Expedition 401 Preliminary Report: Mediterranean-Atlantic Gateway Exchange

Flecker, Rachel
Department of Geography, University of Bristol

Ducassou, Emmanuelle
Environnements Paléoenvironnements Océaniques et Continentaux, UMR CNRS 5805, Université de Bordeaux

Williams, Trevor
International Ocean Discovery Program, Texas A&M University

Amarathunga, Udara
The Department of Geosciences, Princeton University

他

IODP
INTERNATIONAL OCEAN DISCOVERY PROGRAM

International Ocean Discovery Program Expedition 401 Preliminary Report

Mediterranean–Atlantic Gateway Exchange

10 December 2023–9 February 2024

Rachel Flecker, Emmanuelle Ducassou, Trevor Williams, and the Expedition 401 Scientists

Publisher's notes

Core samples and the wider set of data from the science program covered in this report are under moratorium and accessible only to Science Party members until 7 July 2025.

This publication was prepared by the *JOIDES Resolution* Science Operator (JRSO) at Texas A&M University (TAMU) as an account of work performed under the International Ocean Discovery Program (IODP). This material is based upon work supported by the JRSO, which is a major facility funded by the National Science Foundation Cooperative Agreement Number OCE1326927. Funding for IODP is provided by the following international partners:

National Science Foundation (NSF), United States
Ministry of Education, Culture, Sports, Science and Technology (MEXT), Japan
European Consortium for Ocean Research Drilling (ECORD)
Ministry of Science and Technology (MOST), People's Republic of China
Australia-New Zealand IODP Consortium (ANZIC)
Ministry of Earth Sciences (MoES), India

Portions of this work may have been published in whole or in part in other IODP documents or publications.

Disclaimer

Copyright

Citation

Flecker, R., Ducassou, E., Williams, T., and the Expedition 401 Scientists, 2024. Expedition 401 Preliminary Report: Mediterranean–Atlantic Gateway Exchange. International Ocean Discovery Program. https://doi.org/10.14379/iodp.pr.401.2024

ISSN

World Wide Web: 2372-9562

April 2024

Expedition 401 participants

Expedition 401 scientists

Rachel Flecker
Co-Chief Scientist
Department of Geography
University of Bristol
United Kingdom
r.flecker@bristol.ac.uk

Emmanuelle Ducassou
Co-Chief Scientist
Environnements Paléoenvironnements Océaniques et Continentaux, UMR CNRS 5805
Université de Bordeaux
France
emmanuelle.ducassou@u-bordeaux.fr

Trevor Williams
Expedition Project Manager
International Ocean Discovery Program
Texas A&M University
USA
williams@iodp.tamu.edu

Udara Amarathunga
Micropaleontologist (planktonic foraminifers)
The Department of Geosciences
Princeton University
USA
udara.amar@princeton.edu

Barbara Balestra
Micropaleontologist (nannofossils)
Environmental Science Department
American University
USA
balestra@american.edu

Melissa Berke
Organic Geochemist
Department of Civil and Environmental Engineering and Earth Sciences
University of Notre Dame
USA
mberke@nd.edu

Clara Blättler
Inorganic Geochemist
Department of the Geophysical Sciences
University of Chicago
USA
cblattler@uchicago.edu

Shamar Chin
Micropaleontologist (nannofossils)
Earth and Environmental Sciences
University of Iowa
USA
shamar-chin@uiowa.edu

Moumita Das
Micropaleontologist (benthic foraminifers)
Geology Section, MMV
Banaras Hindu University
India
mdas.mmv@bhu.ac.in

Kosuke Egawa
Sedimentologist
Department of Earth Resources Engineering
Kyushu University
Japan
egawa.kosuke.394@m.kyushu-u.ac.jp

Natacha Fabregas
Sedimentologist
Department of Earth Science
University of Bergen
Norway
natacha.fabregas@uib.no

Sarah Feakins
Organic Geochemist
Department of Earth Sciences
University of Southern California
USA
feakins@usc.edu

Simon George
Sedimentologist
School of Natural Sciences
Macquarie University
Australia
Simon.George@mq.edu.au

F. Javier Hernández-Molina
Sedimentologist
Royal Holloway University of London
United Kingdom
javier.hernandez-molina@rhul.ac.uk

Wout Krijgsman
Paleomagnetist
Department of Earth Sciences
Utrecht University
The Netherlands
W.Krijgsman@uu.nl

Zhiyang Li
Sedimentologist
Texas A&M International University
USA
zhiyang.li@tamiu.edu

Jiabo Liu
Paleomagnetist
Institute of Geophysics and Geomatics
China University of Geosciences
China
liujiabo@cug.edu.cn

Danielle Noto
Sedimentologist
CENEX, Department of Geology and Geophysics and Museum of Natural Science
Louisiana State University
USA
notodanielle1@gmail.com

Fadl Raad
Physical Properties Specialist/Downhole Measurements
Università di Corsica Pasquale Paoli, Campus Grimaldi
France
raad_f@univ-corse.fr

Francisco Javier Rodríguez-Tovar
Sedimentologist
Department of Stratigraphy and Paleontology
University of Granada
Spain
fjrtovar@ugr.es

Francisco Javier Sierro
Micropaleontologist (planktonic foraminifers)
Department of Geology
University of Salamanca
Spain
sierro@usal.es

Patricia Standring
Sedimentologist
Institute for Geophysics
University of Texas at Austin
USA
patty.standring@utexas.edu

Jonathan Stine
Physical Properties Specialist
Department of Earth and Environmental Sciences
University of Minnesota Twin Cities
USA
jstine@umn.edu

Erika Tanaka
Inorganic Geochemist
Kochi University
Japan
erikat@kochi-u.ac.jp

Manuel Teixeira
Physical Properties Specialist/Observer
Instituto Dom Luiz, Faculty of Sciences
University of Lisbon
Portugal
macteixeira@ciencias.ulisboa.pt

Xunhui Xu
Physical Properties Specialist
Department of Urban Management
Earth and Resource System
Kyoto University
Japan
xu.xunhui.72x@st.kyoto-u.ac.jp

Shaoru Yin
Physical Properties Specialist
Second Institute of Oceanography
Ministry of Natural Resources
China
shaoru2017@outlook.com

Mohamed Zakaria Yousfi
Micropaleontologist (planktonic foraminifers)/Observer
Office National des Hydrocarbures et des Mines
Morocco
yousfi@onhym.com

Outreach

Erin Winick Anthony
Outreach Officer
Freelance Science Communicator
STEAM Power Media
USA
erin.winick@gmail.com

Kellan Moss
Outreach Officer
Freelance Artist
Rochester Institute of Technology
USA
mossartworks99@gmail.com

Operational and technical staff

Siem Offshore AS officials

Harm Cornelis Theodoor Nienhuis
Master of the Drilling Vessel

Curtis Wayne Lambert Jr.
Drilling Supervisor

JRSO shipboard personnel and technical representatives

Timothy Blaisdell
Applications Developer

Erick Bravo
Marine Laboratory Specialist

Michael Cannon
Marine Computer Specialist

Oscar Cavazos
Marine Laboratory Specialist

Bridgette Cervera
Marine Laboratory Specialist

Etienne Claassen
Marine Instrumentation Specialist

Douglas Cummings
Publications Specialist

Kirby Garrett
Logging Engineer (Schlumberger)

Myriam Kars
Marine Laboratory Specialist

Jan Kotze
Marine Instrumentation Specialist

Carel Lewis
Curatorial Specialist

Nick Logan
Marine Computer Specialist

Zenon Mateo
Marine Laboratory Specialist

Eric Moortgat
Assistant Laboratory Officer

Chieh Peng
Laboratory Officer

Doris Pinero Lajas
Assistant Laboratory Officer

William Rhinehart
Operations Superintendent

Alexander Roth
Marine Laboratory Specialist

Johanna Suhonen
Marine Laboratory Specialist

Kara Vadman
Marine Laboratory Specialist

Maximilian Witek
Marine Laboratory Specialist

Hai Zhao
Applications Developer

Abstract

Marine gateways play a critical role in the exchange of water, heat, salt, and nutrients between oceans and seas. Changes in gateway geometry can significantly alter both the pattern of global ocean circulation and climate. Today, the volume of dense water supplied by Atlantic–Mediterranean exchange through the Gibraltar Strait is among the largest in the global ocean. For the past 5 My, this overflow has generated a saline plume at intermediate depths in the Atlantic that deposits distinctive contouritic sediments and contributes to the formation of North Atlantic Deep Water. This single gateway configuration only developed in the Early Pliocene. During the Miocene, two narrow corridors linked the Mediterranean and Atlantic: one in northern Morocco and the other in southern Spain. Formation of these corridors followed by progressive restriction and closure resulted in extreme salinity fluctuations in the Mediterranean, leading to the precipitation of the Messinian Salinity Crisis salt giant. International Ocean Discovery Program (IODP) Expedition 401 is the offshore drilling component of a Land-2-Sea drilling proposal, Investigating Miocene Mediterranean–Atlantic Gateway Exchange (IMMAGE). Its aim is to recover a complete record of Atlantic–Mediterranean exchange from its Late Miocene inception to its current configuration by targeting Miocene offshore sediments on either side of the Gibraltar Strait. Miocene cores from the two precursor connections now exposed on land will be obtained by future International Continental Scientific Drilling Program (ICDP) campaigns.

Plain language summary

Today, Mediterranean–Atlantic seawater exchange takes place exclusively through the Gibraltar Strait. Around 8 million years ago, however, there were another two gateways: one in northern Morocco and the other through southern Spain. Both connections have subsequently closed and been tectonically uplifted and preserved on land. Extreme narrowing of these pre-Gibraltar Strait connections raised salinity in the Mediterranean substantially, leading to the precipitation of more than 1 km of salt on the Mediterranean's seafloor. This process may have contributed to a major episode of global cooling. The chemical and physical properties of the sediments preserved in and on either side of these corridors are key to understanding and quantifying this global cooling. International Ocean Discovery Program (IODP) Expedition 401 is the offshore drilling component of the Land-2-Sea drilling proposal, Investigating Miocene Mediterranean–Atlantic Gateway Exchange (IMMAGE). The expedition recovered records of exchange preserved off shore in the Atlantic and Mediterranean. Future drilling on shore will target the fossil gateway records that are now preserved on land.

1. Introduction

Marine gateways play a critical role in the exchange of water, heat, salt, and nutrients between oceans and seas. The advection of dense waters helps drive global thermohaline circulation, and because the ocean is the largest of the rapidly exchanging CO_2 reservoirs, this advection also affects atmospheric carbon concentration. Changes in gateway geometry can therefore significantly alter both the pattern of global ocean circulation and associated heat transport and climate, as well as having a profound local impact. Today, the volume of dense water supplied by Atlantic–Mediterranean exchange through the Gibraltar Strait is among the largest in the global ocean. For the past 5 My, this overflow has generated a saline plume at intermediate depths in the Atlantic that deposits distinctive contouritic sediments in the Gulf of Cádiz and contributes to the formation of North Atlantic Deep Water (NADW). This single gateway configuration only developed in the Early Pliocene. During the Miocene, a wide, open seaway linking the Mediterranean and Atlantic evolved into two narrow corridors: one in northern Morocco and the other in southern Spain. Formation and restriction of these corridors permitted Mediterranean salinity to rise and a new, distinct, dense water mass to form and overspill into the Atlantic for the first time. Further restriction and closure of these connections resulted in extreme salinity fluctuations in the Mediterranean, leading to the formation of the Messinian Salinity Crisis salt giant. Investigating Miocene Mediterranean–Atlantic Gateway Exchange (IMMAGE) is a Land-2-Sea drilling proposal

designed to recover a complete record of Atlantic–Mediterranean exchange from its Late Miocene inception to its current configuration. This will be achieved by targeting Miocene offshore sediments on either side of the Gibraltar Strait during International Ocean Discovery Program (IODP) Expedition 401 and recovering Miocene cores from the two precursor connections now exposed on land with future International Continental Scientific Drilling Program (ICDP) campaigns. The scientific aims of IMMAGE are to constrain quantitatively the consequences for ocean circulation and global climate of the inception of Atlantic–Mediterranean exchange, to explore the mechanisms for high-amplitude environmental change in marginal marine systems, and to test physical oceanographic hypotheses for extreme high-density overflow dynamics that do not exist in the world today on this scale.

2. Background

Paleoclimate research is often driven by the need to validate various types of climate models under boundary conditions different from those of the last 150 y for which an instrumental record of climate is available (Intergovernmental Panel on Climate Change, 2014). Quantifying past changes in temperature, momentum, and flux in the ocean and atmosphere is therefore a key target for geologic research. However, the small size of climate change signals relative to climate proxy measurement uncertainty means this is challenging to achieve (Rohling, 2007). A high signal-to-noise ratio typically requires amplification of the climate variable, and in the ocean, this is most commonly found in marginal marine basins where exchange with the open ocean is limited so it cannot buffer and diminish the signal of environmental change (Grant et al., 2017). Unfortunately, limited exchange also makes it difficult to use the enhanced marginal basin record to extrapolate to global-scale oceanographic change (Kaminski et al., 2002). Marine gateways linking the basin to the open ocean represent a sweet spot where on one side climatic changes are amplified in the adjoining marginal basin, whereas on the other side their impact on globally meaningful changes in the open ocean can be directly assessed. In addition, the geometric and hydraulic restriction of the gateway itself places physical limitations on the freedom of the system to change (Nelson et al., 1999). This focuses the deposition of the sedimentologic archive of exchange into a small, well defined geographical area, making it possible to constrain quantitatively responses to exchange that impact global climate (Rogerson et al., 2012b).

The influence of exchanging heat, salt, and momentum through narrow, shallow straits that link the open ocean to marginal basins is profound. The advection of cool or saline waters (Legg et al., 2009) helps drive global thermohaline circulation (Thomas et al., 2004; Álvarez et al., 2005; Rahmstorf, 2006). Because the ocean is the largest of the rapidly exchanging CO_2 reservoirs, this advection also increases the sensitivity of the ocean to atmospheric carbon changes (LaRiviere et al., 2012; Karas et al., 2017; Elsworth et al., 2017; Capella et al., 2019). Although exchange through the Denmark Strait, Indonesian archipelago, and Gibraltar Strait can all overprint both zonal and meridional circulation patterns, global ocean surface circulation and associated heat transport compensating for water mass transformation on the basinward side of gateways forces substantial impacts on sea ice and warming or cooling of adjacent continents and the position of the atmospheric front (Ivanovic et al., 2014a). Unsurprisingly, the opening and closure of oceanic gateways is well recognized as having a profound impact on the Earth's climate, including its periodic switching from Greenhouse to Icehouse conditions (Kennett, 1982; Smith and Pickering, 2003; Knutz, 2008; Bahr et al., 2022).

The impact of regional changes on global-scale processes are generally ideal questions for the Earth System Models theme. However, because of the inherent small scale of marine gateways relative to global circulation model grid cells, the gateways are either hugely enlarged in the model or the transport of heat and water through them is parameterized rather than explicitly modeled (e.g., Dietrich et al., 2008; Ivanovic et al., 2013). An excellent example of the problem occurs at Gibraltar (Figure **F1**), where model grid cells of ~400 km^2, which are suitable for the long global simulations necessary for paleoclimate studies, are ill-equipped to simulate hydraulic control in a strait ~15 km in width and consequently generate exchange behavior that differs from observations (Ivanovic et al., 2013; Alhammoud et al., 2010). Consequently, the codependence of ocean and marginal sea in simulations is reduced, preconditioning models to be insensitive to exchange

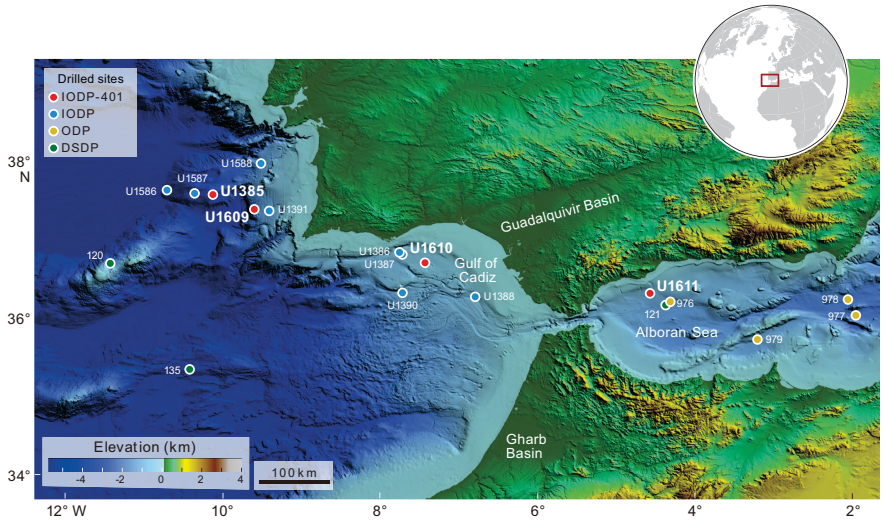

Figure F1. Topographic and bathymetric map of Gibraltar Strait showing locations of Expedition 401 sites and sites from previous expeditions in Atlantic and Alborán Sea. Guadlquivir Basin in Spain and Gharb Basin in Morocco are located at western end of Betic and Rifian Corridors; fossil gateways that closed in the Late Miocene and are the target of ICDP drilling as part of the IMMAGE Land-2-Sea drilling project. ODP = Ocean Drilling Program, DSDP = Deep Sea Drilling Project.

driven change. A view of past and future climate derived from global circulation assessments alone therefore systematically underestimates the role of gateway processes, eliminating a crucial feedback within the Earth system. In summary, exchange through marine gateways is an example of a key climate process that can only be constrained through interrogation of the record of ocean–marginal basin exchange in a specific sedimentary archive.

3. Geologic setting

3.1. Atlantic–Mediterranean exchange now and in the past

In the Atlantic, several marine overflows (Denmark Strait, Mediterranean, and Weddell Sea) supply dense water that collectively feeds the thermohaline circulation system (Smethie et al., 2000; Bahr et al., 2022). The transportation of dense water from the Mediterranean into the interior of the Atlantic (Figure **F2**) is among the largest in the global ocean (Legg et al., 2009), and exchange also provides a key exit point for Atlantic buoyancy, the underlying driver behind Atlantic deep convection (Broecker, 1991).

The dense Mediterranean overflow (MO) is generated as a consequence of its midlatitude setting where evaporation exceeds precipitation (Peixoto and Kettani, 1973), generating a warm, salty water mass. The negative hydrologic budget varies in severity through time, amplifying the climate signal transmitted principally through the Mediterranean's southern catchments and derived from North African monsoon rainfall (Marzocchi et al., 2015). This subtropical monsoonal climate signal with its strong precessional pulse is then propagated into the Atlantic by density-driven exchange (Bahr et al., 2015) through the Gibraltar Strait. Water flowing out of the Mediterranean at depth entrains ambient Atlantic water as it goes (Dietrich et al., 2008), generating first the Mediterranean Overflow Water (MOW) in the Gulf of Cádiz and the Atlantic–Mediterranean Water (AMW) in the rest of the Atlantic (Rogerson et al., 2012b) and large depositional and erosional features including extensive sandy contouritic drifts (Figure **F2**; Nelson et al., 1999; Expedition 339 Scientists, 2013; Hernández-Molina et al., 2003, 2014a, 2014b). AMW flows north, fueling the Norwegian Sea with higher density water that helps sustain the formation and southward flow of NADW (Khélifi et al., 2009; Rogerson et al., 2012b; Kaboth et al., 2018).

Despite the challenges of modeling the gateway, the exchange that occurs through the Gibraltar Strait today is a sufficiently influential component of the Earth System for general circulation models to capture at least part of its impact (Bigg et al., 2003; Bigg and Wadley, 2001). Experiments

without Atlantic–Mediterranean exchange show that its presence makes Greenland warmer and Antarctica cooler (Bigg et al., 2003). This in turn is sufficient to shift the position of the Intertropical Convergence Zone, and hence the location of monsoons, storm tracks, and the hyper-arid zones between them. Atlantic–Mediterranean exchange is also a critical component of Atlantic Meridional Overturning Circulation, particularly at times of weak NADW formation (Bigg and Wadley, 2001; Ivanovic et al., 2014a, 2014b; Penaud et al., 2011; Rogerson et al., 2006, 2010; Voelker et al., 2006). Furthermore, the transport of dense water from the Mediterranean into the interior of the Atlantic entrains ambient Atlantic water en route, contributing significantly to global carbon drawdown (2%–5% of today's total net ocean carbon sink; Tans et al., 1993; Siegenthaler and Sarmiento, 1993; Dixon et al., 1994). Taken altogether, this makes Atlantic–Mediterranean exchange a key teleconnection that links African monsoon precipitation derived from the south Atlantic with the northern high latitudes.

Exchange through a single gateway at Gibraltar is a relatively recent phenomenon (Hernández-Molina et al., 2014b; van der Schee et al., 2016; García-Gallardo et al., 2017a, 2017b). As a result of Africa-Eurasia convergence, westward docking of the Alborán plate, and simultaneous slab retreat (Jolivet and Faccenna, 2000; Faccenna et al., 2004; van Hinsbergen et al., 2014), the Atlantic–Mediterranean connection evolved from a single, wide open seaway (Figure **F3**) linking a Mediterranean that was more of an embayment of the Atlantic than a distinct marginal marine system (Flecker et al., 2015) to two narrow corridors: one in northern Morocco and the other in southern Spain (Figure **F3**; Benson et al., 1991). The onset of episodic organic-rich sedimentation (sapropels) in the Middle Miocene (Hilgen et al., 2005; Taylforth et al., 2014) is the earliest evidence of the Mediterranean operating separately from the Atlantic. Ongoing progressive restriction of the marine corridors permitted Mediterranean salinity to rise, and a distinct, dense water mass formed. This dense water overspill into the Atlantic occurred for the first time at some point during the Middle–Late Miocene (Capella et al., 2017, 2019; de Weger et al., 2020, 2021). Ultimately, the narrowing and closure of these connections resulted in extreme salinity fluctuations in the Mediterranean, leading to the precipitation of more than 1 million km^3 of salt, equivalent to ~6% of the total dissolved oceanic NaCl (Blanc, 2006; Ryan, Hsü, et al., 1973) in the latest Miocene. This event is known as the Messinian Salinity Crisis (MSC; Hsü et al., 1973). Ongoing tectonic convergence coupled with isostatic rebound related to lithospheric mantle dynamics (Duggen et al., 2003) not only severed these earlier marine connections but also uplifted and exposed them on land (Capella et al., 2017; de Weger et al., 2021). In the Early Pliocene, two-way exchange was established through a single conduit, the Gibraltar Strait (Figure **F3**).

During the MSC, the amplified net evaporative flux changed to such an extent that the salinity of water flowing into the Atlantic varied between near-equality with Atlantic water (~36 g/kg) to

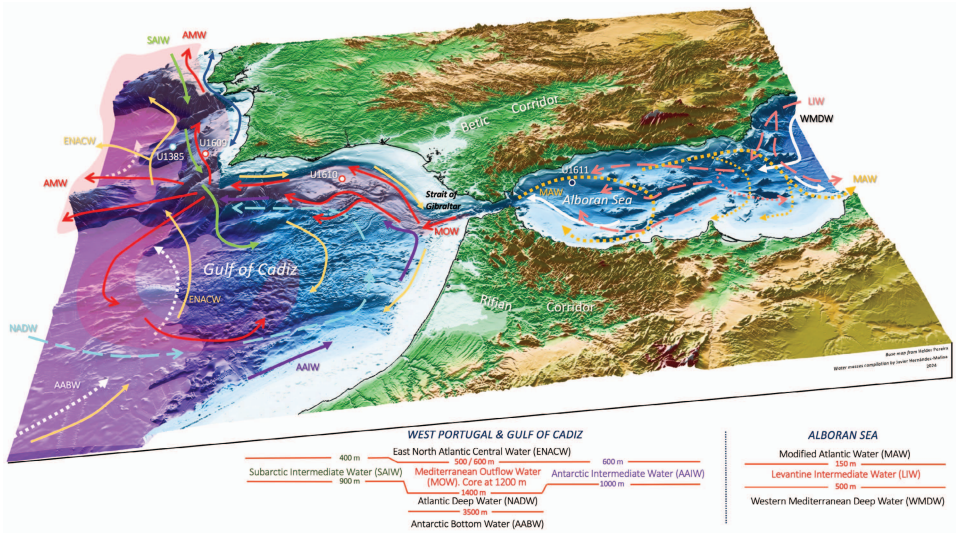

Figure F2. Present-day water mass circulation patterns on either side of Gibraltar Strait in relation to main topographic features and Expedition 401 sites.

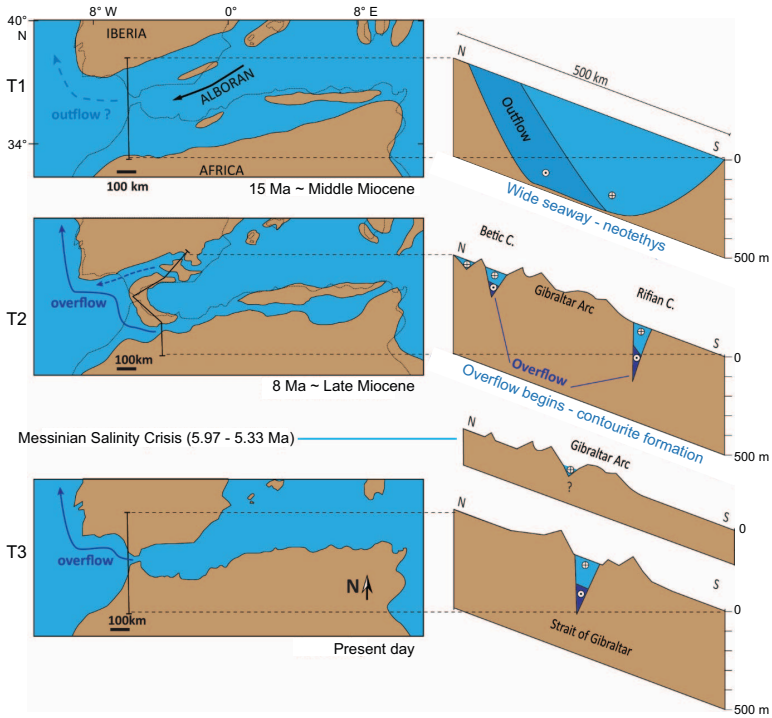

Figure F3. Tectonically controlled reconfiguration of Mediterranean–Atlantic seaways from Middle Miocene to present day. Paleogeography of Western Mediterranean after Do Couto et al. (2016). Rifian/Betic seaways (T2), which replaced a wider seaway (T1), are now exposed on land in northern Morocco and southern Spain. T2 scenario (~8 Ma) is the first with potential impact on Atlantic–Mediterranean salinity gradients and overflow formation. (Figure from Capella et al., 2019.)

halite-depositing brine (>360 g/kg) and brackish water conditions (<20 g/kg). Gibraltar exchange today exhibits one of the largest density contrasts in the modern ocean, but this contrast was up to two orders of magnitude higher during the acme of the MSC. The water flowing into the Atlantic at this time was probably the most extremely dense overflow of oceanographic scale in Earth's history, and all other aspects of the exchange would have been proportionally exaggerated.

4. Scientific objectives

The target of the IMMAGE drilling proposal is the record of Atlantic–Mediterranean exchange during the most dynamic and variable period of its history, from inception (~8 Ma) through salt giant formation (6–5 Ma) to the establishment of an exchange configuration similar to today (5–4 Ma). The sediments on either side of the gateway region, which are preserved both onshore and offshore, record the changing nature of Atlantic–Mediterranean exchange, allowing quantitative evaluation of its role in global-scale climate systems, impact on major climatic events, and influence over extreme environmental change in the Mediterranean. Two of IMMAGE's scientific objectives are therefore paleoclimatic. In addition, a Late Miocene drilling target focused on the gateway also provides an unparalleled opportunity to test physical oceanographic representations of extreme high-density overflow dynamics that do not exist in the world today on this scale. IMMAGE's third objective is therefore testing a physical oceanography hypothesis.

4.1. Objective 1: to document the time at which the Atlantic first started to receive a distinct overflow from the Mediterranean and to evaluate quantitatively its role in Late Miocene global climate and regional environmental change

Today, dense water (13°C, 37 g/kg; Price et al., 1993) pools on the floor of the Mediterranean behind a shallow (300 m), narrow (15 km) sill, the Gibraltar Strait. Mediterranean waters overspill the sill and cascade down the continental slope. The density contrast between Mediterranean and

ambient Atlantic water generates substantial current speed, leading to extensive contouritic drifts (Hernández-Molina et al., 2016). Recent fieldwork in Morocco has revealed that the Rifian Corridor in northern Morocco contains Upper Miocene contouritic sediments (Capella et al., 2017) that resemble the Pliocene–Pleistocene contourites in the Gulf of Cádiz (Integrated Ocean Drilling Program Expedition 339; Expedition 339 Scientists, 2013).

The presence of 7.8–6.3 Ma contourites in Morocco (Capella et al., 2017) indicates that an overspill geometry had already formed in the Late Miocene, ~2 My before the MSC, allowing a density contrast between the Mediterranean and Atlantic to develop and feeding saline Mediterranean water into the North Atlantic (Capella et al., 2017, 2019). The outstanding question is whether these exposed Rifian contourites are the first products of MO or whether older, buried contourites exist in either the Rifian and/or Betic Corridors (Figures **F2**, **F3**).

One possibility is that initiation of MO contributed to the cooling that ultimately triggered the formation of permanent Northern Hemisphere ice by altering the North Atlantic density structure and increasing CO_2 drawdown through the entrainment of Atlantic surface water and its dissolved CO_2 in the dense AMW plume (Capella et al., 2019). Correlation with similarly high-resolution sites in the North Atlantic will be required to test this mechanism and assess its importance in modulating NADW formation.

Hypotheses that will be tested as part of this scientific objective include the following:

- Hypothesis 1.1: the earliest contourites formed as a result of Atlantic–Mediterranean exchange and correlate with the onset of Late Miocene sea surface temperature (SST) decline in the mid- and high latitudes. Dating the first Atlantic–Mediterranean contourites will test this hypothesis.
- Hypothesis 1.2: atmospheric CO_2 sequestration in the deeper ocean through the initiation and development of AMW can account for the degree and distribution of SST cooling observed. Reconstructing the velocity, density, and flux of AMW through time, quantifying its impact on CO_2 advection (Capella et al., 2019), and then modeling the resulting SST distribution (e.g., Ivanovic et al., 2014a) tests this hypothesis.
- Hypothesis 1.3: AMW modulates NADW formation, triggers glacial inception, and influences continental-scale aridification. Model-based testing of this hypothesis requires the correlation of IMMAGE records with existing high-resolution records globally.

4.2. Objective 2: to recover a complete record of Atlantic–Mediterranean exchange before, during, and after the Messinian Salinity Crisis and to evaluate the causes and consequences of this extreme oceanographic event locally, regionally and globally

Today, Mediterranean seawater flows through the Gibraltar Strait forming a saline plume at intermediate depths in the Atlantic (Figure **F2**; Iorga and Lozier, 1999). The plume's record of Pliocene–Quaternary contouritic sediments was recovered from the Gulf of Cádiz (Expedition 339) and documents a Mediterranean contribution to Atlantic thermohaline circulation since the Pliocene (Hernández-Molina et al., 2014b; van der Schee et al., 2016; Garcia-Gallardo et al., 2017a, 2017b). However, there was also a Late Miocene episode of Mediterranean influence on the Atlantic (Capella et al., 2017, 2019), although the conduit for Atlantic–Mediterranean exchange is unclear because Gibraltar may have already been open alongside marine corridors in northern Morocco and southern Spain (Figure **F3**) (Flecker et al., 2015; Martín et al., 2009; Krijgsman et al., 2018), and the Alborán Basin may have been an intermediate system separated from the Mediterranean by the Alborán volcanic arc (Booth-Rea et al., 2018). The sedimentary expression of restriction and closure of these Miocene connections in the Mediterranean comprises both thick evaporites (e.g., Roveri et al., 2014) and brackish "Lago Mare" sediments (Iaccarino and Bossio, 1999; Orszag-Sperber, 2006; Rouchy et al., 2007; Guerra-Merchán et al., 2010). Understanding the causes of high-amplitude salinity change in the Mediterranean and its global consequences depends on recovering a complete record of Atlantic–Mediterranean exchange before, during, and after the MSC. Hypotheses that will be tested as part of this scientific objective include the following:

- Hypothesis 2.1: the Alborán Basin was an intermediate marine system influenced by the Atlantic and separated from the Mediterranean by the Alborán volcanic arc during the MSC.
- Hypothesis 2.2: extreme environmental fluctuations in the Mediterranean had negligible impact on AMW.

4.3. Objective 3: to test our quantitative understanding of the behavior of ocean overflow plumes during the most extreme exchange in Earth's history

There are ~20 major ocean-scale overflow systems in the world today (Legg et al., 2009), including some of the most important and sensitive oceanic transport systems (e.g., Denmark Strait and Weddell Sea). All of these systems are driven by source water density anomalies upstream of the overflow (Price and O'Neill Baringer, 1994). However, the range of source water density today is rather small; 27.7 σ units (Red Sea) to 28.95 σ units (Mediterranean Sea). In comparison, the density of Mediterranean water during gypsum and halite deposition would have been enormous (110 and ~300 σ units, respectively). This presents an opportunity and a challenge for existing representations of oceanographic overflow physics (e.g., Legg et al., 2009) because we can test hypotheses derived from physical theory through scientific drilling. This is the first experiment of its type that we are aware of and is ground-breaking in the field of quantitative paleoceanography. The application of physical theory to the paleoceanography of MO is well established (Rogerson et al., 2012a) and suggests the following hypotheses:

- Hypothesis 3.1: the velocity of the plume is a function of the Atlantic–Mediterranean density contrast, limitation on flow through the strait (Bryden et al., 1994), the gradient of the slope, and the degree of mixing (Price et al., 1993).
- Hypothesis 3.2: mixing with ambient water causes a strong negative feedback on the size of the plume, limiting the degree of its variability (Price et al., 1993). This means that only minor changes in the physical size of the plume are expected, despite the proportion of plume water derived directly from the outflow varying significantly. As a result, changes in Mediterranean density have little impact on the plume position.
- Hypothesis 3.3: the main control on the settling depth of MO is the vertical density gradient in the North Atlantic, which is a product of North Atlantic overturning circulation (Rogerson et al., 2012a).

5. Connections to the 2050 Science Framework

Using the newly obtained Expedition 401 cores, we can now describe the changes in Mediterranean–Atlantic water exchange through geologic time and understand the mechanisms governing those changes and their downstream effects on the Earth's climate system. This will allow us to address the following strategic objectives and initiatives from the 2050 Framework for scientific ocean drilling:

5.1. Strategic objectives

- Earth's climate system: opening and closure of oceanic gateways is recognized as having a profound impact on Earth's climate, changing the distribution of heat and salt in the world's oceans. Dense salty water from the Mediterranean contributes to global thermohaline circulation, NADW formation, and associated carbon drawdown.
- Tipping points in Earth's history: flooding of the Mediterranean basin at the end of the Miocene is one of the most vivid examples of a tipping point in Earth's history. However, the history of water flow through this gateway remains to be described in detail, and it has consequences not just for the Mediterranean but also for the global ocean.
- Global cycles of energy and matter: the Mediterranean–Atlantic gateway has a controlling influence on the distribution of salt, heat, and nutrients in the ocean.

5.2. Flagship initiatives

- Groundtruthing future climate change: sediment cores from this expedition covered the last ~8 Ma of Earth's climate, including analogs for future warm climates under CO_2 levels up to ~500 ppm. In particular, the combination of gateway and climate history recorded in the cores will help us understand global climate from 5 to 8 Ma, a relatively understudied interval compared to the last 5 My.

5.3. Enabling elements

- Broader impacts and outreach: during the expedition, we reached a broad audience to communicate the expedition's science and real-time progress (see **Outreach**). Because of the unusually long duration of this Land-2-Sea drilling project, we have an opportunity to develop a more ambitious outreach endeavor than is typical and will be targeting, in particular, communities that do not normally engage with scientific narratives.
- Land to sea: this IODP expedition is the first element of the first ever Land-2-Sea drilling project. The onshore ICDP drilling will happen in the years following Expedition 401 at sites in southern Spain and northern Morocco. Integrated results from both the land and sea drilling are necessary to fully understand Late Miocene gateway history and deliver IMMAGE's scientific objectives. Expedition 401 scientific results provide the foundation and momentum on which the two ICDP projects will build.

6. Site summaries

During Expedition 401, core was recovered from 7 holes at 4 different sites (Figures **F4**, **F5**). At Sites U1385 and U1609, where two holes were cored at each site and the physical properties data showed regular cyclic patterns, splices have been constructed.

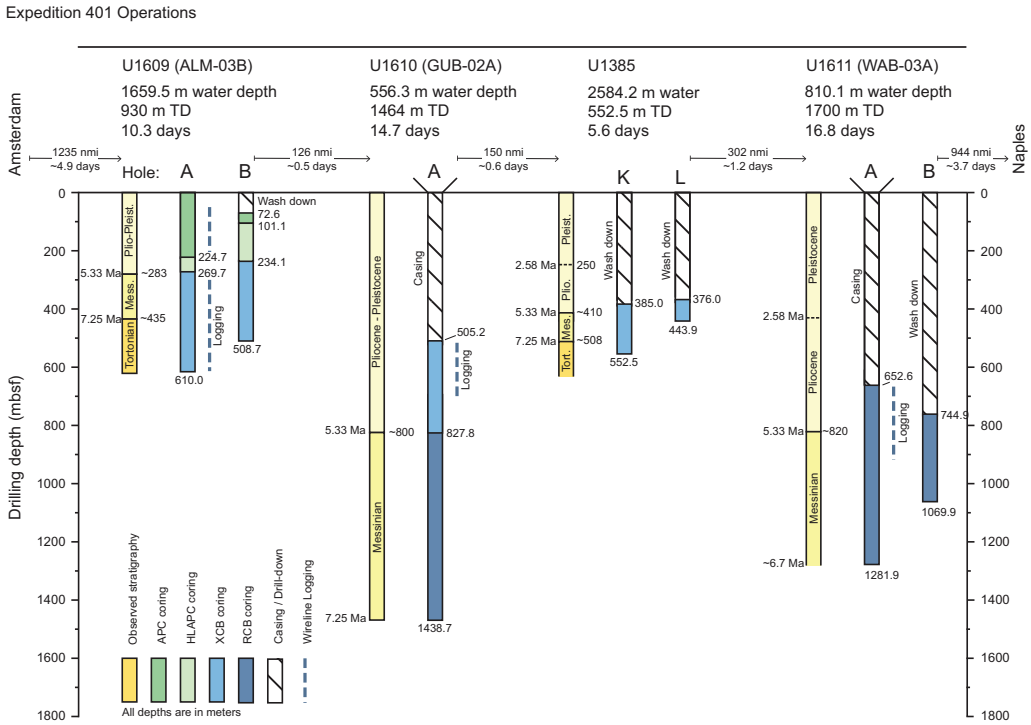

Figure F4. Drilling summary, Expedition 401. Original strategy for these deep holes was to wash down through Pliocene, which had been extensively recovered previously, and core from just above 4.5 Ma bioevent down to target depth of 8 Ma. Logging at each site was planned but proved difficult or impossible to implement fully. However, recovery was excellent and there was time to drill a second hole at three of the four sites. TD = total depth.

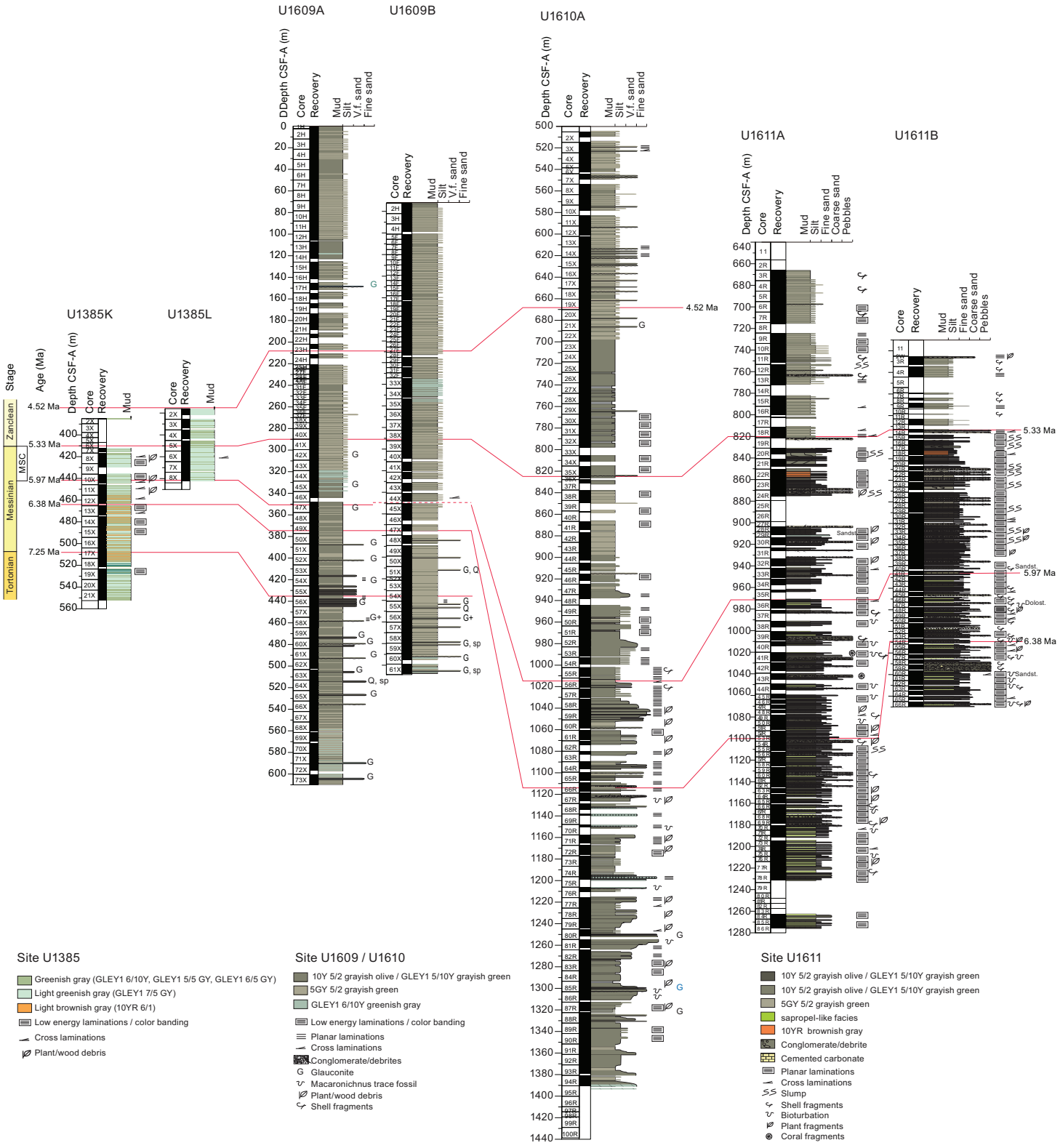

Figure F5. Correlation of Expedition 401 sites. Red lines = position of key intervals at each site including top and bottom of Messinian Salinity Crisis (MSC).

6.1. Site U1609

6.1.1. Background and objectives

Site U1609 (37°22.6159′N, 9°35.9119′W; proposed site ALM-03B) is located at 1659.5 meters below sea level (mbsl) on the continental slope of the Portuguese margin (Figures F6, F7; Table T1). The primary scientific objective of Site U1609 was to recover a distal record of the Late Miocene–Pliocene MO plume (Figure F2). The aim was to capture the evolution of the plume's equilibrium depth through time, from the earliest evidence of overflow through the Rifian Corridor in present-day Morocco, through the Mediterranean's MSC (5.97–5.33 Ma), to the Early Pliocene (~4 Ma). This interval of major gateway and Mediterranean environmental change is likely to have substantially influenced both the density and the chemistry of the overflow on subprecessional to million-year timescales.

Site U1609 is 17 km west and downslope from Integrated Ocean Drilling Program Site U1391, drilled during Expedition 339, which comprised Pliocene–Quaternary muddy contourites with interbedded sands, hemipelagites, and several layers of mass movement deposits. On the seismic profile linking Site U1391 with Site U1609, packages of the contouritic drift migrate landward with

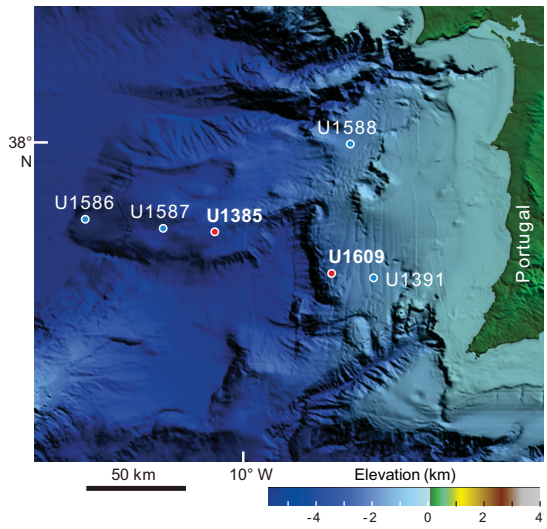

Figure F6. Bathymetric map of the Portuguese continental margin showing Sites U1609 and U1385 in relation to previously drilled sites in the area. See Figure F1 for legend.

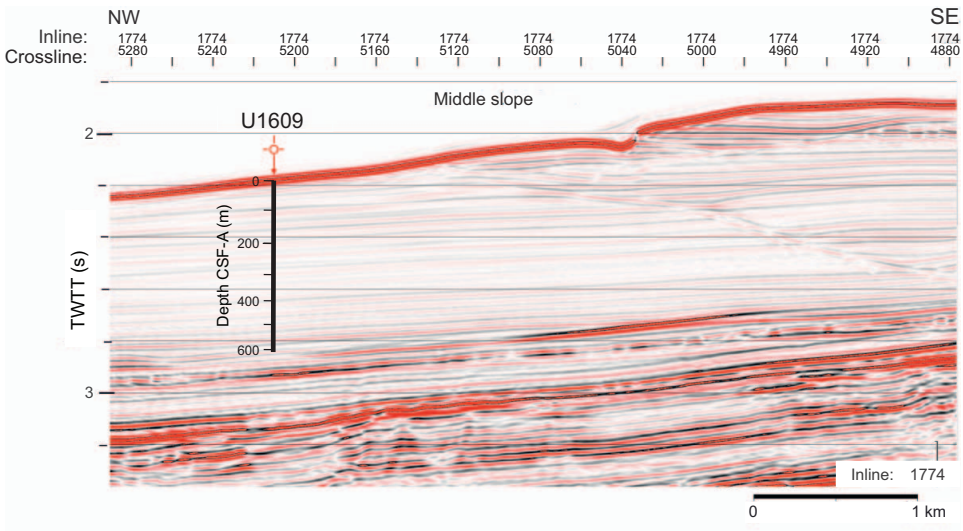

Figure F7. Seismic Profile IL1774 with location and approximate penetration, Hole U1609A. TWTT = two-way traveltime.

time. Site U1609 took advantage of this landward migration and surface erosion, which is also visible in the seismic profiles, to access the target Miocene–Pliocene strata at relatively shallow depths. The seismic data also suggest that the Late Miocene succession at Site U1609 is more likely to provide a more complete record of the MO plume than Site U1610 (proposed Site GUB-02A) in the Gulf of Cádiz, which is closer to the source of the plume.

Site U1609's distal location was selected to recover a less clastic, more hemipelagic succession suitable for high-resolution astrochronological tuning and a strong age framework for subprecessional investigation of the driving mechanisms causing changes in the plume. This record of the Miocene MO plume also provides an important constraint on the upper part of the northeast Atlantic water mass structure in the Late Miocene (Figure **F2**). This record will be correlated with a deeper water site to the north, Site U1385 (drilled during Expedition 401), and the Miocene successions recovered along the IODP Expedition 397 depth transect.

In combination with other Expedition 401 Atlantic sites, the record from Site U1609 also allows the investigation of more specific objectives including the following:

- To establish the age of the earliest contourites formed as a result of MO.
- To evaluate the impact of extreme environmental fluctuations in the Mediterranean on its overflow plume and the structure of the Atlantic water masses (Figure **F2**).
- To provide quantitative constraints on the mixing behavior of dense overflows by reconstructing the strength and attenuation rate of the Atlantic–Mediterranean exchange signal beyond the gateway.

6.1.2. Operations

Site U1609 consists of two holes and 983.0 m of sediment collected over a 1046.1 m cored interval (Figures **F4**, **F5**). Hole U1609A penetrated 610.0 m with a sedimentary recovered length of 572.4

Table T1. Operations summary, Expedition 401. — = not applicable.

Hole	Latitude	Longitude	Water depth (mbsl)	Total penetration (m)	Drilled interval (m)	Cored interval (m)	Recovered length (m)	Recovery (%)	Total cores (*N*)	APC cores (*N*)	HLAPC cores (*N*)	XCB cores (*N*)	RCB cores (*N*)
U1609A	37°22.6259′N	9°35.9120′W	1659.5	610.0	—	610.0	572.23	94	73	25	12	36	0
U1609B	37°22.6159′N	9°35.9119′W	1659.5	508.7	72.6	436.1	410.75	94	60	3	28	29	0
		Site U1609 totals:		1118.7	72.6	1046.1	982.98	94	133	28	40	65	0
U1610A	36°41.9812′N	7°25.8844′W	556.3	1438.7	505.2	933.5	751.20	80	99	0	0	35	64
		Site U1610 totals:		1438.7	505.2	933.5	751.20	80	99	0	0	35	64
U1385K	37°34.0099′N	10°7.6370′W	2584.2	552.5	385.0	167.5	127.89	76	20	0	0	20	0
U1385L	37°34.0197′N	10°7.6367′W	2584.2	443.9	376.0	67.9	58.44	86	7	0	0	7	0
		Site U1385 totals:		996.4	761.0	235.4	186.33	79	27	0	0	27	0
U1611A	36°18.7537′N	4°34.2717′W	810.1	1281.9	656.3	625.6	431.22	69	85	0	0	0	85
U1611B	36°19.3779′N	4°34.7520′W	784.0	1069.9	744.9	325.0	253.38	78	65	0	0	0	64
		Site U1611 totals:		2351.8	1401.2	950.6	684.60	72	150	0	0	0	149
		Expedition 401 totals:		5905.6	2740.0	3165.6	2605.11	82	409	28	40	127	213

Hole	Date started	Time started UTC (h)	Date finished	Time finished UTC (h)	Time on hole (h)	Time on site (days)
U1609A	17 Dec 2023	1715	23 Dec 2023	2230	149.25	
U1609B	23 Dec 2023	2230	28 Dec 2023	0000	97.50	
				Site U1609 totals:		10.28
U1610A	28 Dec 2023	1030	12 Jan 2024	0345	353.25	
				Site U1610A totals:		14.72
U1385K	12 Jan 2024	1645	15 Jan 2024	1330	68.75	
U1385L	15 Jan 2024	1330	18 Jan 2024	0730	66.00	
				Site U1385 totals:		5.61
U1611A	19 Jan 2024	1345	30 Jan 2024	1400	264.25	
U1611B	30 Jan 2024	1400	5 Feb 2024	0930	139.50	
				Site U1611 totals:		16.82
				Expedition 401 totals:		47.43

m (93% recovery). Hole U1609B cored 436.1 m with a sedimentary recovered length of 410.8 m (94% recovery).

6.1.2.1. Hole U1609A

The ship arrived at Site U1609 at 1655 h on 17 December 2023 after completing the 1220 nmi voyage from Amsterdam (Netherlands) in 4.5 days. All thrusters were down and secure at 1712 h, and the ship switched to full auto dynamic positioning (DP) mode at 1720 h, marking the start of operations at Site U1609. Operations started on the rig floor assembling the bottom-hole assembly (BHA). We used a polycrystalline diamond compact (PDC) drill bit for Hole U1609A, and for the extended core barrel (XCB) cores we used a PDC cutting shoe. This combination had been found during recent IODP expeditions, including during Expedition 397 in the same area, to yield very good recovery of XCB cores.

At 0430 h on 18 December after one missed mudline, we were successful in starting Hole U1609A (37°22.6259′N, 9°35.9120′W), with the seafloor calculated at 1659.5 mbsl based on the core recovery and mudline depth in Core 1H. Cores 1H–25H penetrated from the seafloor to 224.7 meters below seafloor (mbsf) and recovered 224.7 m (85%). Advanced piston corer temperature (APCT-3) tool measurements were made during Cores 4H, 7H, 10H, and 13H, and all measurements recorded smooth 10 min long temperature equilibration curves. At 0300 h on 19 December, we switched to the half-length advanced piston corer (HLAPC). Cores 26F–37F penetrated from 224.7 to 269.7 mbsf and recovered 45 m (102%). At 1430 h at 269.7 mbsf, we changed to XCB coring. Cores 38X–73X penetrated from 269.7 to 610.0 mbsf and recovered 340.3 m (99%). Over the course of the hole, the driller pumped eight 30 bbl sepiolite mud sweeps from 274.7 to 571.0 mbsf.

After confirming that early Tortonian sediments had been reached and thus that we had recovered the Messinian to late Tortonian target succession, we stopped coring. The last core, 73X, reached 610.0 mbsf and came on deck at 2015 h on 22 December.

We prepared the hole for downhole logging by sweeping it with 30 bbl of sepiolite mud to flush out any loose sediment, displacing it with 230 bbl of barite-weighted mud to stabilize the borehole walls, and setting the end of the pipe to 56.4 mbsf. The triple combo downhole logging tool string was assembled by 0130 h on 23 December, but before it could be run down the pipe, the wireline heave compensator control computer was found to be unresponsive. After troubleshooting diagnosed a probable hard drive failure, we decided to log without heave compensation. Ship heave was around 2.5 m throughout the day—higher than desirable but not atypical for logging from the ship. The triple combo logged borehole physical properties data down to within 5 m of the bottom of the hole. The second tool string, the Versatile Seismic Imager, also reached close to the bottom of the hole for the check shot survey. Concurrently, we observed for protected marine species; none were observed. Only two of the 13 check shot stations gave reliable first-arrival times because most of the borehole was too wide to achieve good coupling. Fortunately, those two stations were in the lower part of the hole where the data are most useful for tying borehole depth to the seismic profiles. Because of the wide borehole and the lack of heave compensation, we decided not to run the Formation MicroScanner tool and instead to run a sonic velocity and natural gamma radiation (NGR) tool string as the third and final logging run. This tool string also reached close to the base of the hole. The logging equipment was rigged down by 2230 h on 23 December. We raised the pipe, and the bit cleared the seafloor at 2235 h, ending Hole U1609A.

6.1.2.2. Hole U1609B

The ship was offset 20 m south of Hole U1609A along the slope, and at 0305 h on 24 December we started Hole U1609B (37°22.6159′N, 9°35.9119′W) by drilling down without recovery. The plan was to drill down without coring to spend more time coring the Early Pliocene to Late Miocene target interval; however, in these clay-rich sediments, drilling was no faster than taking cores. At 0930 h, we retrieved the center bit and started taking advanced piston corer (APC) cores at 72.6 mbsf. Cores 2H–4H penetrated from 72.6 to 101.4 mbsf and recovered 28.5 m (95%), but after Core 4H had partial recovery and required 20,000 lb overpull to retrieve, we switched to coring with the HLAPC coring system at 101.1 mbsf. Cores 5F–32F penetrated from 101.4 to 234.1 mbsf and recovered 133.0 m (101%). We ran the Sediment Temperature 2 (SET2) tool after Core 32F at

234.1 mbsf to measure formation temperature deeper than had been possible with the APCT-3 tool in Hole U1609A.

At 1630 h on 25 December, we switched to the XCB coring system. At 1600 h on 26 December, after taking Core 48X at 389.3 mbsf, we ran the SET2 tool a second time. XCB coring proceeded until cores reached the age of 8.4 Ma, old enough to cover the main events in the history of the Mediterranean–Atlantic gateways. Cores 33X–61X penetrated from 234.1 to 508.7 mbsf and recovered 264.9 m (91%). At 1700 h on 27 December, we set back the top drive and started to pull up the drill pipe. The bit cleared the seafloor at 1905 h, and the BHA was on deck by 2345 h. The thrusters were raised, and we started the transit to Site U1610 at 2354 h, ending Site U1609.

Overall, we spent 10.2 days at Site U1609, about two days shorter than in the original operations plan because the age targets were shallower than anticipated. For this reason, we were also able to recover two cored records of the target interval rather than the single core record that originally had been planned in the expedition *Scientific Prospectus* (Flecker et al., 2023).

6.1.3. Principal results

6.1.3.1. Lithostratigraphy

Three main lithologies are described at Site U1609: calcareous mud, calcareous silty mud, and clayey calcareous ooze. Minor coarser grained deposits (e.g., calcareous silt, sandy silt, and calcareous sand) are also observed. On the basis of subtle lithologic changes, Holes U1609A and U1609B are divided into four lithostratigraphic units (Figure **F8**). Contacts between these units and the lithologies within them are mainly gradational, characterized by subtle changes in color and grain size (Figure **F9**). Only the coarser silts and sandier beds are characterized by sharp to erosive basal contacts. In Hole U1609A, Unit I ranges 0–344 mbsf and is characterized by alternating calcareous mud and calcareous silty mud. Unit II ranges 344–457 mbsf and consists of alternating calcareous mud and clayey calcareous ooze. Unit III ranges 457.7–531.5 mbsf and contains triplets of calcareous mud of two different shades (lighter/darker) and clayey calcareous ooze, repeating on a meter scale. Unit IV ranges 531.5–609.3 mbsf and contains two distinct types of calcareous muds and clayey calcareous ooze, with brown calcareous muds as the dominant lithology. In this unit, bed thickness is usually <1 m and the beds occur rhythmically. Coarser sandy and silty deposits at ~10 cm scale are observed primarily in Units II and III.

The sedimentary facies and facies associations identified at Site U1609 can be mainly attributed to hemipelagic and bottom current processes. This site recovered part of the Sines drift (middle-slope plastered drift) during deposition of Unit I (Pliocene and late Messinian). Beneath this, a few early Messinian and the Tortonian turbidite deposits are intercalated (Units II–IV). These coincide with regional tectonic events (Suarez et al., 1989; Riaza and Martines del Olmo, 1996; Sierro et al., 1996; Maldonado et al., 1999; Ledesma, 2000; Martinez del Olmo and Martín, 2016), but relative sea level falls may also have triggered gravity flows during this time interval.

The regular cyclicity visible in both the sedimentary facies and the physical properties data may be explained by local precessional climatic fluctuations as well as bottom current variability. Bottom currents during deposition of Unit I were weak but vigorous enough at intermediate depths to develop a plastered drift along the middle continental slope. On the longer timescale, the Tortonian to Pliocene shallowing identified from trace fossil assemblages may be related to long-term sea level regression (landward) and later progradation (basinward) of the margin (Riaza and Martinez del Olmo, 1996; Sierro et al., 1996; Maldonado et al., 1999; Ledesma, 2000; Martinez del Olmo and Martín, 2016).

6.1.3.2. Biostratigraphy

The sedimentary record recovered at Site U1609 is mostly continuous, although minor discontinuities cannot be totally excluded based on the low resolution of the biostratigraphic sampling on board. Preservation of microfossils is generally good with abundant calcareous nannofossils and planktonic foraminifers; benthic foraminifers are rare.

Based on the calcareous nannoplankton assemblage, the top of the sequence recovered in Hole U1609A is estimated to be >1.24 Ma, indicating that a significant proportion of the Pleistocene

sequence has been eroded at this location. A continuous series of calcareous nannoplankton and planktonic foraminiferal events were recorded in this site spanning from the Calabrian to the earliest Tortonian (Figure **F8**). Some of the calcareous nannofossil bioevents, specifically the highest occurrence (HO) events, may have been affected by reworking and redeposition. However, the ages derived from both the nannofossils and the foraminifers suggest that this is not a major issue. Sedimentation rates combined with the oldest bioevent, suggest an age close to the Tortonian/Serravallian boundary for the base of Hole U1609A.

During the Pliocene, bioevent-derived sedimentation rates range 37–90 m/My, which is in line with those estimated from the paleomagnetic records. Miocene successions have lower sedimentation rates (39–71 m/My).

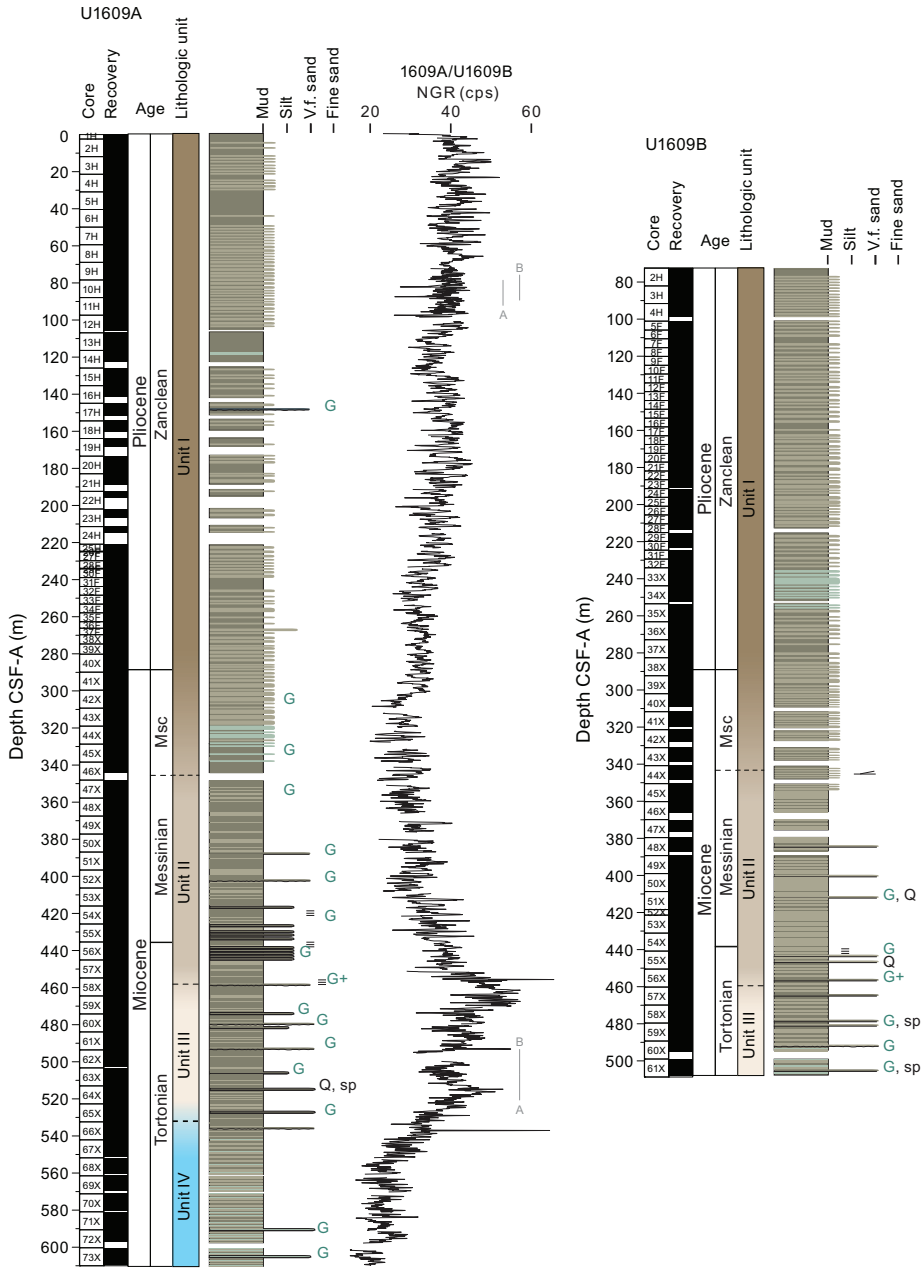

Figure F8. Site U1609 synthesis. NGR data shown is derived mainly from Hole U1609B, with upper and lower intervals from Hole U1609A. See Figure F5 for lithology and symbol legend. V.f. = very fine. Labeled vertical lines = transition between hole NGR datasets. cps = counts per second. MSC = Messinian Salinity Crisis.

6.1.3.3. Paleomagnetism

Paleomagnetic investigation of cores from Holes U1609A and U1609B focused on demagnetization of the natural remanent magnetization (NRM) of archive-half core sections and discrete samples of the working-half core sections. The Icefield MI-5 core orientation tool was used to orient the uppermost 24 cores in the APC section of Hole U1609A. The NRM intensity is very weak, ranging from about 1.4×10^{-5} to 4.0×10^{-1} A/m, with an average of 2.5×10^{-3} A/m.

In Hole U1609A, NRM removed by 10 mT alternating field (AF) demagnetization is likely related to an overprint caused by core drilling. Inclination values after 20 mT AF demagnetization roughly show polarity reversals, but with a lot of values scattered between expected normal and reversed values, and with very few of the reversed values reaching the expected geomagnetic axial dipole inclination at the site (56.8°). The weak magnetization and scattered directions may be due to dissolution of most of the original magnetic minerals and precipitation of authigenic iron sulfides. However, after running a 1 m smoothing window on the inclination values, normal and reversed polarity intervals can be tentatively recognized and, constrained by the biostratigraphic framework, correlated to the geomagnetic polarity timescale (GPTS) from about 1.2 to 8.7 Ma.

6.1.3.4. Geochemistry

Salinity, pH, alkalinity, concentrations of major anions and cations, ammonium, phosphate, and trace elements were measured on 66 interstitial water (IW) samples and a mudline (bottom water) sample from Hole U1609A. IW was extracted by squeezing a 5–7 cm whole-round sample, and the squeeze cake residues were then sampled for sedimentary geochemistry. One IW sample was collected in every APC and XCB core (Cores 401-U1609A-1H through 25H and 38X–73X) and one in every other HLAPC core (Cores 28F–36F). Alkalinity increased from 2.4 mM at the mudline to >15 mM between 44.8 and 256.1 mbsf, driven primarily by sulfate reduction, and pH varied

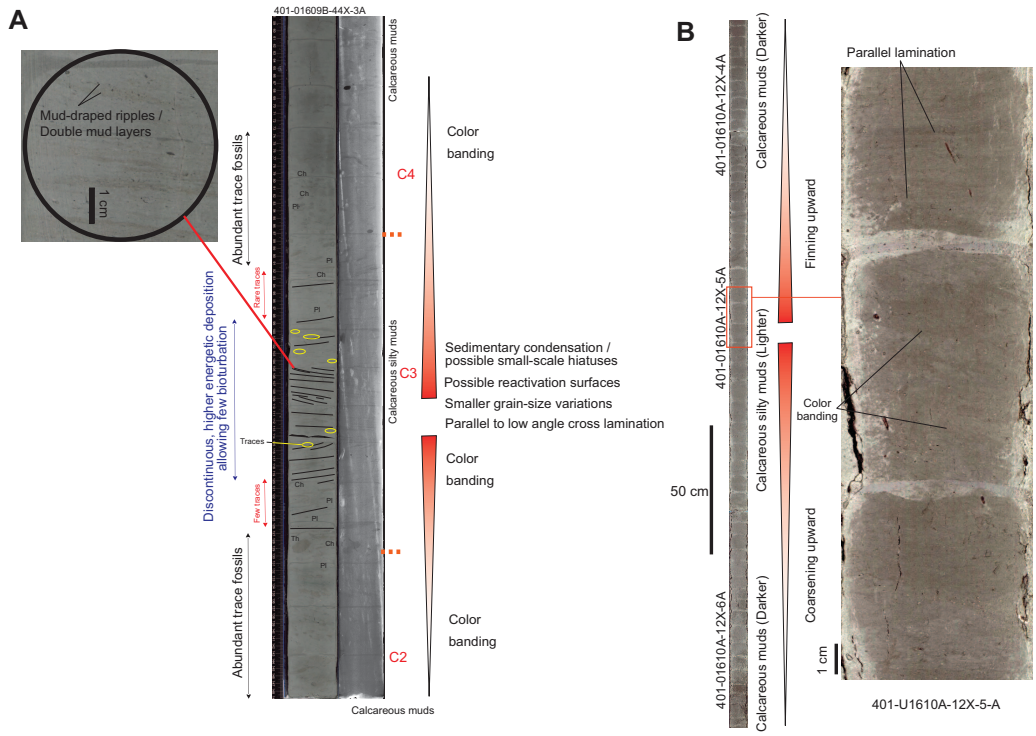

Figure F9. Examples of bigradational sequences of contourites. A. Fine-grained contourite with typical expression of subtle lithologic change observed, Site U1609. This section is a rare example showing trace fossil distribution, primary sedimentary structures, and subdivision intervals (C1–C5) according to contourite facies model for bigradational sequences (Stow and Faugères, 2008). Original core section images (LSIMG, left) and X-ray images (XSCAN, right) are shown. Ch = *Chondrites*, Pl = *Planolites*, Th = *Thalassinoides*. Yellow circles = occurrence of discrete traces on central division of bigradational sequence. B. Fine-grained contourite showing coarsening- and fining-upward sequence, as well as some subtle sedimentary structures, such as parallel lamination and small grain size variations, Site U1610.

between 7.4 and 7.8. Major ion concentrations, nutrient concentrations, and alkalinity reflect a variety of subsurface diagenetic processes including sulfate reduction, carbonate mineral precipitation and dissolution, organic matter remineralization, and water uptake into clay minerals. The sulfate–methane transition zone occurs around Core 6H at ~45 mbsf.

Weight percent total inorganic carbon (TIC), sedimentary carbon (TC), and total nitrogen (TN) were measured on the squeeze cake residues from the Hole U1609A IW sampling. Headspace gas was also measured from a discrete sample taken at the top of the core section below each of the 66 IW samples. Methane and ethane were commonly detected, whereas ethene and propane were detected in trace amounts in <10 samples. Methane concentrations ranged 0–42,000 parts per million by volume (ppmv), and ethane concentrations ranged 0–3.3 ppmv, with highest abundances between 100 and 300 mbsf. Calcium carbonate content ($CaCO_3$ wt%) was calculated from the TIC content, assuming that all inorganic carbon is present as calcium carbonate. Total organic carbon (TOC) was determined as the difference between TC and TIC. Calcium carbonate varied between 20 and 75 wt%, increasing toward the bottom of Hole U1609A, whereas TOC and TN remained low (<1% and <0.08%, respectively) throughout.

6.1.3.5. Physical properties and downhole measurements

Analysis of physical properties data allowed us to define four units at Site U1609 with boundaries at 344, 458, and 531 mbsf that correspond to the lithostratigraphic units defined in Site U1609 **Lithostratigraphy** (Figure **F8**). In general, there is a correlation between magnetic susceptibility (MS), NGR, and gamma ray attenuation (GRA) bulk density, all presenting a slight decrease from the top to the bottom of Unit I. The correlation is even better between NGR and MS. Unit II shows an increasing trend for both NGR and GRA toward the bottom of the unit (458 mbsf). Unit III contains several coarser sandy layers and is followed by greater variations on physical properties that present a global decreasing trend toward the bottom of the unit (531 mbsf). Unit IV represents a decrease in all the measured physical properties. This is reflected in the sedimentologic data by the transition to a less siliciclastic sequence of clayey calcareous oozes and calcareous muds. Generally, variations in physical properties are associated with color changes in visual core descriptions and in the red-green-blue (RGB) and reflectance data. This suggests that color changes are associated with changes in grain size and mineralogical composition.

Logging data from the downhole logging operations in Hole U1609A were processed at Lamont-Doherty Earth Observatory, Columbia University (USA). The sonic velocity logs and check shot interval velocity values reached 2.25 km/s at the base of the logging interval, 578 mbsf. These in situ velocity data enabled the Hole U1609A stratigraphy to be more accurately tied to the seismic stratigraphy. Based on downhole temperature measurements (see Site U1609 **Operations**), the seafloor temperature is 6.9°C.

6.2. Site U1610

6.2.1. Background and objectives

Site U1610 (proposed Site GUB-02A) is the closest of the expedition's Atlantic sites to the Gibraltar Strait and by extension to the Mediterranean–Atlantic gateway during the Late Miocene (Figures **F1**, **F10**). It is located at 556.3 mbsl in the Gulf of Cádiz (36°41.9812′N, 7°25.8844′W; Table **T1**). The aim of drilling at Site U1610 was to provide a proximal record for the proximal–distal transect along the path of the MO plume during the Late Miocene and Early Pliocene (Figure **F2**).

There is considerable uncertainty about the Late Miocene timing of opening and closure of the three different Mediterranean–Atlantic gateways (the Betic corridor through southern Spain, the Gibraltar Strait, and the Rifian corridor through Morocco; Figure **F3**; Krijgsman et al., 2018), and establishing this history is one of the main objectives of the expedition. Site U1610 was positioned in a location that would capture a record of the MO plume, whichever possible gateway it was coming from, throughout the 8–4 Ma interval of interest. The Miocene target interval also needed to be sufficiently shallowly buried (<1700 mbsf) and in deep enough water to be accessible to the R/V *JOIDES Resolution* drilling capability. However, the Pliocene–Pleistocene succession in the Gulf of Cádiz derives both from more recent MO and substantial clastic deposition from mainland Spain and Portugal, so in many places this Miocene–Pliocene interval of interest is too deeply bur-

ied. Additionally, all potential IODP sites need to be in locations where hydrocarbon accumulations are demonstrably absent, which was challenging for the Gulf of Cádiz. Within these constraints, there was little choice about the location of Site U1610, and even then the target depth of 1460 mbsf was very deep for IODP drilling (Figures **F4**, **F11**).

The two-way traveltime (TWT) to depth conversion used for the Pliocene–Pleistocene succession at Site U1610 was derived from adjacent Expedition 339 Sites U1386 and U1387 (Expedition 339 Scientists, 2013), which lie ~20 km to the northwest. This indicated that the Pliocene–Pleistocene succession at Site U1610 was ~750 m thick. Our drilling strategy was to drill ahead without coring the Pleistocene and the top of the Pliocene, casing the hole to 550 mbsf, to increase the chances of recovering the target interval.

Site U1610 is located in the Deep Algarve Basin of the Gulf of Cádiz (Ng et al., 2022). Based on regional correlations to Expedition 339 sites and industry wells, the Late Miocene seismic stratigraphic sequence at the site location was divided into four distinct stages, charting the progradation of a submarine fan (channel/levee/lobes system) influenced by bottom currents. The seismic packages transition upward from distal submarine lobes (a low-amplitude reflection unit below 2

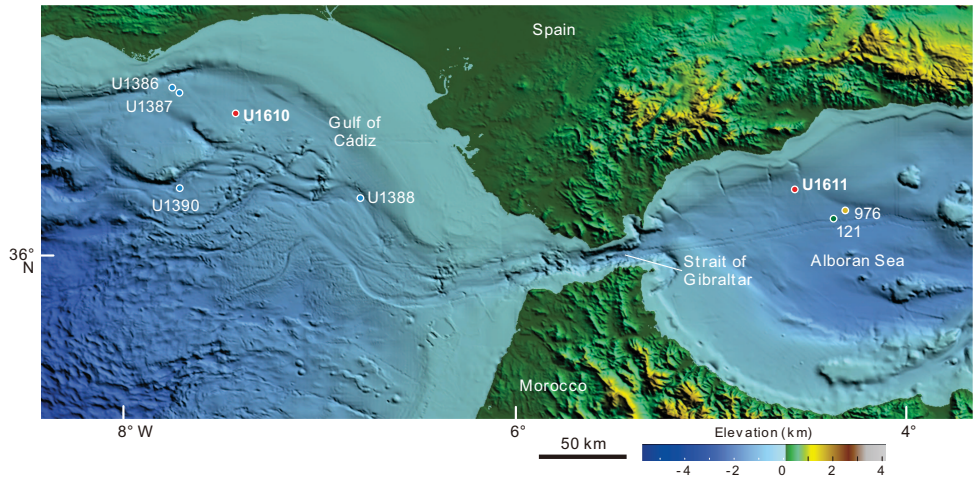

Figure F10. Bathymetric map of Gulf of Cádiz and Alborán Sea showing Sites U1610 and U1611 in relation to previously drilled sites in the area. See Figure F1 for legend.

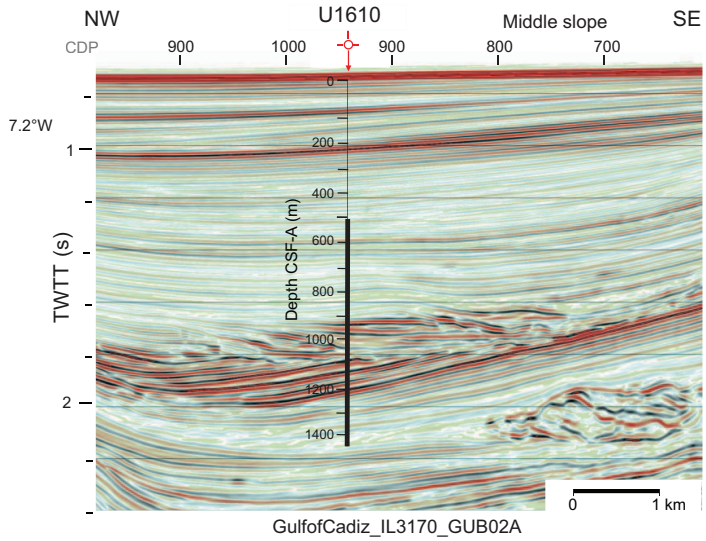

Figure F11. Seismic Profile IL3170 with location and approximate penetration, Hole U1610A. TWTT = two-way traveltime. CDP = common depth point.

s TWT) to more proximal, coarser grained (higher amplitude) submarine lobes, overlain by a transparent unit (Messinian Transparent Unit [MTU]) thought to reflect hemipelagic deposition, and then a Pliocene–Pleistocene MO-derived contouritic drift.

Expedition 339 drilled the top of the MTU at Site U1387 and recovered hemipelagic sediments (Expedition 339 Scientists, 2013). Beneath this we anticipated a migrating channel fill succession, below which is an unconformity and a succession of dipping bright reflectors (Ng et al., 2022). Beneath this is a package of parallel-bedded, lower amplitude reflectors that is thought to be of Tortonian age. At around 2.1 s TWT is a wedge-shaped unit that is interpreted to be the toe of a seismic unit with irregular internal reflections that thickens to the southeast and is thought to be an olistostrome, equivalent to the olistostrome seen in outcrop in southern Spain. The 8 Ma target age was anticipated to lie just below this chaotic interval.

6.2.2. Operations

Site U1610 consists of one hole, U1610A, and 751.2 m of sediment was collected from over a 933.5 m cored interval (81% recovery). The upper 501.9 m of the hole was cased to prevent caving and make it easier to flush cuttings out of the borehole (Figure **F4**), with the aim of increasing the chances of coring and logging successfully to the target depth of 1460 mbsf. The Pleistocene and Late Pliocene stratigraphy, which was not recovered in the top 501 m at Site U1610, is already known from nearby Expedition 339 Site U1387, located ~27 km northwest.

6.2.2.1. Hole U1610A

The ship completed the 122 nmi voyage to Site U1610 at a speed of 11.5 kt, arriving at 1010 h on 28 December 2023. The hydraulic release tool (HRT) and casing was prepared, consisting of the HRT assembly, HRT base, and 498 m of 10¾ inch casing. The rig team then made up the BHA, including the bit, underreamer bit, and mud motor. The BHA and drill pipe were lowered down through the casing until the bit and underreamer extended below the casing by 3 m. The HRT running tool was attached to the casing, and the funnel was welded on; then, the entire casing system was lowered down through the moonpool and the ship was positioned over the hole coordinates.

Hole U1610A started at 1200 h when the seafloor was tagged at 561.7 mbsl. The funnel's base landed on the seafloor with the casing shoe at 501.9 mbsf. After the casing was released, the bit was raised, clearing the seafloor at 2215 h on 30 December and clearing the rotary table at 0302 h on 31 December, completing casing operations.

We elected to start coring in Hole U1610A with the XCB coring system because it had recovered good quality cores at equivalent depths in Hole U1609A. The nonmagnetic drill collar was left out of the assembly to improve the robustness of the BHA, and a lockable float valve was included for potential downhole logging.

Hole U1610A was reentered at 0940 h on 31 December, and during this process the depth to the seafloor was found to be 556.3 mbsl, identical to the precision depth recorder (PDR) reading but shallower than the previous estimate of 561.7 mbsl. The bit was lowered to the base of the hole, 505.2 mbsf, and the first science activity at the site was to run the SET2 tool. At 1430 h, we started coring Core 2X and continued into the new year.

At 0340 h on 4 January 2024, we started a more rigorous headspace gas sampling protocol for the depth interval 754–960 mbsf at this site, following the recommendation by the IODP Environmental Protection and Safety Panel and Texas A&M University Safety Panel. Beginning with Core 27X at 747.7 mbsf, the headspace gas results from each core were analyzed before advancing the bit to collect the next core. This protocol was in effect because a detailed preexpedition analysis of 3D seismic data showed that there is a nonzero, but very low, risk of finding gas at the Site U1610 location. Headspace gas results from all XCB cores were found to be in the normal (safe) range of methane/ethane ratios and absolute methane values. Cores 2X–36X penetrated from 505.2 to 827.8 mbsf and recovered 322.6 m (93%).

At 0700 h on 4 January, there was a failure in the top drive brake system, causing the brake to engage and overheat. We stopped coring and pulled up Core 36X, which had advanced 3 m. The

bit was raised to 793.5 mbsf, the top drive was racked to allow repair, and the bit was raised to 495.2 mbsf just inside the casing. The first interval of top drive inspections and repair ran from 0945 to 1330 h. The cause for the failure appeared to be the exhaust valve on the brake. A portion of the diaphragm in the exhaust valve had broken off, lodged in the valve, and kept air pressure to the energizing bladder behind the brake bands. This kept the brake engaged. There was significant damage to the brake and bladder assembly from the resultant overheating, and the entire brake assembly needed to be replaced with the spare unit from the warehouse.

Meanwhile, we decided to change the coring system from XCB to rotary core barrel (RCB) for the remainder of the hole. We raised the bit to the ship, clearing the seafloor at 1423 h and the rig floor at 1630 h. Repairs to the top drive continued and were complete by 0215 h on 5 January. The rig floor team then assembled the RCB BHA with a new 9⅞ inch PDC bit, and Hole U1610A was reentered at 0548 h. Core 50R marked the end of the special headspace gas protocol, and results were within the normal range for the interval where the enhanced gas safety protocol was in effect. The procedure resulted in a delay of ~45 min per core across 23 cores.

Coring continued with very good recovery until Core 95R, which recovered just 15 cm of hard dolostone rock pieces. Core 96R was empty, so we ran the bit deplugger to remove any potential obstructing rock lodged in the bit. Although the drilling rate indicated that we were drilling recoverable sediments and had passed below the hard lithified sediments that had been partly recovered in Core 95R, no sediments were recovered; therefore, we stopped coring at 0515 h on 11 January with Core 100R. Cores 37R–100R penetrated from 827.8 to 1438.7 mbsf and recovered 610.9 m (74%).

We prepared for downhole logging by releasing the bit at the bottom of the hole, filling the hole with 354.3 bbl of heavy (10.5 lb/gal) barite mud, and raising the pipe. When the end of the pipe reached 779.4 mbsf, the drill pipe became stuck. After an overpull of 60,000 lb would not free the pipe, the circulating head was attached so that fluid could be pumped and the top drive was picked up so that the pipe could be rotated. After several attempts, the pipe came free at 1215 h on 11 January with 90,000 lb overpull and a pump pressure of 600 psi. The end of the pipe was set at 516.6 mbsf for logging, 14.7 m below the casing shoe.

At 1415 h, we started to assemble the quad combo tool string, including NGR, density, resistivity, and sonic velocity tools. The tool string was lowered down the hole, passing out of the casing into the open hole at 1640 h. At ~726 mbsf, the tool string encountered an obstruction and after eight attempts, could not pass any further down the hole. This is the same depth interval at which the drill pipe was stuck earlier in the day. However, useful log data were acquired from the ~208 m open hole logged interval.

The inclinometer in the cable head of the quad combo logging tool string showed that Hole U1610A was inclined between 13° and 15° from vertical in the logged interval. The hole had been suspected to deviate from vertical from observations of inclined beds in the cores.

The downhole logging equipment was rigged down by 0045 h on 12 January, and the pipe was raised, clearing the seafloor at 0130 h and the rig floor at 0300 h. The rig floor was secured for transit, we raised the thrusters at 0336 h, and we started the sea passage to Site U1385 at 0348 h, ending Site U1610.

6.2.3. Principal results

6.2.3.1. Lithostratigraphy

Seven primary lithologies were described in Hole U1610A: calcareous clay, calcareous mud, calcareous silty mud, calcareous (sandy) silt(stone), calcareous (silty) sand(stone), clayey calcareous ooze, and dolostone. Minor coarser grained lithologies were also observed. Based on these lithologic descriptions, Site U1610 is divided into five lithostratigraphic units (Figure **F12**). Contacts between lithologies are predominantly gradual, with subtle color and grain size changes; however, some contacts are sharp to erosive.

Unit I ranges 505.2–699.4 mbsf and is composed of alternating calcareous mud and calcareous silty mud, with minor coarser, sandy intervals. Unit II ranges 699.2–831.7 mbsf and consists of

calcareous mud and calcareous clay. Unit III ranges 837.5–934.8 mbsf and consists of interbedded calcareous mud and clayey calcareous ooze to calcareous silty mud, with minor coarser, sandy intervals. Unit IV ranges 934.8–1388.8 mbsf and is divided into three subunits (Figure **F12**). Subunit IVa consists of alternating calcareous silty mud, calcareous sandy silt, calcareous mud, and coarser grained sand and silty sand intervals (Figure **F13**), with minor clayey calcareous ooze to calcareous clay (934.8–1112.7 mbsf). Subunit IVb consists of calcareous mud, calcareous silty mud, calcareous sandy silt, and calcareous sand (very fine, fine, and medium), with some clayey calcareous ooze to calcareous clay, and minor lithified siltstone, sandstone (fine to medium), and conglomerate (1112.7–1220.3 mbsf). Subunit IVc consists of alternating calcareous mud, calcareous silty mud, calcareous sandy silty, and coarser grained sand and silty sand intervals, with minor

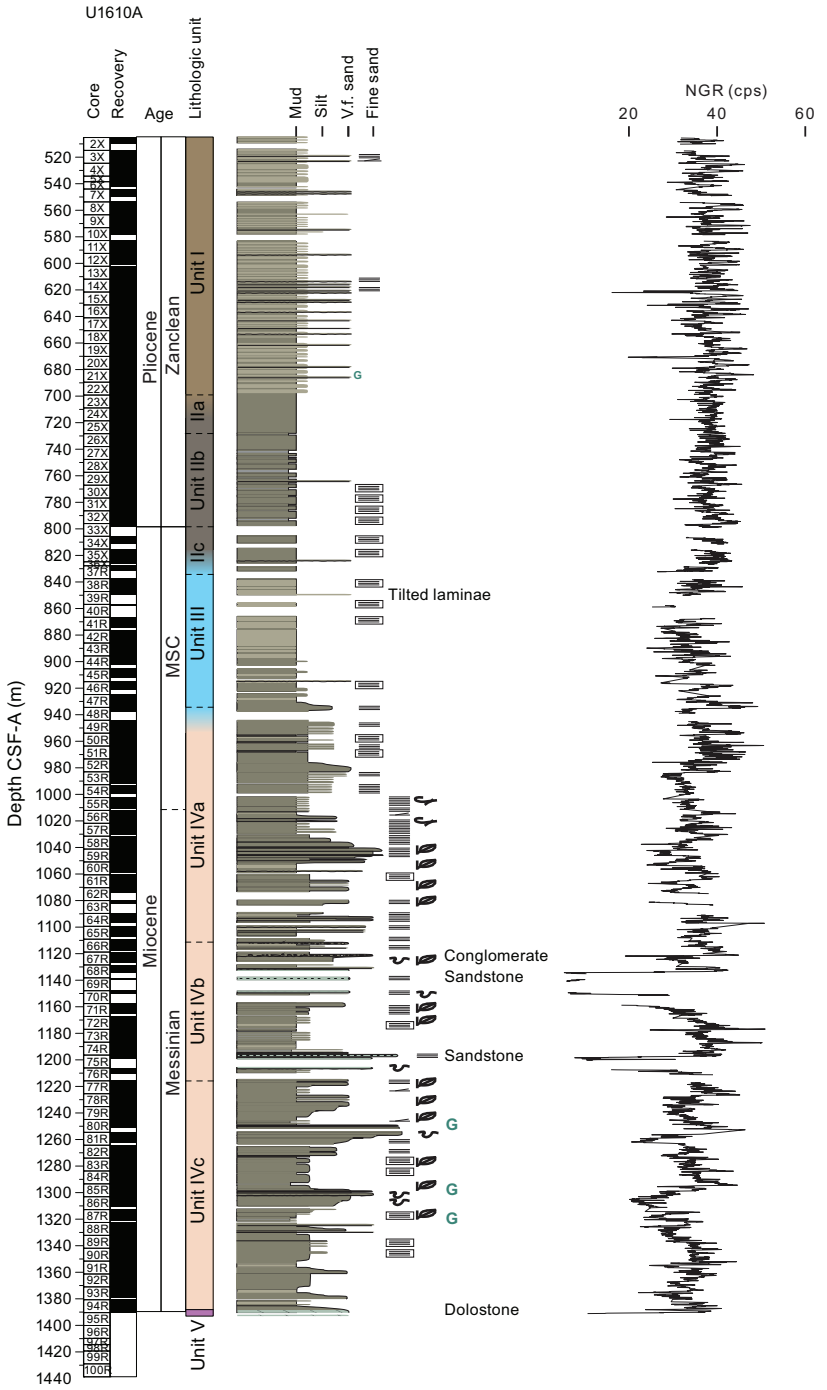

Figure F12. Site U1610 synthesis. See Figure F5 for lithology and symbol legend. V.f. = very fine. cps = counts per second.

clayey calcareous ooze to calcareous clay and calcareous clay (1220.3–1388.8 mbsf). Unit V ranges 1388.6–1388.8 mbsf and consists entirely of dolostone. Cores 401-U1610A-96R through 100R (1388.6–1438.7 mbsf) had 0% recovered sediments and are not included in the unit definition.

Hole U1610A is located in the southern part of the Deep Algarve Sedimentary Basin, within the Gulf of Cádiz. During deposition of Unit IV in the early to late Messinian (<6.9–7.1 Ma to around 5.78 Ma), there was an interplay of gravity processes, (contouritic) bottom currents, and pelagic/hemipelagic deposition that determined the evolution of a mixed (turbidite-contourite) depositional system, where turbiditic deposits were reworked by bottom currents. The bottom current processes are associated with an intermediate water mass flowing along the middle slope of the margin. This mixed depositional system underwent a long-term evolution from Subunit IVc to IVa, with a wide spectrum of features and deposits formed under synchronous and asynchronous interactions of gravity and contouritic processes. Turbidite deposits have been described in both the Guadalquivir Basin and the Deep Algarve Basin during the Messinian and are associated with continental margin progradation, tectonic instability, and relative sea level variations.

During deposition of Units III and II in the latest Messinian–Early Pliocene (5.78 to >4.52 Ma), an important change in the depositional style with respect to Unit IV took place, with the development of hemipelagic deposits, and with very occasional, very fine grained turbidites not affected by bottom currents. This result agrees with the previous interpretation for the upper part of the Messinian in the Gulf of Cádiz that proposed hemipelagic sedimentation during the late Messinian and no significant MOW influx during the earliest Pliocene (e.g., Llave et al., 2011; Expedition 339 Scientists, 2013; Hernández-Molina et al., 2016, van der Schee et al., 2016), but at Site U1610 it appears that this change happened earlier than previously documented based on seismic data from the same area (Ng et al., 2022). However, this hypothesis for the lack of bottom water current reworking and contourite deposition is contrary to other authors who consider a MOW influence since the Miocene/Pliocene boundary (e.g., Nelson et al., 1999).

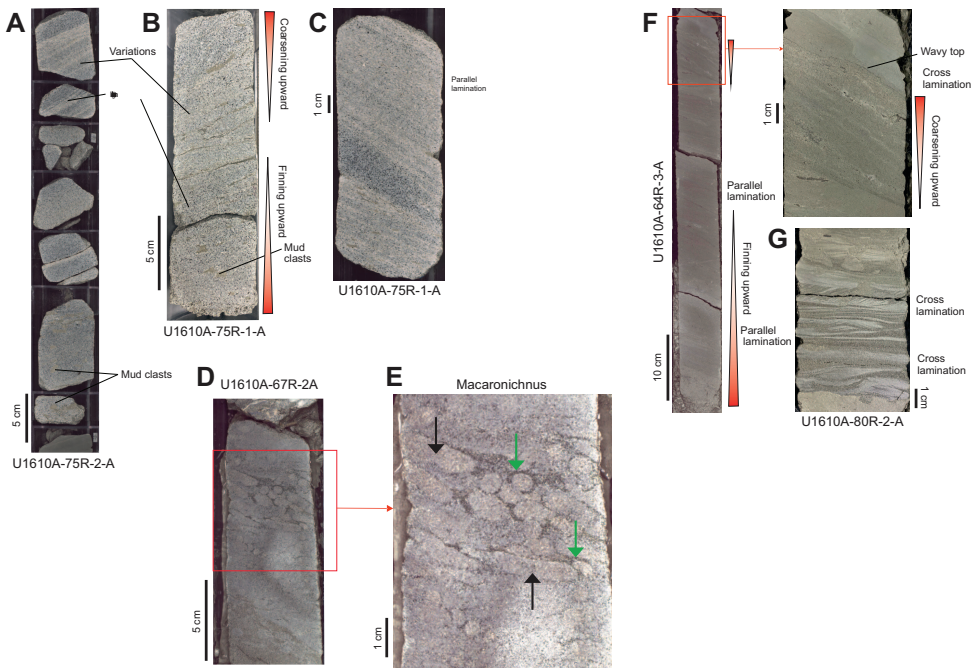

Figure F13. Examples of sandy deposits, Site U1610. Core photographs showing (A) lithified sandstones with sharp bases and mud clasts; (B) sandstone with mud clasts, fining-upward interval, and coarsening-upward interval; (C) sandstones with parallel and cross laminations and marked color banding. Dark laminations in C are caused by high proportion of glauconite. D, E. *Macaronichnus* trace fossil (red box in D) and typical mineralogical segregation shown between cylinder tube core (lighter minerals; black arrows) and surrounding rim (darker and heavy minerals; green arrows). F, G. Core photographs showing examples of turbidite deposits with evidence of reworking by bottom currents (F: reworking at top of turbidite; G: stacked sets of cross laminations in turbidite).

During deposition of Unit I later in the Pliocene (4.6–3.57 Ma), bottom water current (contouritic) and pelagic/hemipelagic sediments dominated the succession. Similar Pliocene sequences observed elsewhere in the Gulf of Cádiz are considered to result mainly from MOW bottom currents (e.g., Nelson et al., 1999; Rodrigues et al., 2020).

6.2.3.2. Biostratigraphy

Based on the calcareous nannoplankton and foraminifer assemblage, an age between 3.61 and 3.57 Ma is estimated for the top of the recovered sequence (510.3 mbsf). Below this, a continuous series of calcareous nannoplankton and planktonic foraminifer events were recorded. The presence of *Globorotalia miotumida* and *Reticulofenestra rotaria* at the bottom of the hole constrains the age to between 6.38 and ~7.2 Ma (Figure **F12**). The Miocene/Pliocene boundary is placed at ~800 mbsf (the Subunit IIb–IIc transition) based on the HO of *Orthorhabdus rugosus*. However, this bioevent is used with caution because of the scarcity of the specimen in the core catcher (CC) sample analyzed. The subsequent highest common occurrence of *Neogloboquadrina incompta* (sinistral) recorded at ~939 m indicates a Messinian/Miocene age.

During the Pliocene, sedimentation rates determined from biostratigraphy are on the order of ~160 m/Ma and were higher during the Miocene, reaching up to 240 m/Ma. The preservation of microfossils is generally good with abundant calcareous nannofossils and planktonic foraminifers, but the concentration and preservation of planktonic foraminifers decreases with depth in the Late Miocene samples. The benthic/planktonic ratio is indicative of intermediate water depths during the Miocene and Pliocene.

6.2.3.3. Paleomagnetism

Paleomagnetism measurements of NRM were performed on all the archive-half core sections from Hole U1610A on the superconducting rock magnetometer (SRM). AF demagnetization was performed at 5, 10, 15, and 20 mT, with measurement of the remaining NRM being taken at 2 cm resolution after each step. A drilling overprint was mostly removed by 10 mT demagnetization.

In addition, NRM was measured on 134 cube samples on the AGICO JR-6A spinner magnetometer. The samples were then AF demagnetized. The NRM of discrete samples is significantly stronger than at Site U1609, with an average of 10×10^{-4} A/m. In general, steps of 5, 10, 15, 20, 30, 40, 50, and 60 mT, and in some cases up to 100 mT, were added to fully demagnetize the characteristic magnetic component.

Results from 501 to 540 mbsf clearly show normal inclinations in both SRM and JR-6A records. Between 540 and 1010 mbsf, reversed directions are dominant and many SRM inclination values approach the expected antipodal geocentric axial dipole (GAD) inclination at the site (57°). Some short (<20 m) normal polarity depth intervals are present, but they are not clear, and only a few show successive inclinations with the expected GAD value. Normal polarities dominate from 1010 to 1390 mbsf. Correlations to the GPTS are tentative, but the lack of reversals in the lower 1010–1390 mbsf are consistent with the high sedimentation rates observed by biostratigraphy.

We measured the anisotropy of magnetic susceptibility (AMS) and bulk MS of all the discrete samples using the MFK2 KappaBridge instrument. Results show that all the κ_{min} axes have a tilt of ~15°–17° deviating from the vertical. Because κ_{min} is generally perpendicular to the sedimentary bedding plane, this value indicates that drilling was not vertical but must have occurred with an angle of 15°–17° and is consistent with the observation of inclined beds in the visual core descriptions and the logging data. In principle, we think it should be possible to reconstruct the strike of the dipping borehole, provided the paleomagnetic signal is robust enough, which will allow AMS results to be interpreted in terms of current flow direction.

6.2.3.4. Geochemistry

In Hole U1610A, the safety protocol for drilling between 740 and 960 mbsf required the methane concentration in headspace gases and methane/ethane ratios to be reported to the drilling team prior to advancing to drill the next core. In all headspace samples in this interval, the methane concentrations remained <12,000 ppmv (well below the 100,000 ppmv safety threshold), ethane concentrations were <12 ppmv, and the minimum ratio of these two gases (C_1/C_2) was 406. These low concentrations of methane and ethane and the dominance of methane (low C_1/C_2 ratio) pre-

sented no concerns for drilling safely as they indicate a microbial rather than petrogenic source. Methane and ethane were commonly detected, whereas ethene, propane, isobutane, and isopropane were detected in trace amounts.

Void space was also sampled directly when gas pockets appeared in the core. In void spaces, the absolute concentrations are not meaningful because they are essentially methane pockets (measured methane is close to 100%), but we found similar trace constituent composition to that measured with the standard interstitial headspace gas protocol. In void spaces, the C_1/C_2 ratio minimum was 1930, indicative of microbial rather than petrogenic sourcing.

Two bottom water samples and 54 IW samples were collected from Hole U1610A for salinity, pH, and alkalinity measurements. One IW sample was collected from every core, except where recovery was limited (<3 m core) or poor quality (abundant fractures), in which case the IW sample was not taken. Approximately 10 mL of IW was extracted initially, which decreased to ~6 mL of water during RCB coring. Sampling continued until water yields decreased below ~1 mL at Core 401-U1610A-61R. An additional IW sample was obtained from Core 72R with insufficient yield for most measurements. Alkalinity ranges 1.4–4.8 mM, pH varies between 7.5 and 8.0, and salinity is 32–35 in IW samples. Major and trace elements in the IW samples were measured by ion chromatography (IC) and inductively coupled plasma–atomic emission spectroscopy (ICP-AES). The bottom water samples each have an elevated salinity of 36, indicating we were sampling MOW.

Overall, $CaCO_3$ ranges 25.4–79.8 wt%, with a mean of 35.3 wt% and a standard deviation of 7.3 wt%. Standard reproducibility was 1.12 wt% (n = 13). $CaCO_3$ is generally relatively invariant at Site U1610, with most samples falling within 28–40 wt% downcore. This included some selected for color variations, implying that color variations are driven by changes in components other than carbonates, likely the siliciclastic fraction.

6.2.3.5. Physical properties and downhole measurements

In the upper part of the cored interval, 510–685 mbsf, ~2 m scale cycles are evident in the MS and NGR data (Figure **F12**) and they have higher amplitude in the underlying interval, 685–975 mbsf. The 975–1130 mbsf interval is characterized by a downhole increase in MS values by two orders of magnitude and a decrease in NGR values. From 1130 to 1295 mbsf, MS and NGR return to lower values and lower amplitude variations, with longer wavelength changes and less-evident cyclicity. Below 1295 mbsf, shorter wavelength variability is again seen in the MS and NGR data sets.

Downhole logging in Hole U1610A unfortunately did not reach deeper than 726 mbsf. Caliper logs show that the hole was alternately washed out to greater than 15 inches and closed in to narrower than the bit diameter. However, the 220 m long open hole logged interval shows cyclic variation that can be used to cover stratigraphic gaps in Lithostratigraphic Unit I. The density log is strongly affected by borehole conditions, but in narrower borehole intervals, the readings are probably valid and reach a maximum of 2.0 g/cm^3. Perhaps the most important logging result is quantifying that the hole is inclined from vertical by 13°–15° in the logged interval. Hole inclination will have to be considered in calculating bed thicknesses and depths to seismic reflectors because coring depth along the borehole overestimates true vertical depth.

The SET2 probe results gave a temperature of 24.8°C at 505.2 mbsf. Using this result and the seafloor temperature of 12°C (measured during the Conductivity-Temperature-Depth tool deployment), the geothermal gradient at the site is 25.3°C/km.

6.3. Site U1385

6.3.1. Background and objectives

Site U1385 (37°34.2849′N, 10°7.5616′W) (Figures **F6**, **F14**) was first drilled during Expedition 339 to provide a marine reference section of Pleistocene millennial climate variability. Five holes were cored (Holes U1385A–U1385E) to a maximum penetration of 151.5 mbsf using the APC system (Expedition 339 Scientists, 2013). The record extends to 1.45 Ma (Marine Isotope Stage 47) with an average sedimentation rate of 11 cm/ky (Hodell et al., 2015).

Site U1385 (37°34.0128′N, 10°7.6580′W) was reoccupied during Expedition 397 (2022) to deepen the sequence to 400 mbsf, just above the Miocene/Pliocene boundary (~5.3 Ma; Hodell et al., 2023). Five more holes were cored (Holes U1385F–U1385J) ~500 m from the Expedition 339 location, using the APC system to about 110 mbsf and the XCB system beneath that depth (Table T1). During Expedition 397, Site U1385 was part of a four site depth transect designed to capture and reconstruct water mass changes during the Pliocene and Pleistocene (Hodell et al., 2023). The two deeper water sites, U1587 and U1586, also recovered Late Miocene successions. Results from Site U1385 demonstrate that the Iberian margin yields long, continuous records of millennial Pliocene–Pleistocene climate variability permitting detailed land–sea comparisons (Hodell et al., 2023).

Expedition 401 used the same site designation for this site, coring Holes U1385K and U1385L, and we distinguish between the intervals recovered by the different expeditions by prefixing the expedition number to the site (i.e., 339-U1385, 397-U1385, and 401-U1385). Site 401-U1385 is located ~20 m from Site 397-U1385 at a water depth of 2590 mbsl, placing it in the core of Lower Northeast Atlantic Deep Water (NEADW). Seismic data indicate the stratigraphy is continuous between the locations.

6.3.2. Objectives

Extending this remarkable sediment archive back into the Late Miocene was one of the primary goals of reoccupying Site U1385 during Expedition 401. Equivalent aged sediments recovered at the deeper Site U1587 (Hodell et al., 2023) can be traced upslope on the seismic profile to Site U1385. These Late Miocene sediments at Site U1587 display well-developed precessional cyclicity. However, the poor carbonate preservation at this greater water depth (3480 m water depth) means that high-resolution carbonate-based proxy records cannot be generated (Hodell et al., 2023). The

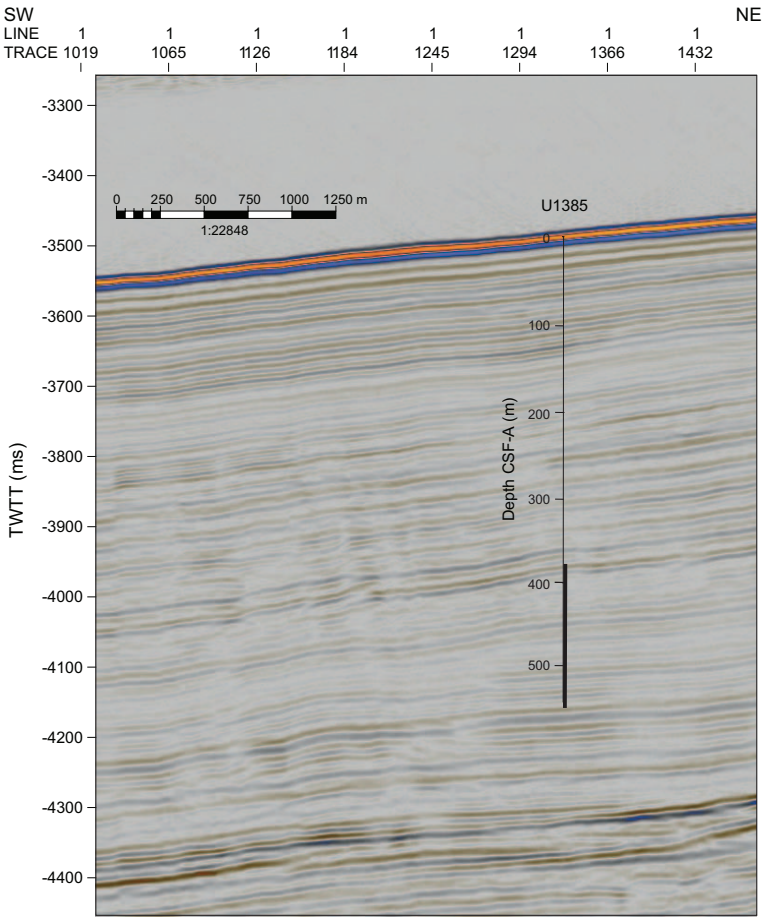

Figure F14. Seismic Profile JC89-9 with location and approximate penetration, Hole U1385K. TWTT = two-way traveltime.

shallower water depth of Site U1385 (2590 m water depth) means it was likely to have better carbonate preservation, making these essential proxy records viable.

Site U1385 is Expedition 401's deepest site. It is located on an elevated ridge, minimizing the chances of disturbance by downslope transport (Figure **F6**). In combination with Site U1609 and the two deeper water Expedition 397 sites, U1587 and U1586, the Late Miocene records from Site U1385 complete a Miocene depth transect equivalent to the Pliocene–Pleistocene transect generated by Expedition 397. The initial objective in the expedition's scientific prospectus was to recover the deeper part of the section at Site 397-U1385 up to a maximum depth of 873 mbsf. However, the late Tortonian to Messinian age interval of interest was likely not to require that full depth.

The specific objectives of coring Site 401-U1385 are as follows:

- To document the nature, amplitude, and pacing of climate cycles in the Atlantic before, during, and after the MSC and
- To examine water mass variability during this time period characterized by extreme regional changes in oceanographic context.

6.3.3. Operations

Holes U1385K and U1385L were cored after drilling down to start coring a little shallower than the 400 mbsf depth reached at this site during Expedition 397 (Figures **F4**, **F14**).

6.3.3.1. Hole U1385K

The 154 nmi voyage from Site U1610 to Site U1385 took 12.8 h at a speed of 12.0 kt. We lowered the thrusters at 1622 h on 12 January 2024, and switched to DP mode at 1652 h. Site U1385 was cored to 151 mbsf during Expedition 339 in 2011 and to 400 mbsf during Expedition 397 in 2022. The APC/XCB BHA was assembled with a PDC bit and was lowered toward the seafloor, and a pipe-cleaning "pig" was pumped down to clean the inside of the drill pipe. The ship was positioned 20 m east of Hole 397-U1385J.

Hole U1385K was started at 0035 h on 13 January and was drilled ahead, reaching 385.0 mbsf at 1615 h. The center bit was retrieved, and we started coring. Cores 2X–6X returned nearly empty, so we ran the bit deplugger to ensure that the bottom of the BHA was free from loose sediment, which may have entered during the preceding drill down. Recovery improved in subsequent cores, and we continued coring until Core 21X at 1035 h on 15 January, having reached the age target of 8 Ma. Cores 2X–21X penetrated from 385.0 to 552.5 mbsf and recovered 127.9 m (76%). We pulled up the pipe, clearing the seafloor at 1328 h on 15 January and ending Hole U1385K.

6.3.3.2. Hole U1385L

The ship was offset 20 m north, and we started Hole U1385L at 1455 h on 15 January 2024, drilling ahead without coring to 376 mbsf. Coring began at 0330 h on 16 January, and Cores 2X–8X penetrated from 376.0 to 443.9 mbsf, recovering 58.4 m (86%). We stopped coring at 1645 h because of the high wind and wave conditions forecast for the evening and next day. The bit cleared the seafloor at 1835 h and was pulled up to a depth of 332 mbsl while the ship began waiting on weather (WOW). (After coring Hole U1385K, we had a choice between going directly to the next site or staying to core Hole U1385L; we prioritized collecting core from Hole U1385L, knowing that it would mean WOW the following day.)

The ship began WOW at 2315 h on 16 January. At midmorning on 17 January, the average wind speed reached 35 kt, gusting to 65 kt, and then it eased throughout the day. After WOW for 28.25 h, we were able to resume operations at 0330 h on 18 January. The BHA was raised, disassembled, and stowed. The thrusters were raised at 0720 h, and at 0736 h we started the transit to Site U1611 (proposed Site WAB-03A), ending operations at Site U1385.

6.3.4. Principal results

6.3.4.1. Lithostratigraphy

Four lithostratigraphic units are defined at Site U1385, and they are characterized by alternating light-colored (light greenish gray) and dark-colored (greenish gray and gray) beds composed of

clayey calcareous ooze and calcareous clay with lighter and darker shades and gradational and sharp boundaries (Figures **F15**, **F16**). Minor lithologies include clay- and pyrite-rich intervals and horizons exhibiting multiple hues, including shades of orange-brown and blue-green. Trace fossils include *Chondrites, Planolites, Thalassinoides*, and *Zoophycos*, and rare *Asterosoma, Palaeophycos*, and *Schaubcylindrichnus*. Pyrite nodules and shell fragments are disseminated throughout. Sediments are initially interpreted to be deepwater hemipelagic deposits.

Unit I extends from 385 to 430 mbsf in Cores 401-U1385K-2X and 7X–9X and from 376 to 430.5 mbsf in Sections 401-U1385L-2X-1 to 7X-4, and comprises clayey calcareous ooze (light greenish gray) and calcareous clay (greenish gray). Unit II extends from 436 to 458.5 mbsf in Sections 401-U1385K-10X-1 to 12X-2 and from 430.5 to 442.6 mbsf in Sections 401-U1385L-7X-5 to 8X-CC. Unit III extends from 458.5 to 519.6 mbsf in Sections 401-U1385K-12X-3 to 18X-4. Units II and III contain clayey calcareous ooze (light greenish gray) and calcareous clay (variable greenish gray and gray). Unit IV extends from 519.6 to 552.65 mbsf in Sections 401-U1385K-18X-5 to 21X-CC and is dominated by calcareous clay (variable greenish gray and gray) with minor clayey calcareous ooze (light greenish gray).

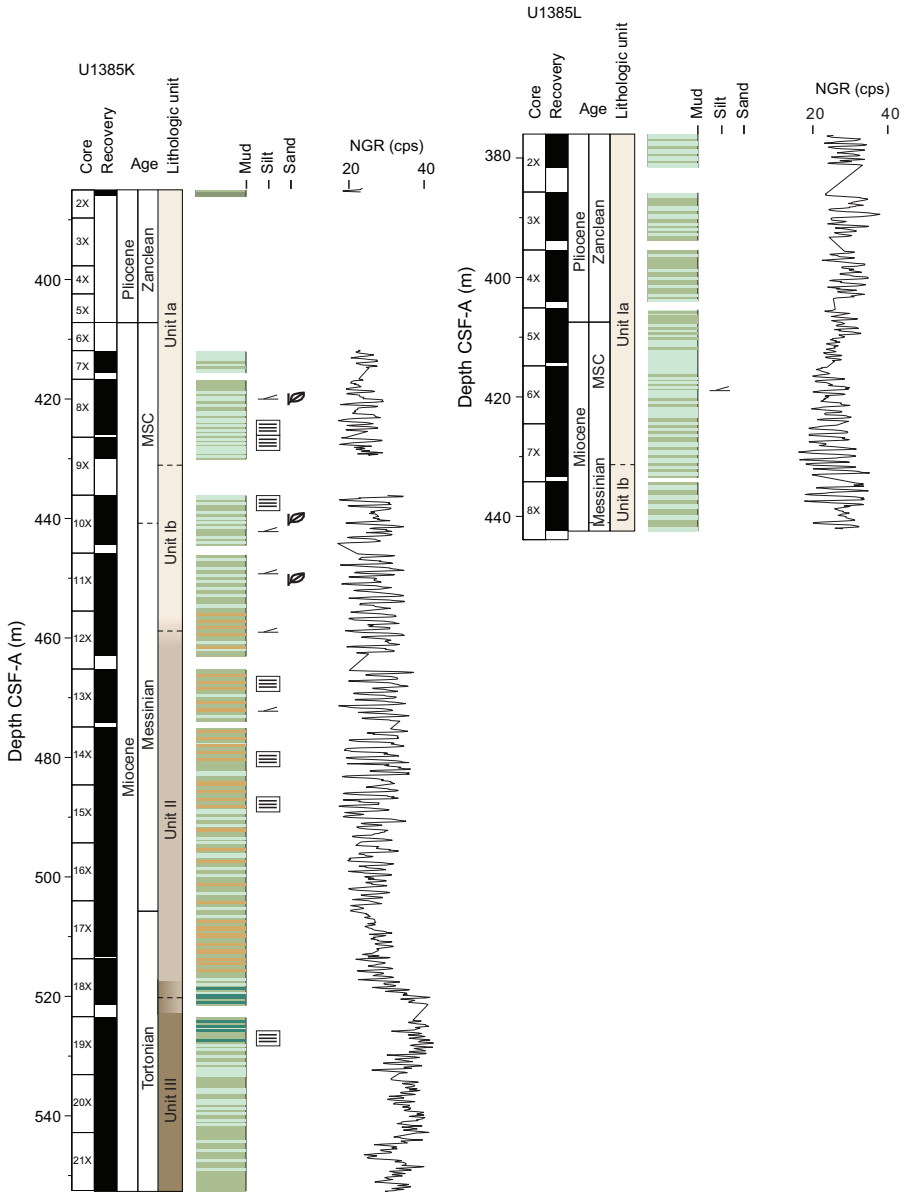

Figure F15. Site U1385 synthesis. See Figure F5 for lithology and symbol legend. cps = counts per second. MSC = Messinian Salinity Crisis.

Site U1385 is located on a plateau (Promontório dos Príncipes de Avis) below the water depth of the present-day Mediterranean outflow plume. This area is protected from sedimentary input from slope deposition or submarine canyons. The Miocene sediments recovered from Site U1385 are dominated by pelagic clayey calcareous ooze and calcareous clay deposits, consistent with this setting. Precessional-scale variability in the Miocene and late Tortonian sediments recovered may have resulted from fluctuations in carbonate and/or siliciclastic input, generating pelagic deposits with color-carbonate cycles. This may be driven either by local climatic variability or result from nepheloid layers higher in the water column (e.g., associated with MOW; Abrantes et al., 2000; Ambar et al., 2002; Magill et al., 2018) containing significant quantities of suspended sediment.

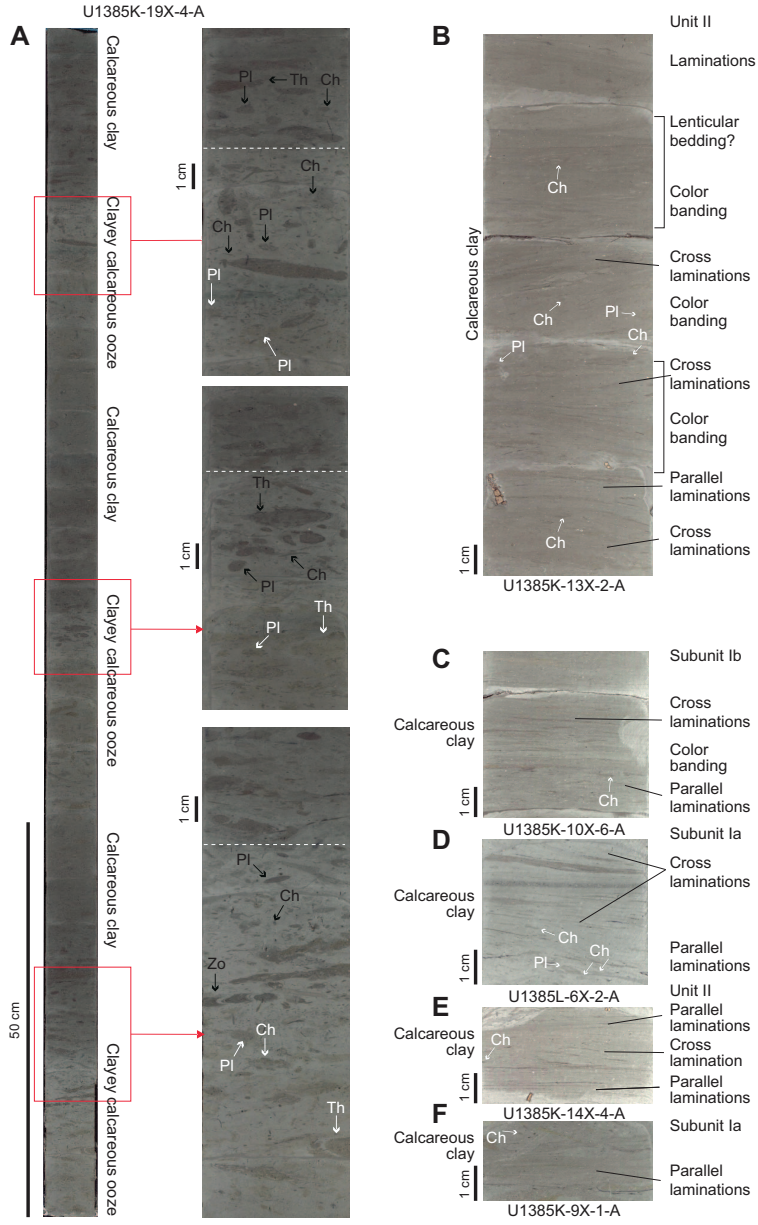

Figure F16. Examples of sedimentary structures, Site U1385. A. Alternating lithologies showing regular sedimentary cycles between calcareous clays (darker facies) and clayey calcareous ooze (lighter facies), with detail of trace fossils in the contact (dashed white line) between facies. Note differentiation between dark (black arrows) and light (white arrows) trace fossil assemblages and penetration of dark traces into lighter sediments. B–F. Color banding, parallel laminations, cross laminations, and lenticular bedding associated with calcareous clays. Ch = *Chondrites*, Pl = *Planolites*, Th = *Thalassinoides*, Zo = *Zoophycos*.

Future research will evaluate the influence of regional water masses on the dominant pelagic sedimentation at Site U1385. The interplay between NEADW and Antarctic Bottom Water (van Aken, 2000; Hernández-Molina et al., 2011; Glazkova et al., 2022) would have been particularly important during the latest Miocene when Atlantic intermediate and deepwater circulation evolved into a pattern similar to the one observed today (Sykes et al., 1998; Billups, 2002; Nisancioglu et al., 2003; Uenzelmann-Neben et al., 2017; Hernández-Molina et al., 2017).

6.3.4.2. Biostratigraphy

Calcareous microfossils are typically abundant with moderate and good preservation, and planktonic foraminifers are well preserved with evidence of fragmentation in only a few samples. The age of the succession is constrained by eight nannofossil events and four foraminifer events. The HO of *O. rugosus* (5.23 Ma) and the lowest occurrence of *Ceratolithus acutus* (5.36 Ma) are recorded between Sections 401-U1385L-4X-CC and 5X-CC at ~409 mbsf, constraining the Messinian/Pliocene boundary to Core 5X (Figure **F15**). The oldest bioevent identified was the base of the paracme of *Reticulofenestra pseudoumbilicus* (8.8 Ma) between Sections 401-U1385K-19X-CC and 20X-CC at ~517 mbsf. CC samples were also analyzed for benthic foraminifer content; the assemblage seems well preserved. Nannofossil smear slides from Site U1610 were reexamined for minerals and reworked coccoliths.

6.3.4.3. Paleomagnetism

Pass-through paleomagnetic measurements were performed using the SRM to investigate the NRM on a total of 132 archive-half sections (91 sections from Hole U1385K and 41 sections from Hole U1385L). AF demagnetization was performed on the SRM by applying stepwise peak fields of 5, 10, 15, and 20 mT, with measurement of the remaining magnetization taken at 2 cm resolution. In addition, we collected and measured 117 discrete samples of the working-half sections, using 3–7 discrete samples from each core. First, the AMS and bulk MS were measured on all samples using the MFK2 KappaBridge instrument. Next, the NRM of 61 cube samples, 47 samples from Hole U1385K and 14 samples from Hole U1385L, was measured on the AGICO JR-6A spinner magnetometer. Stepwise AF demagnetization was performed at successive peak fields of 0, 5, 10, 15, 20, 30, 40, 50, 60, and 70 mT, up to a maximum of 80 mT for samples from Hole U1385K and a maximum of 40 mT for samples from Hole U1385L where the magnetic signal was weaker. When magnetization became erratic, demagnetization was stopped.

Constrained by stratigraphic correlation to Hole 397-U1385J, the topmost core of Hole U1385L is <5 Ma. We then correlated the reversal pattern in inclination values of SRM measurements after 20 mT and JR-6A measurements after 20 mT to the most recent GPTS. Based on this magnetostratigraphy, the base of Hole U1385K is slightly older than 8.2 Ma, and the average sediment accumulation rate is ~5 cm/ky for the Messinian part of the record.

The AMS results of Holes U1385K and U1385L show an overall vertical direction of the κ_{min} axis, in agreement with a sedimentary fabric and a vertically drilled hole.

6.3.4.4. Geochemistry

For Hole U1385K, one headspace gas sample and IW sample were taken per core. Gas content in Hole U1385K was within the safety range; only methane and ethane were detected, but no higher hydrocarbons. IW samples from Hole U1385K were measured for salinity, pH, and alkalinity. Salinity remained invariant at 32 throughout the cored interval. IW major and trace elements were measured by IC and ICP-AES. Sediment samples were obtained from the IW squeeze cake residues in Hole U1385K and one sample per core from Hole U1385L to understand geochemical variations. Sediment samples were dried, ground, and weighed to measure C, N, and $CaCO_3$. Calcium carbonate abundance varies from 39 to 69 wt% and correlates well with NGR, showing that mixing of carbonate and siliciclastic fractions is controlling the observable cyclicity at this location. Carbonate geochemistry shows lithology-dependent variations and signs of carbonate diagenesis.

6.3.4.5. Physical properties and downhole measurements

The full suite of physical properties measurements was made on cores and samples from Holes U1385K and U1385L. Moisture and density measurements show a compaction trend with depth: bulk density increases from ~1.9 g/cm^3 at 378 mbsf to 2.0 g/cm^3 at 548 mbsf, and porosity

decreases from 50% to 43% over the same depth interval. NGR and MS records contain cyclic alternations on a meter to submeter scale throughout the cored interval (Figure **F15**), with relatively higher amplitude cycles from ~420 to 505 mbsf. No downhole measurements were made at Site U1385.

6.4. Site U1611

6.4.1. Background and objectives

Site U1611 (proposed Site WAB-03A) is located inside the Mediterranean just to the east of the Strait of Gibraltar, in the Alborán Sea (Figure **F10**). It marks the eastern end of Expedition 401's transect of sites that track MOW from its source, through the Atlantic–Mediterranean gateway into the Gulf of Cádiz (Site U1610), and around to the west of the Iberian margin (Sites U1609 and U1385) (Figure **F2**). Today, the Alborán Basin is a relatively narrow (150 km wide, north to south), shallow (maximum depth of 1800 m), elongate (350 km long, east to west) area that links the deeper parts of the Mediterranean Sea to the Atlantic. Atlantic water flows into the Mediterranean through the Gibraltar Strait at the surface as a coherent layer of warm and relatively fresh marine water, while deeper cooler and more saline water generated in the Mediterranean flows through the Alborán Sea and out into the Atlantic at depth (Figures **F17**, **F18**). The stratified water mass structure in the Alborán Sea reflects this exchange as well as the densities of the different water masses generated within the Mediterranean, principally the Levantine Intermediate Water and Western Mediterranean Deep Water (WMDW; Ercilla et al., 2016). Site U1611 is located on the north side of the basin on the Spanish continental slope at a water depth of 810 m (Figure **F10**). Today, this area is bathed in WMDW with a temperature of ~12.9°C and a salinity of ~38.45 (Figure **F19**). It is directly impacted by westward flowing currents that produce contourite deposition along the Spanish margin (Figure **F17**) as well as receiving the input of gravity deposits from upslope (Ercilla et al., 2016).

Exchange through a single gateway at Gibraltar is a relatively recent (Pliocene–Pleistocene) phenomenon (Hernández-Molina et al., 2014a; van der Schee et al., 2016; García-Gallardo et al., 2017a; Flecker et al., 2015). As a result of Africa-Eurasia convergence, westward docking of the Alborán plate, and simultaneous slab retreat (Jolivet and Faccenna, 2000; Faccenna et al., 2004; van Hinsbergen et al., 2014), the Atlantic–Mediterranean connection evolved from a single, wide open seaway in the Tortonian (Figure **F3**) linking a Mediterranean that was more of an embayment of the Atlantic than a distinct marginal marine system (Flecker et al., 2015) to two narrow corridors

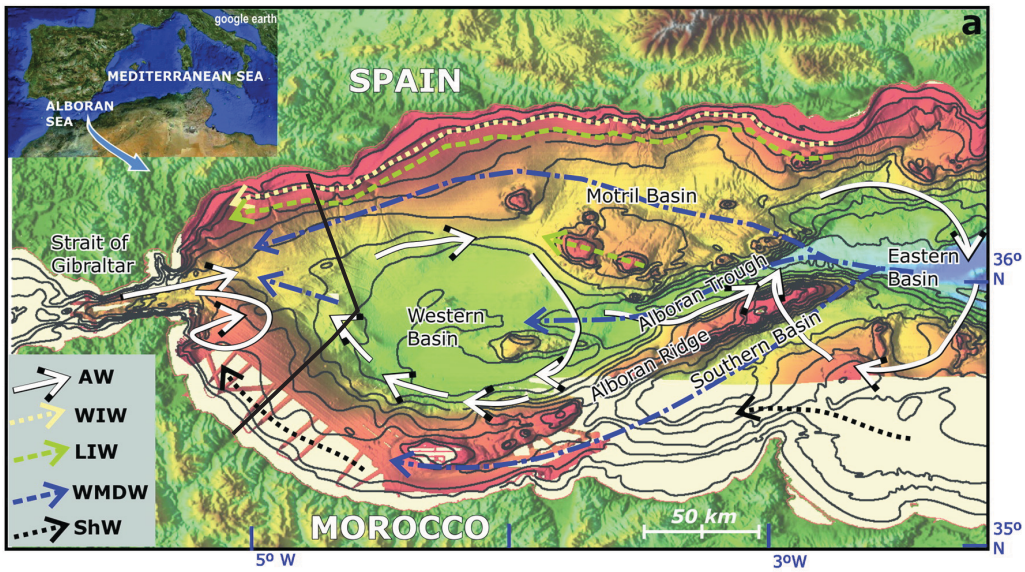

Figure F17. Bathymetric map of Alborán Sea showing present-day water masses and currents. AW = Atlantic Water, WIW = Western Intermediate Water, LIW = Levantine Intermediate Water, WMDW = Western Mediterranean Deep Water, ShW = shelf water (mix of AW and WMDW). (Figure from Ercilla et al., 2016.)

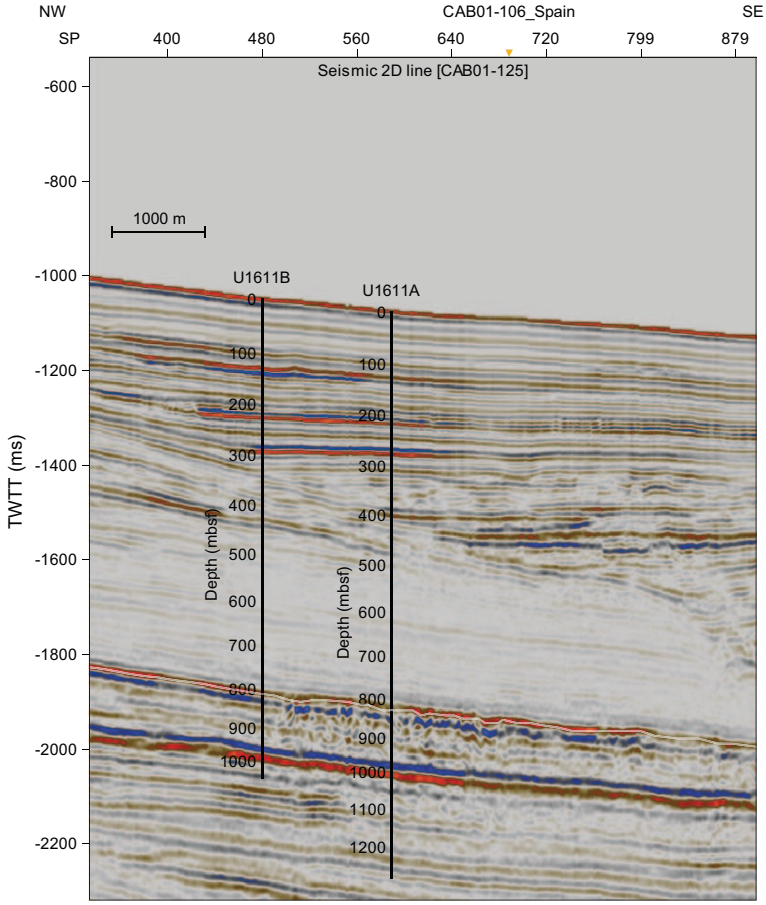

Figure F18. Seismic Profile CAB01-125 with location and approximate penetration, Holes U1611A and U1611B. TWTT = two-way traveltime. SP = shotpoint.

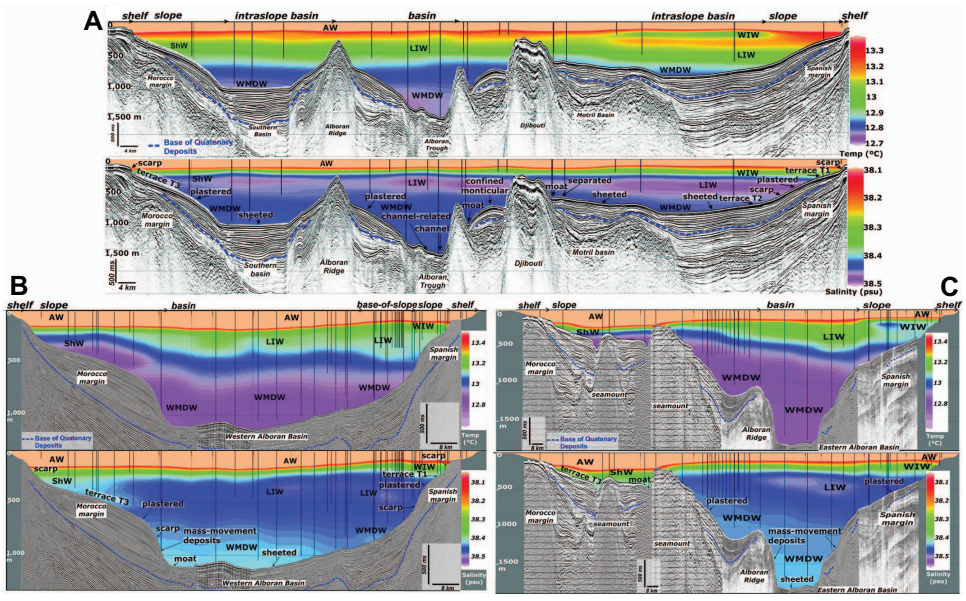

Figure F19. A–C. Water mass structure in Alborán Sea (Ercilla et al., 2016). AW = Atlantic Water, WIW = Western Intermediate Water, LIW = Levantine Intermediate Water, WMDW = Western Mediterranean Deep Water, ShW = shelf water (mix of AW and WMDW).

in the early Messinian: one in northern Morocco and the other in southern Spain (Figure **F20**; Martín et al., 2014).

Ongoing restriction of the marine corridors permitted Mediterranean salinity to rise, and a distinct, dense water mass formed. Ultimately, the narrowing and closure of these connections resulted in extreme salinity fluctuations in the Mediterranean, leading to the precipitation of more than 1 million km^3 of salt, equivalent to ~6% of the total dissolved oceanic NaCl (Blanc, 2006; Ryan, Hsü, et al., 1973) in the latest Miocene. This event is known as the MSC (Hsü et al., 1973). Progressive tectonic convergence coupled with isostatic rebound related to lithospheric mantle dynamics (Duggen et al., 2003) not only severed these earlier marine connections but also uplifted and exposed them on land (Capella et al., 2017). In the Early Pliocene, two-way exchange was established through a single conduit, the Gibraltar Strait. This reconnection event is known as the Zanclean deluge. Many authors suggest that catastrophic failure of the Atlantic-Mediterranean barrier at Gibraltar led to the swift refilling of the Mediterranean Sea associated with major erosion in the Alborán Basin (Estrada et al., 2011; Lofi, 2018; Garcia-Castellanos et al., 2020).

6.4.2. Objectives

Site U1611 targets one of the few thick late Messinian sedimentary successions in the Alborán Basin. The record recovered from this location will provide key constraints on the chemistry and physical properties of MO during the Late Miocene. The major objective for Site U1611 was to recover an 8–4 Ma succession that records the evolution of the Alborán Sea before, during, and after the MSC. This information will then be used to test the following hypotheses:

- The Alborán Basin was an intermediate marine system influenced by the Atlantic and separated from the Mediterranean by the Alborán volcanic arc during the MSC,
- Mediterranean–Atlantic exchange occurred through the Gibraltar Strait before the start of the MSC, and

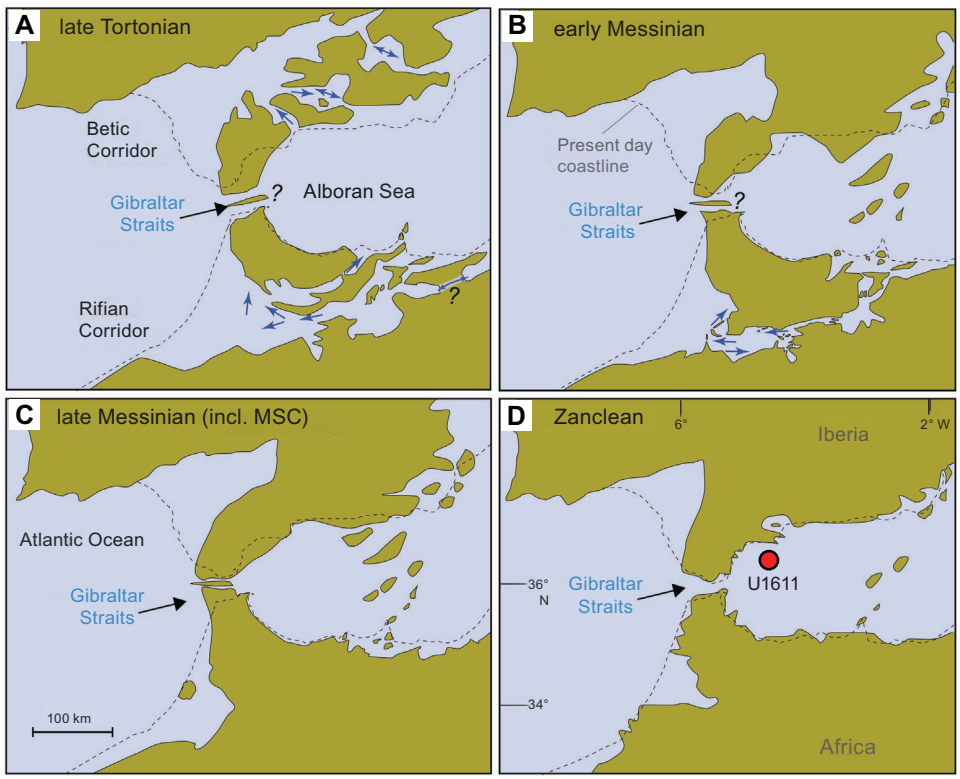

Figure F20. Schematic maps showing closure and opening of Mediterranean–Atlantic gateways from late Tortonian to Zanclean (updated after Martín et al., 2014).

- Extreme environmental fluctuations in the Mediterranean are mirrored by both environmental conditions in the Alborán Sea and visible perturbations down the MO plume in the Atlantic.

6.4.3. Operations

On the morning of 19 January 2024, *JOIDES Resolution* sailed through the Strait of Gibraltar, one of the Mediterranean–Atlantic gateways in the title of Expedition 401. The 333 nmi transit from Site U1385 to Site U1611 in the Alborán Basin of the Mediterranean Sea took 29.8 h at an average speed of 11.2 kt. We arrived on site at 1315 h on 19 January, lowered the thrusters, and started to unstow the BHA. At 1745 h, high winds made it unsafe for the derrickman to work at the monkey board in the derrick, so we waited until 2015 h for the wind to drop before resuming operations (a 2.5 h delay).

The rig floor team assembled ~650 m of 10¾ inch casing, hung it below the ship, and made up the casing stinger BHA, including the bit, underreamer bit, and mud motor. The BHA and drill pipe were lowered down through the casing until the bit and underreamer extended below the casing by 3 m. The HRT running tool was attached to the casing, and the funnel was welded on. The funnel was lowered through the moonpool at 1540 h, and the whole casing system was lowered to 792.1 mbsl before installing the top drive. Hole U1611A was started at 1730 h, and we continued to drill the casing into Hole U1611A until the reentry cone base landed on the seafloor at 810.1 mbsl with the bit at 654.6 mbsf and the casing shoe at 652.6 mbsf. The subsea camera was deployed to observe the release of the casing, and at 0405 h on 22 January the casing assembly was released from the pipe and BHA. The bit was raised back to the ship, clearing the rig floor at 1103 h and completing the casing portion of operations in Hole U1611A. The RCB BHA was then assembled with a PDC bit and lowered to 584.9 mbsl, and the subsea camera was deployed again to guide reentry into the hole.

Hole U1611A was reentered at 1832 h, and the top of the cone was confirmed to be at 807.3 mbsl and the seafloor was confirmed to be at 810.1 mbsl, very close to the PDR estimate of seafloor depth at 810.2 mbsl. The bit was lowered down the casing to 613 mbsf, where it took weight, probably because it met sediments that had come up into the casing. The top drive was installed, and the bit was washed down to 656.3 mbsf, followed by a 30 bbl mud sweep to clear any remaining loose sediment from the casing. At 0000 h on 23 January, the core line winch electrical controller failed, specifically the Veeder-Root counter in the controller. It was replaced, and the winch was back online by 0545 h. The first run on the core line was the SET2 tool. The Icefield MI-5 tool, usually run to orient APC cores, was run by piggybacking on the SET2 tool deployment to estimate any deviation of the casing from vertical. It showed a small angle at the top of casing, deviating to 10° at the base of casing. This result was subsequently confirmed by the downhole logging inclinometer data. Coring started at 0815 h with Core 2R, but it recovered only 3 cm of sediment, so we ran the bit deplugger. Recovery improved for subsequent cores. Cores 2R–24R penetrated from 656.3 to 879.4 mbsf and recovered 223.1 m (74%). Cores 25R and 26R returned nearly empty, probably because coarse-grained sediments in the formation entered the base of the pipe. The bit deplugger was deployed again. We made five 30 bbl mud sweeps per day to flush cuttings and loose sediment out of the borehole, and coring continued with moderate to good recovery. At 0815 h on 26 January, following Core 44R, we switched to half-core advances, which improved core recovery (on 26 January full-core advances yielded 69% recovery and half-core advances yielded 87%).

We switched from half-length to full-length RCB core advances with Core 77R. Core 79R returned empty, so we ran the bit deplugger again and switched back to half-length advances for Cores 80R–83R, each of which recovered less than 10 cm. Because hole conditions were difficult, at 1945 h we started a wiper trip to clear bridges in the hole prior to further coring and downhole logging. Overpulls of 20,000–30,000 lb were observed at 1104.9, 949.4, 881.7, and 872.0 mbsf before the bit could be raised to the casing shoe. On washing down, 12 tight spots were encountered and 6 m of fill was found at the base of the hole. From 0730 to 1030 h on 29 January, we washed out the fill and swept the hole with 30 bbl sepiolite mud in preparation for coring. Cores 84R–86R penetrated to 1281.9 mbsf, the final depth of the hole, and recovered 13.2 m (68%). Cores 2R–86R penetrated from 656.3 to 1281.9 mbsf and recovered 625.6 m of core (69%).

At 1545 h, we started to prepare the hole for downhole logging. The bit was released at the base of the hole, the hole was displaced with barite-weighted mud, and the end of pipe was raised to 672.7 mbsf. The rig floor team assembled the triple combo logging tool string, without the source, and started lowering it down the pipe at 2145 h. The tool string reached an impassable obstruction at 909.6 mbsf and made a repeat and main pass, which together cover the open hole interval from 672.7 to 909.6 mbsf. Borehole diameter varied between narrower than 6 inches to wider than the maximum extent of the caliper measurement, 17 inches, and the logged interval of the borehole was inclined from the vertical by between 10° and 15°. The triple combo tool string was back on deck at 0410 h on 30 January, and a sonic-inclinometry tool string was assembled for the second logging run. This tool string was lowered into the borehole but could not pass below 743.6 mbsf. It recorded data for the short interval up to the bit and was back on deck by 0910 h, and the logging equipment was disassembled by 1100 h. The BHA was raised back to the ship, clearing the rotary table at 1400 h and ending Hole U1611A. A new mechanical bit release and PDC RCB bit were added to the BHA and were lowered back down close to the seafloor.

The ship was offset 1316 m northwest and Hole U1611B was started at 1725 h on 30 January at a water depth of 784 mbsl. The relatively large offset was made to core part of the seismic profile where reflectors had greater horizontal continuity than in Hole U1611A. We drilled ahead from 211.6 to 744.9 mbsf and pumped 30 bbl sepiolite mud sweeps after adding every two stands of pipe to keep the hole clear. When the center bit was retrieved, 1.7 m of sediment was found behind it in the core barrel, which was curated as a wash core, 2W. Coring started at 1830 h on 31 January. Cores 3R and 4R had 91% recovery, but the following two cores, 5R and 6R, returned nearly empty, so we ran the bit deplugger and then switched to half-core RCB advances. Coring proceeded with half-core advances for the next 3 days, until operations needed to stop to start preparing for the transit to Napoli, Italy. Core 66R arrived on the catwalk at 2330 h on 4 January and was the last core of the site and the expedition. Cores 3R–66R penetrated from 744.9 to 1069.9 mbsf and recovered 77.3 m (89%).

6.4.4. Principal results

6.4.4.1. Lithostratigraphy

Four main lithologies were described in Site U1611: (calcareous) mud, (calcareous) silty mud, sandy silt, and silty sand. Minor lithologies include sandy mud, conglomerate, breccia, and cemented carbonate (e.g., dolostone and limestone). On the basis of lithologic changes, Holes U1611A and U1611B are divided into three lithostratigraphic units (Figure **F21**). Contacts between these units and the lithologies within them are mainly gradational in Unit I (Early Pliocene), characterized by subtle changes in color and grain size, and become more commonly sharp in Units II and III (Messinian), associated with distinct color changes and frequent laminations. The coarser silts and sandier beds typically have sharp to erosive basal contacts.

Unit I ranges 656.3–820.4 mbsf in Hole U1611A and 746.4–814.2 mbsf in Hole U1611B. In Hole U1611A, Unit I comprises three subunits, consisting of alternating calcareous mud and calcareous silty mud. The 733.9–772.3 mbsf interval contains more occurrences of coarser lithologies including conglomerates and calcareous sandy silt (Figure **F22**). In Unit I in Hole U1611B, calcareous muds also alternate with calcareous silty muds, with the frequency of coarser lithologies increasing with depth.

Unit II ranges 820.4–996.5 mbsf in Hole U1611A and 814.2–996.9 mbsf in Hole U1611B. In Hole U1611A, it is characterized by the presence of laminated beds alternating with nonlaminated and sometimes coarse graded beds. Unit II consists of two subunits. Subunit IIa (820.4–964.3 mbsf) is composed of lithologies with variable carbonate content, including mud, calcareous mud, calcareous silty mud, sandy silt, and silty sand, with minor aragonite, cemented carbonate, breccia, and conglomerate (Figure **F22**). Subunit IIb (971.5–996.5 mbsf) is composed of similar lithologies as Subunit IIa, but with a lower carbonate content, with beds of calcareous muds and calcareous silty muds alternating with muds, sandy silts, and sands. In Hole U1611B, Unit II mostly consists of the same lithologies as those in Hole U1611A, typically with a lower calcareous content with increasing depth. However, in Hole U1611B more silty muds were described in the deeper part of Unit II, and in general there are more coarser beds.

Unit III ranges 1000.6–1275.9 mbsf in Hole U1611A and 997.1–1069.69 mbsf in Hole U1611B. In Hole U1611A, Unit III consists of two subunits. Subunit IIIa (1000.6–1144.9 mbsf) consists of frequent alternations of silty mud and calcareous silty mud in the shallower parts, with numerous intervals of sandy silt and silty sand. The proportion of calcareous silty mud is lower in the deeper part of Subunit IIIa. There is also minor conglomerate typically associated with contorted, slump-like sediment deformation, and cemented carbonate. Subunit IIIb (1146.1–1275.9 mbsf) consists of similar lithologies to Subunit IIIa, except that Subunit IIIb lacks the rapid interbedding of calcareous silty mud and silty mud and contains more frequent occurrences of coarser grained intervals (e.g., sandy silt and silty sand). In Hole U1611B, Unit III is similar to the upper part of Subunit IIIa in Hole U1611A, except that there is a notable thick conglomerate (8.5 m) that was not recovered in Hole U1611A. Unit III is characterized by the presence of laminated beds alternating with nonlaminated and normally graded beds, but the laminations appear subtler than in Unit II (Figure **F22**).

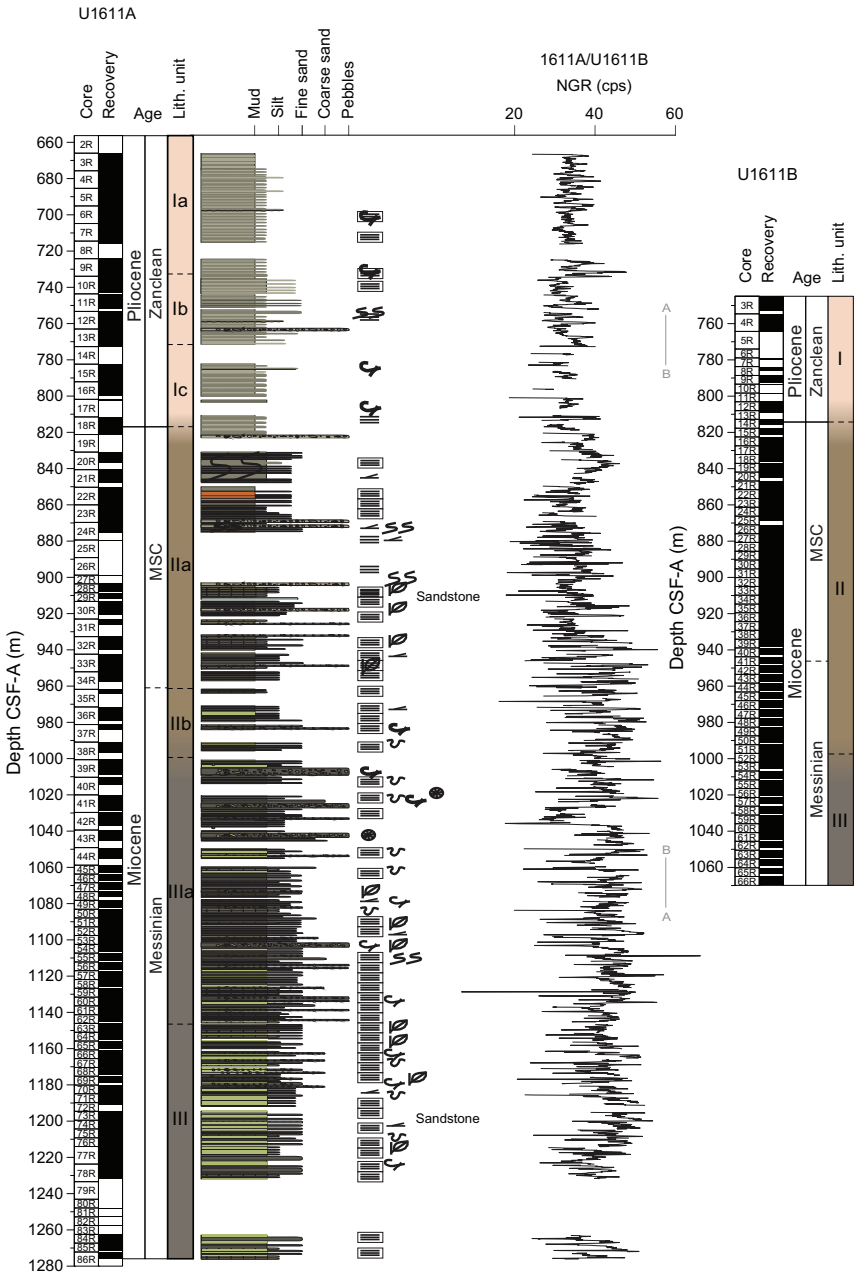

Figure F21. Site U1611 synthesis. See Figure F5 for lithology and symbol legend. Labeled vertical lines = transition between hole NGR datasets. cps = counts per second.

During the Messinian, particularly in Unit III, there is evidence of an interplay of gravitational and pelagic/hemipelagic processes. This produced a complex depositional system, where the slumps, debrites, and turbiditic deposits are volumetrically the most important deposits in the succession, resulting in a high sedimentation rate. Unit II is characterized by the development of laminations throughout, along with the presence of thin aragonite layers, dark muds, etc. During this time, the basin likely became more restricted, and the relatively high sedimentation rate and low bottom water oxygenation led to a benthic-poor habitat, limiting macrobenthos trace-fossil maker community sufficiently to prevent bioturbation, preserving the finely laminated sediments (Schimmelmann et al., 2016). These processes and the precipitation of aragonite are possible in stratified "marine lakes" with restricted seawater access and water column stratification (Schimmelmann et al., 2016). Turbidite and debrite deposits are also present in Unit II, and according to the literature on this sector of the Alborán Sea, these deposits are considered to be chaotic mass transport deposits that accumulated during the Messinian Salinity Crisis (Martínez del Olmo and Comas, 2008; Estrada et al., 2011; Martínez del Olmo, 2012; Bulian et al., 2021). Based on the results from this expedition, Unit II has thinner and finer gravitational deposits that occur less commonly than Unit III.

The Pliocene sediments of Unit I display clear evidence of bottom water currents (contouritic) and pelagic/hemipelagic sedimentation. Similar Pliocene sequences observed elsewhere in the

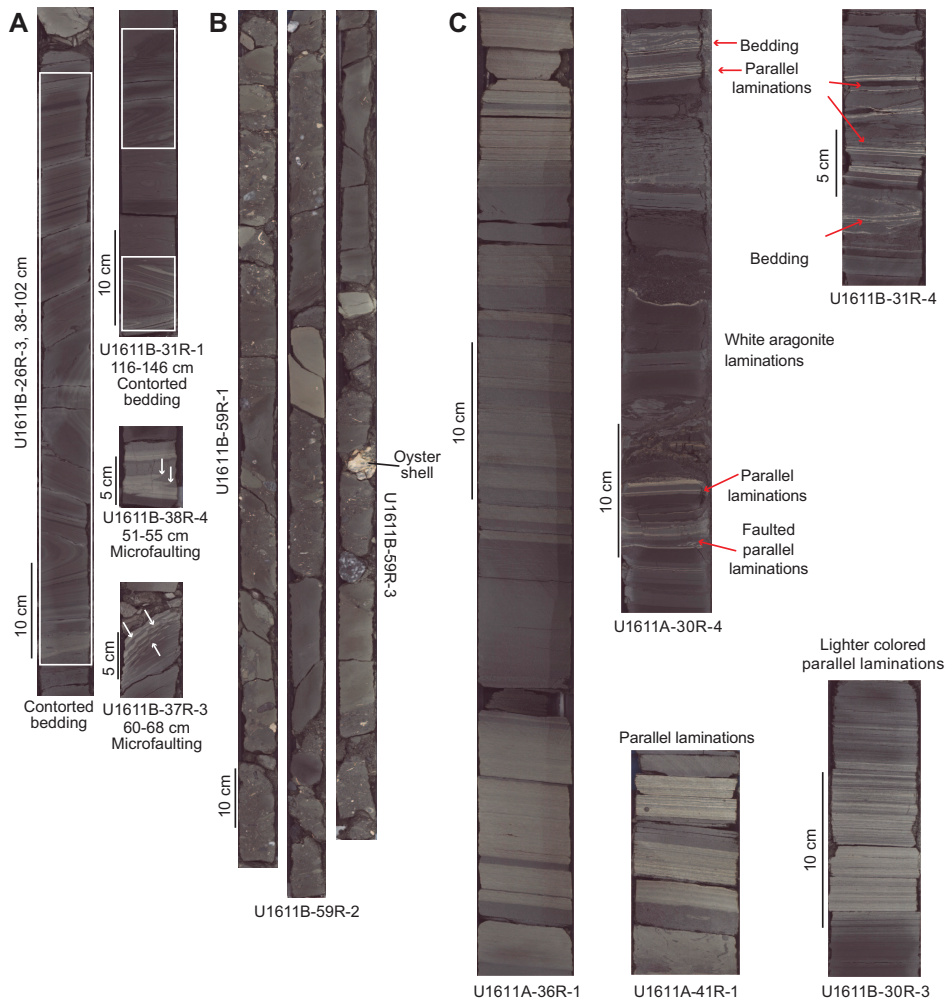

Figure F22. Linescan images of deformational and laminated structures, Site U1611. A. Contorted bedding (slump), microfaulting, and chaotic deposits. B. Conglomerate >1 m long with mud clasts and large bioclasts. C. Examples of lighter colored laminations reflecting variable carbonate content (401-U1611A-36R-1 and 401-U1611B-30R-3), white laminations composed of aragonite that are parallel (401-U1611A-30R-4 and 401-U1611B-31R-4), and deformed (contorted and faulted), parallel, and cross laminations (401-U1611A-41R-1).

Alborán Basin are considered to result mainly from the regional circulation of the deep, intermediate, and surface Mediterranean water mass currents (e.g., Juan et al., 2016, 2020; Ercilla et al., 2016; Llave et al., 2020). The transition from the low-oxygen finely laminated sediments of Unit II to the well-oxygenated contouritic sediments of Unit I occurs over a 2 m interval that was not recovered in either Hole U1611A or U1611B. Dating of the uppermost Miocene and lowermost Pliocene sediments on either side of this recovery gap is necessary to determine the duration of this transition, which may be associated with the catastrophic refilling of the Mediterranean at the Miocene/Pliocene boundary (Garcia-Castellanos et al., 2020).

6.4.4.2. Biostratigraphy

This site is characterized by some intervals poor in microfauna, particularly planktonic foraminifers. However, despite some core catchers being barren in foraminifers, they were rich in fish teeth and scales, wood fragments, and shell fragments, providing valuable information about the site's paleoenvironment.

Both holes were designed to start retrieving cores in the Early Pliocene, and this age was confirmed by the calcareous nannoplankton and foraminifer assemblages recovered in the uppermost core catcher samples (656 m in Hole U1611A and 744 m in Hole U1611B). Below Samples 401-U1611A-18R-CC (821.2 mbsf) and 401-U1611B-14R-CC (815.7 mbsf), close to the Lithostratigraphic Unit I/II boundary, planktonic foraminifers are absent (with rare exceptions) in the fraction larger than 150 µm, although they continue to be present in the 63–150 µm fraction. We interpret this change to be the Messinian/Zanclean boundary. There is also a significant change in the composition of the sediments below this boundary, with almost no biogenic particles in the coarse fraction except for fish and wood fragments. The near total absence of >150 µm planktonic foraminifers continues to Sample 401-U1611A-42R-CC (1037.2 mbsf). Beneath this, to the bottom of Hole U1611A the sediments typically contain some planktonic foraminifers in the >150 µm fraction but few benthic foraminifers. The presence of calcareous nannofossils *R. pseudoumbilicus* and *Nicklithus amplificus* in the lowermost sample from Hole U1611A (1281.9 mbsf) constrains the age at the base of the hole to be between 6.82 and 7.10 Ma. (Figure **F21**).

6.4.4.3. Paleomagnetism

Pass-through paleomagnetic measurements were performed using the SRM to investigate the NRM of all the archive-half sections of Holes U1611A and U1611B. AF demagnetization was performed on the SRM by applying stepwise peak fields of 5, 10, 15, and 20 mT, with measurement of the remaining magnetization taken at 2 cm resolution.

In addition, we collected discrete samples of all the working-half sections of Hole U1611A. We measured the AMS and bulk MS using the MFK2 KappaBridge unit and the NRM on the AGICO JR-6A spinner magnetometer. Stepwise AF demagnetization was performed at successive peak fields of 0, 5, 10, 15, 20, and 30 mT up to a maximum of 60 mT. In addition, we performed stepwise thermal demagnetization up to a maximum temperature of 600°C on six sawed samples. The paleomagnetic intensities are weak, and inclinations are scattered between expected normal and reversed polarities. This makes it unclear if it was the primary magnetic signal or a pervasive overprint that was measured. Thermal demagnetization experiments show the presence of iron sulfides in the sediment.

The AMS results from Hole U1611A show an overall vertical direction of the κ_{min} axis with a scatter on the order of 10°, in agreement with observations of subhorizontal strata in the split cores.

6.4.4.4. Geochemistry

Headspace gas samples and IW in Hole U1611A were taken at one per recovered core or one every other half advance. Gas contents in both holes remained within a safe range, and the downhole pattern of methane/ethane ratios and absolute methane values are similar between the holes, despite a horizontal separation of 1361 m. IW salinities reached a maximum of 70 at ~1050 mbsf and then decreased below that level. Major ion chemistry was used to interpret the origin of these saline IW to be a possible remnant of late Messinian brine. Partly because of this observation, we consulted with onshore microbiologists and took 5 cm whole-round samples from Hole U1611B at 20 m intervals using clean equipment and immediately froze them at −80°C for possible future microbiological analysis.

$CaCO_3$ varies from 5.0 to 92.0 wt% at Site U1611, with a mean of 28.3 wt%. $CaCO_3$ is generally between 30 and 60 wt% in the Pliocene Unit I. In Unit II, carbonate decreases to between 14 and 36 wt%, and in Unit III it decreases further to the range of 15–25 wt%. In Unit III, these low carbonate concentrations are interrupted by decimeter-scale dolomitic or cemented carbonate beds with high values, typically greater than 60 wt% (7 samples).

6.4.4.5. Physical properties and downhole measurements

Large-scale downhole patterns in the whole-round physical properties data of Holes U1611A and U1611B typically match well, but the same horizons are approximately 5–15 m shallower in Hole U1611B compared to Hole U1611A. Coarser lithologies tend to have lower NGR values. Cemented carbonate layers are distinguished by low NGR and MS values and relatively high GRA density values (Figure **F21**).

Downhole logging in Hole U1611A was only partially successful, with the triple combo tool string reaching 909 mbsf, logging a 236 m open hole interval. However, this interval includes the Messinian/Zanclean boundary at ~820 mbsf, providing stratigraphic continuity there, and also covers some poorly recovered Messinian intervals. The sonic-inclinometry tool string reached 743 mbsf before the hole became impassible. The borehole was characterized in the caliper borehole diameter log by washouts, bridges, and ledges. According to both the General Purpose Inclinometry Tool logs, at the end of the pipe the borehole was inclined at ~9° from vertical and the inclination increased with depth to more than 12° at 750 mbsf.

7. Preliminary scientific assessment

7.1. Objective 1: to document the time at which the Atlantic first started to receive a distinct overflow from the Mediterranean and to evaluate quantitatively its role in Late Miocene global climate and regional environmental change

- Hypothesis 1.1: the earliest contourites formed as a result of Atlantic–Mediterranean exchange and correlate with the onset of Late Miocene SST decline in the mid- and high latitudes. Dating the first Atlantic–Mediterranean contourites will test this hypothesis.
- Hypothesis 1.2: atmospheric CO_2 sequestration in the deeper ocean through the initiation and development of AMW can account for the degree and distribution of SST cooling observed. Reconstructing the velocity, density, and flux of AMW through time, quantifying its impact on CO_2 advection (Capella et al., 2019), and then modeling the resulting SST distribution (e.g., Ivanovic et al., 2014a) tests this hypothesis.
- Hypothesis 1.3: AMW modulates NADW formation, triggers glacial inception, and influences continental-scale aridification. Model-based testing of this hypothesis requires the correlation of IMMAGE records with existing high-resolution records globally.

Hypothesis 1.1 will require the coring of the fossil corridors in Spain and Morocco to test entirely. However, the records in the Atlantic also hold part of the story. The information collected that is relevant to this hypothesis is as follows:

- Site U1385: no contourites were recovered. This is consistent with its water depth, which is substantially below the core of the MOW plume today. However, the Miocene successions here, like the even deeper records cored during Expedition 397 at Sites U1586 and U1587 (Hodell et al., 2023), do record strong precessional cyclicity in NGR that does appear to correlate very precisely with the timing of major changes occurring in the Mediterranean during the MSC that have direct implications for Atlantic–Mediterranean exchange (Flecker et al., 2015).
- Site U1609: fine-grained silty mud contourites were recovered from the surface to a depth of 320 mbsf in Hole U1609A and 352 mbsf in Hole U1609B. The gradational nature of the transitions between subtle grain size differences make it difficult to be sure exactly where the onset is, and this will need resolving with detailed grain size analysis after the expedition. However,

the identified onset corresponds broadly to the onset of the MSC in the Mediterranean (5.97 Ma). There is no evidence of contourites deeper in the succession.
- Site U1610: the top 200 m recovered from Hole U1610A (500–700 mbsf) comprised silty mud contourites. These beds were both siltier (e.g., coarser) and thicker than the equivalent-aged Early Pliocene contourites at Site U1609. This is consistent with their more proximal position relative to the Gibraltar Strait. At Site U1610, however, there is an interval between 700 and 935 mbsf where no contourites were recovered, nor is there any clear evidence of bottom water current activity of any sort, although again this will need testing with high-resolution grain size analysis. Between 935 and 1030 mbsf, there are clear contourites. This interval is Messinian and is equivalent to the period just before and during the lower part of the MSC. More detailed correlation and dating will be required to ascertain exactly when these contouritic sediments start and end here. The succession from 1030 mbsf to the bottom of the hole (1400 mbsf) is dominated by sandstones deposited by turbidity currents and mass flows. However, there is almost always evidence of reworking by bottom currents.
- Site U1611: the Pliocene succession recovered at this site in the Mediterranean is dominated by silty mud contourites. There is no evidence of contourite deposition below the Miocene/Pliocene boundary.

In summary, Site U1609 will be the best location for evaluating the timing of the initial onset of bottom water currents in the Tortonian when MO is thought to have started. It will also be necessary to establish that the bottom current features are not generated by other water masses. The contouritic information derived from the other sites is Messinian–Pliocene in age and provides interesting insights into bottom current variability through time.

Testing Hypotheses 1.2 and 1.3 will require detailed postcruise analysis and modeling. However, a critical first step was to recover successions that could be tuned to the insolation curve as a means to achieving precessional-scale correlation between Expedition 401 sites and far-field locations of the same age. Given the depth our succession was buried, we anticipated 30%–40% recovery, consistent with typical RCB recovery rates. However, not only was the recovery much better than this (>82% overall), but in addition because our 8 Ma target was not buried as deeply as we had thought there was time to drill not one but two holes at Site U1609, generating a splice that is nearly complete. We also have a close to complete record at Site U1385 that can be correlated peak-to-peak to the adjacent orbitally tuned NGR records from Sites U1586 and U1587 (Hodell et al., 2023). Finally, although the recovery of the single hole at Site U1610 was only 80%, most of the poor recovery is toward the bottom of the hole. The upper part of the succession is strongly cyclic, making it likely that it will be possible to tune the record to the insolation curve.

Taken together, the cores recovered during Expedition 401 place us in a far better position to test these hypotheses than could ever have been anticipated before the expedition.

7.2. Objective 2: to recover a complete record of Atlantic–Mediterranean exchange before, during, and after the Messinian Salinity Crisis and to evaluate the causes and consequences of this extreme oceanographic event locally, regionally, and globally

- Hypothesis 2.1: the Alborán Basin was an intermediate marine system influenced by the Atlantic and separated from the Mediterranean by the Alborán volcanic arc during the MSC.
- Hypothesis 2.2: extreme environmental fluctuations in the Mediterranean had negligible impact on AMW.

Cores recovered at Site U1611 in the Alborán Sea record a thick succession of organic-rich laminated fine-grained sediments interbedded with turbidites, debrites, and slumps, overlain by Pliocene contourites. The fauna and ichnofossils identified in the pre-Pliocene sequence indicate that subaqueous deposition occurred throughout but that the water mass was highly stratified with low oxygen or anoxic conditions at the sediment/water interface. The bottom of the hole is probably around 6.8 Ma, and this sequence continues with these same features right up to the Miocene/Pliocene boundary. We drilled two holes at this site, and Hole U1611B in particular is largely complete (78%) because of the drilling configuration we employed (half-advance coring

using the RCB coring system and a PDC bit). The majority of what was not recovered was in the Pliocene, so the record from the Miocene–Pliocene downward (with the exception of a 2 m gap just below the Miocene/Pliocene boundary) is close to continuous. This will make testing Hypothesis 2.1 possible with additional postcruise analysis.

Hypothesis 2.2 requires the tuning of both Mediterranean and Atlantic records to the insolation curve to compare the timing of changes in the physical properties reflecting Late Miocene water mass and sedimentation changes. Although the details of this tuning require refinement, particularly in Site U1611, the changes in the physical properties records at times consistent with major changes in the Mediterranean associated with gateway changes are clear. Exploration of the mechanisms for achieving these synchronous changes can now be implemented through postcruise empirical and modeling studies.

7.3. Objective 3: to test our quantitative understanding of the behavior of ocean overflow plumes during the most extreme exchange in Earth's history

- Hypothesis 3.1: the velocity of the plume is a function of the Atlantic–Mediterranean density contrast, limitation on flow through the strait (Bryden et al., 1994), the gradient of the slope, and the degree of mixing (Price et al., 1993).
- Hypothesis 3.2: mixing with ambient water causes a strong negative feedback on the size of the plume, limiting the degree of its variability (Price et al., 1993). This means that only minor changes in the physical size of the plume are expected, despite the proportion of plume water derived directly from the outflow varying significantly. As a result, changes in Mediterranean density have little impact on the plume position.
- Hypothesis 3.3: the main control on the settling depth of MO is the vertical density gradient in the North Atlantic, which is a product of North Atlantic overturning circulation (Rogerson et al., 2012a).

Testing these physical oceanography hypotheses will require detailed physical and chemical analysis and modeling. However, this is only possible because of the high recovery rates with clear and tunable cyclicity enabling site-to-site correlation down the MO plume on a precessional timescale. The cores we have recovered will permit us to test whether the representations of overflows within general circulation models are effective when overflow density is higher than the range of validation provided by the modern ocean. If general circulation model representation of these Messinian high density overflows are inadequate, this casts doubt on all modeling experiments in which part of the ocean-atmosphere system is outside the range exhibited today.

8. Outreach

Expedition 401 had two Education and Outreach Officers: Erin Winick Anthony, a science communicator and founder of STEAM Power Media based out of Texas (USA), and Kellan Moss, a freelance artist and scientific illustrator based out of Washington (USA). Both officers conducted outreach from aboard *JOIDES Resolution*, communicating the science objectives of the expedition to students and the general public across the world through numerous platforms. These included live ship-to-shore events, digital portraits, pastel drawings, social media, videos, media interviews, and blog posts.

8.1. Tours

The Outreach Officers hosted live ship-to-shore video tours on Zoom for formal and informal groups all over the world. These events introduced students and members of general audiences to the scientific goals of Expedition 401 and the broader history, significance, and process of scientific ocean drilling.

Broadcasts began with an introduction to *JOIDES Resolution*, an explanation of the importance of scientific ocean drilling, and a description of the scientific goals of the expedition. In some cases, a

scientist who shared a non-English language with the audience hosted the tour. Participants received a 45 min tour of the ship that included the bridge, lifeboats, derrick, rig floor, catwalk, and laboratories. Viewers learned about the core flow process from scientists in each laboratory including physical properties, core description, paleomagnetism, biostratigraphy, and geochemistry. Tours ended with question-and-answer sessions with scientists and the Onboard Outreach Officer.

Over the course of the expedition, the Onboard Outreach Officers facilitated 75 Zoom tours to many international groups, including primary and secondary schools, colleges and universities, podcasts, museums, after school programs, and informal public groups. These tours were completed in 15 different countries in 6 different languages to about 465,000 people.

Some special occasion tours were given to groups such as Centro Ciência Viva do Algarve, which also hosted a Portugal based exhibit about the exhibition; the Smithsonian National Museum of Natural History, which reached visitors to the institute; and CBS Mission Unstoppable, which live streamed the tour on Twitch. Student audiences ranged from Pre-K to graduate university level.

The Expedition Project Manager, both Co-Chief Scientists, and every member of the science party assisted with the tours. Many of the scientists recruited tour audiences in their home countries. Two Chinese scientists worked with IODP China to arrange a live tour with primary schools around the country. That connection was facilitated by the Xinhua official Chinese news agency, which live streamed the event, reaching an audience of approximately 460,000 people in China. Multiple members of the science party recorded tours with their universities for later use, including a PhD student who will use the recording for a seminar at their weekly Geology and Geophysics Department meetings.

The following includes some of the feedback sent by groups who received tours:

- "It was hard to believe we were at sea, the images looked so stable, clean, beautiful and undisturbed, they were. The audio was also so good, and everyone was so excited." —Yukari Kido, Women for One Ocean, Japan.
- "Seriously the best ship to shore I have ever seen. And I have seen a lot." —Sarah Kachovich, Australia-New Zealand IODP Consortium, Australia.
- "The tour was so informational, and they loved every moment of it. I really liked the time allowed for asking questions, too!" - Taryn Page, Charlotte Country Day School, United States.
- "That was really interesting, and pitched just right for my class. They are buzzing right now, having some more great questions and chatting to each other about what they saw and even talking about what they want to do with science when they grow up." —Margaret Tokunaga, Cutthrope Primary, United Kingdom.
- "The link has really stimulated some interesting discussions and I think we might have one or two who want to follow in similar careers-I suspect applications for earth sciences at university will be quite popular ☺ Evie is still asking questions! Even the lady from our marketing department who took a few photos stayed to listen as she found it so fascinating." —Jacky Gill, Woodbridge School, United Kingdom.
- "The kids really enjoyed it! We had about 150 people in attendance total. While my new department members were dubious at first about the relevance, they really see the importance of this type of interaction now!" —Jennifer Field, Weston High School, United States.
- "THANK YOU SO MUCH! That was so fun and they have not stopped talking about how much fun they had." —Peyton Early, Hallsville Middle School, United States.

A letter from the CEO of National Youth Science Forum (NYSF), Dr. Melanie Bagg GAICD, was also sent to the outreach officers, thanking them for the tour and their efforts to the NYSF program.

Additionally, eight of the tours from the expedition have been or will be posted publicly, furthering the impact of the events. A sampling can be viewed at the following links:

- Solve it For Kids Podcast (**https://youtu.be/9ksqg3hfF5Y**),
- Erin Winick–Tour of the *JOIDES Resolution* Science Ship! (**https://youtu.be/Eqq-8I9CB4A**),

- Shadow The Scientists 1 (**https://youtu.be/MtTHuFGdqlI**),
- Shadow the Scientists 2 (**https://youtu.be/_yGnhT73Lvc**), and
- Shadow the Scientists 3 (**https://youtu.be/jTS3HHPPMvU**).

8.2. Social media

The Outreach Officers maintained six online platforms during the expedition: Facebook, Instagram, X, Threads, YouTube, and the *JOIDES Resolution* Expedition 401 web page.

The Outreach Officers posted 100 Facebook posts, 254 Facebook stories, 79 Instagram posts, 611 Instagram stories, 108 Tweets, 10 short YouTube videos, and 35 Threads posts on the *JOIDES Resolution* accounts over the course of Expedition 401. Across all platforms, these posts reached approximately 2.3 million impressions and received nearly 100,000 interactions (e.g., likes, shares, and comments).

One Outreach Officer used their own social media accounts with a following of more than 100,000 to reach an additional audience during the expedition. More than 110 posts were published across their professional Facebook and Instagram accounts. These posts achieved millions of impressions and directed this audience to the *JOIDES Resolution* accounts.

Because of the success of posts on both sets of accounts, *JOIDES Resolution* gained more than 1200 new Facebook followers, 500 Instagram followers, and 150 X followers.

Expedition 401 content also performed exceptionally well on the platform Threads. Although the platform does not yet offer analytics tools, the *JOIDES Resolution* account gained at least 700 new followers from the success of these posts.

More than 50 of the social media posts were vertical videos created as one of the outreach officer's shipboard projects. These videos covered topics ranging from sleep shifts on the ship to science highlights of the expedition. Some of the top performing videos included the following:

- Time-lapse of thrusters descending at the third drilling site (1.1 million views on Facebook),
- Sleep schedule explainer (780,000 views on Facebook and 13,700 views on Instagram),
- Explainer of the black bag signals on ship (64,000 views on Facebook),
- Guide to how to make a shrunken Styrofoam cup at sea (30,800 views on Instagram), and
- Favorite geology movies of the science team (23,300 views on Instagram).

The Science in 60 Seconds video series featured nearly half of the science party taking on the challenge to explain their work in 60 s or less. This video series received more than 65,000 views and will be packaged together for future educational use.

Three videos created during the expedition have been or will also be shared by CBS Mission Unstoppable, a women in STEM focused television show and social media platform. The National STEM Challenge also reposted the video created about shrinking cups using ocean pressures. Xena Workwear, a women's steel toe boot company, will feature a day in the life vlog created by one of our Outreach Officers after the end of the expedition.

A total of 11 blog posts were written and published on the *JOIDES Resolution* web page during Expedition 401. These blogs covered topics including scientific explainers, expedition news updates, and questions-and-answers with scientists. One of these blogs was also adapted into a sharable infographic for social media.

8.3. Media coverage

Expedition 401 received coverage by several high-profile organizations including the BBC and the Weather Channel. The Outreach Officers pitched Expedition 401 to climate and STEM focused media outlets, resulting in coverage in outlets such as the Weather Channel, CBS Mission Unstoppable, and Solve It for Kids. The Weather Channel team also requested that a follow up live interview is done after the expedition to share the initial results.

The ship's proximity to and visibility from Malaga, Spain, resulted in additional news coverage from local publications. After this coverage, the science team reached out to the outlet that first covered the ship, resulting in the featuring of the three Spanish scientists aboard the ship.

Additional articles were written by the science party for publications such the UK-IODP newsletter and U.S. Science Support Program's Drilling Dispatch newsletter. Multiple universities including Princeton and the University of Bristol published articles covering the participation of their respective scientists in the expedition.

Links to a sampling of news clippings covering the expedition are in Table **T2**.

8.4. Visual art

An Onboard Outreach Officer completed over a dozen original pieces of artwork that were shared to the various *JOIDES Resolution* social media pages. Currently, at least 12 more pieces are scheduled to be completed postcruise, half in digital format and half traditional chalk pastel. Coordination to feature this artwork at an exhibit or conference is in progress for the next fiscal year.

8.4.1. Traditional artwork

Six original pieces of artwork were completed during the duration of Expedition 401 using chalk pastels and colored pencils (Figure **F23**). Each piece is based on a photo taken by the artist and sketched onto roughly 30 cm × 42 cm colored cotton paper. Firm, vivid chalk pastels were used to color these drawings and a fixative was used to prevent smearing. Colored pencils were used for finer details. Each piece was completed in 6–14 h. Four of these pieces featured specific scientists at work, and the other two pieces featured the SIEM Offshore drilling crew. Each piece featured a different area of work from various fields of study. Once completed, the artwork was turned into a social post, either in picture or video format.

Two of these pieces were featured in the SIEM Offshore newspaper.

In additional to these six pieces, the onboard artist also completed warm-up sketches of various equipment around the ship. These were also posted to the *JOIDES Resolution* social media pages as a photo set and a video.

8.4.2. Digital artwork

Six original portraits of various members of the Science Party were completed during the duration of Expedition 401 using a digital software program. These portraits took between 4–10 h to complete and were shared to the *JOIDES Resolution* social media pages in video format. After the expedition, these same members will be redrawn, showcasing any physical or emotional changes each of them underwent during the 2 month cruise.

Additional warm-up sketches were completed for this medium. These warm-ups were also turned into a video for the *JOIDES Resolution* social media pages.

Table T2. Sampling of news clippings, Expedition 401.

Outlet	Link	Format	Country
BBC World Service	**https://www.bbc.co.uk/programmes/w3ct4sdk**	Radio	UK
The Weather Channel		Live TV	USA
H5 News	**https://my-h5news.app.xinhuanet.com/h5activity/yunzhibo-pc/#/?isFull=0&roomId=65a9e21ce4b0f3656467b8e4**	Online Broadcast	China
Solve It for Kids	**https://solveitforkids.libsyn.com/why-do-science-at-sea**	Podcast	USA
Books, Kids, and Creations	**https://open.spotify.com/episode/3j0RCeNhzjb3zLA56Rn31V?si=wxUZaFEcTg27ytZgNsbsoA**	Podcast	USA
CBS Mission Unstoppable		Twitch Live Stream	USA
Smoko Podcast	**https://www.smokopodcast.ca/2129026/14355093-episode-27-erin-winick-anthony-founder-of-steam-power-media-stem-creator-science-communicator**	Podcast	USA
Hazard Girls Podcast	Not yet released	Podcast	USA
SUR In English	**https://www.surinenglish.com/malaga/what-that-big-tower-the-horizon-off-20240126144731-nt.html**	Article	Spain
SUR	**https://www.diariosur.es/malaga-capital/gran-torre-horizonte-frente-malaga-20240126114835-nt.html**	Article	Spain
SUR	**https://www.diariosur.es/malaga/barco-gran-torre-estudia-formo-mediterraneo-frente-20240129142420-nt.html**	Article	Spain
Huffington Post	**https://www.huffingtonpost.es/sociedad/una-torre-flotante-mitad-mar-desconcierta-poblacion-malaga.html**	Article	Spain
Kochi Shibun	**https://www.kochinews.co.jp/article/detail/714287**	Article	Japan

8.5. Additional outreach projects

The Education and Outreach Officers each undertook additional side projects to share the scientific objectives of Expedition 401.

8.5.1. A picture from space

Through coordination with the Crew Earth Observation team at Johnson Space Center, the outreach officers arranged for a picture to be taken of *JOIDES Resolution* from the International Space Station. The image taken by NASA astronaut Jasmin Moghbeli shows the ship as a tiny dot in the North Atlantic. Given that the space station and the ship are both major international collaborations and remote floating laboratories, a product is being created to show the similarities between the two missions.

8.5.2. 3D printing at sea

An Outreach Officer used the 3D printer on the ship to create a portable model of one of the coring bits. Smaller versions of the model were also turned into necklaces and earrings. These served as models used in the ship-to-shore events to better explain the technology of the ship. A video was created about this project to share the manufacturing tools on the ship online.

8.5.3. Documentary coordination

Expedition 403 will have a documentary crew sailing on *JOIDES Resolution*. This crew is also planning to include part of the story of Expedition 401. The Onboard Outreach Officers coordinated with this team to set up interviews with the Expedition 401 science team and record any additional shipboard footage that the documentary crew needs.

8.5.4. Article writing

Before sailing, one of the outreach officers coordinated with Beanz: The Kids STEAM Magazine and Engineering.com to write articles covering the expedition. An article written for Beanz covered the preparations for the expedition (**https://kidscodecs.com/preparing-ocean-expedition**). The Engineering.com article will cover the topic of remote manufacturing and the tools available

Figure F23. Outreach officer artwork of Siem Offshore AS crew at work in the derrick, Expedition 401.

on the ship. The Outreach Officer performed interviews on the ship for this article and will write it upon return to shore.

8.5.5. Photography

One of the Outreach Officers took over 5000 photos of the various scientists and crew members. These photos were used to highlight specific events and members at work as social media posts. In addition, they were used in various videos produced for social media and for the Family & Friends page for the expedition. There are future plans for these photos to be made into a mixed media animation by said photographer after the expedition.

Recreation photos of Leg 13 staff and scientists with Expedition 401 staff and scientists were also taken. These photos showcased the similarity between the two expeditions while highlighting the women-centric party we sailed with today.

References

Abrantes, F., 2000. 200,000 yr diatom records from Atlantic upwelling sites reveal maximum productivity during LGM and a shift in phytoplankton community structure at 185 000 yr. Earth and Planetary Science Letters, 176(1):7–16. **https://doi.org/10.1016/S0012-821X(99)00312-X**

Alhammoud, B., Meijer, P.T., and Dijkstra, H.A., 2010. Sensitivity of Mediterranean thermohaline circulation to gateway depth: a model investigation. Paleoceanography, 25(2):PA2220. **https://doi.org/10.1029/2009PA001823**

Álvarez, M., Pérez, F.F., Shoosmith, D.R., and Bryden, H.L., 2005. Unaccounted role of Mediterranean water in the drawdown of anthropogenic carbon. Journal of Geophysical Research: Oceans, 110(C9):C09S03. **https://doi.org/10.1029/2004JC002633**

Ambar, I., Serra, N., Brogueira, M.J., Cabeçadas, G., Abrantes, F., Freitas, P., Gonçalves, C., and Gonzalez, N., 2002. Physical, chemical and sedimentological aspects of the Mediterranean outflow off Iberia. Deep Sea Research, Part II: Topical Studies in Oceanography, 49(19):4163–4177. **https://doi.org/10.1016/S0967-0645(02)00148-0**

Bahr, A., Kaboth, S., Jiménez-Espejo, F.J., Sierro, F.J., Voelker, A.H.L., Lourens, L., Röhl, U., Reichart, G.J., Escutia, C., Hernández-Molina, F.J., Pross, J., and Friedrich, O., 2015. Persistent monsoonal forcing of Mediterranean Outflow Water dynamics during the late Pleistocene. Geology, 43(11):951–954. **https://doi.org/10.1130/G37013.1**

Bahr, A., Kaboth-Bahr, S., and Karas, C., 2022. The opening and closure of oceanic seaways during the Cenozoic: pacemaker of global climate change? Special Publication - Geological Society of London, 523:SP523-2021-2054. **https://doi.org/10.1144/SP523-2021-54**

Benson, R.H., Rakic-El Bied, K., and Bonaduce, G., 1991. An important current reversal (influx) in the Rifian Corridor (Morocco) at the Tortonian-Messinian boundary: the end of Tethys Ocean. Paleoceanography, 6(1):165–192. **https://doi.org/10.1029/90PA00756**

Bigg, G.R., Jickells, T.D., Liss, P.S., and Osborn, T.J., 2003. The role of the oceans in climate. International Journal of Climatology, 23(10):1127–1159. **https://doi.org/10.1002/joc.926**

Bigg, G.R., and Wadley, M.R., 2001. Millennial-scale variability in the oceans: an ocean modelling view. Journal of Quaternary Science, 16(4):309–319. **https://doi.org/10.1002/jqs.599**

Billups, K., 2002. Late Miocene through early Pliocene deep water circulation and climate change viewed from the sub-Antarctic South Atlantic. Palaeogeography, Palaeoclimatology, Palaeoecology, 185(3–4):287–307. **https://doi.org/10.1016/S0031-0182(02)00340-1**

Blanc, P.-L., 2006. Improved modelling of the Messinian salinity crisis and conceptual implications. Palaeogeography, Palaeoclimatology, Palaeoecology, 238(1):349–372. **https://doi.org/10.1016/j.palaeo.2006.03.033**

Booth-Rea, G., R. Ranero, C., and Grevemeyer, I., 2018. The Alboran volcanic-arc modulated the Messinian faunal exchange and salinity crisis. Scientific Reports, 8(1):13015. **https://doi.org/10.1038/s41598-018-31307-7**

Broecker, W.S., 1991. The great ocean conveyor. Oceanography, 4(2):79–89. **http://www.jstor.org/stable/43924572**

Bryden, H.L., Candela, J., and Kinder, T.H., 1994. Exchange through the Strait of Gibraltar. Progress in Oceanography, 33(3):201–248. **https://doi.org/10.1016/0079-6611(94)90028-0**

Bulian, F., Sierro, F.J., Ledesma, S., Jiménez-Espejo, F.J., and Bassetti, M.-A., 2021. Messinian West Alboran Sea record in the proximity of Gibraltar: Early signs of Atlantic-Mediterranean gateway restriction. Marine Geology, 434:106430. **https://doi.org/10.1016/j.margeo.2021.106430**

Capella, W., Flecker, R., Hernández-Molina, F.J., Simon, D., Meijer, P.T., Rogerson, M., Sierro, F.J., and Krijgsman, W., 2019. Mediterranean isolation preconditioning the Earth sSystem for Late Miocene climate cooling. Scientific Reports, 9(1):3795. **https://doi.org/10.1038/s41598-019-40208-2**

Capella, W., Hernández-Molina, F.J., Flecker, R., Hilgen, F.J., Hssain, M., Kouwenhoven, T.J., van Oorschot, M., Sierro, F.J., Stow, D.A.V., Trabucho-Alexandre, J., Tulbure, M.A., de Weger, W., Yousfi, M.Z., and Krijgsman, W., 2017. Sandy contourite drift in the late Miocene Rifian Corridor (Morocco): Reconstruction of depositional environments in a foreland-basin seaway. Sedimentary Geology, 355:31-57. **https://doi.org/10.1016/j.sedgeo.2017.04.004**

de Weger, W., Hernández-Molina, F.J., Flecker, R., Sierro, F.J., Chiarella, D., Krijgsman, W., and Manar, M.A., 2020. Late Miocene contourite channel system reveals intermittent overflow behavior. Geology, 48(12):1194–1199. **https://doi.org/10.1130/G47944.1**

de Weger, W., Hernández-Molina, F.J., Miguez-Salas, O., de Castro, S., Bruno, M., Chiarella, D., Sierro, F.J., Blackbourn, G., and Manar, M.A., 2021. Contourite depositional system after the exit of a strait: case study from the late Miocene South Rifian Corridor, Morocco. Sedimentology, 68(7):2996–3032. **https://doi.org/10.1111/sed.12882**

Dietrich, D.E., Tseng, Y.-H., Medina, R., Piacsek, S.A., Liste, M., Olabarrieta, M., Bowman, M.J., and Mehra, A., 2008. Mediterranean Overflow Water (MOW) simulation using a coupled multiple-grid Mediterranean Sea/North Atlantic Ocean model. Journal of Geophysical Research: Oceans, 113(C7):C07027. **https://doi.org/10.1029/2006JC003914**

Dixon, R.K., Solomon, A.M., Brown, S., Houghton, R.A., Trexier, M.C., and Wisniewski, J., 1994. Carbon pools and flux of global forest ecosystems. Science, 263(5144):185–190. **https://doi.org/10.1126/science.263.5144.185**

Do Couto, D., Gorini, C., Jolivet, L., Lebret, N., Augier, R., Gumiaux, C., d'Acremont, E., Ammar, A., Jabour, H., and Auxietre, J.-L., 2016. Tectonic and stratigraphic evolution of the Western Alboran Sea Basin in the last 25 Myrs. Tectonophysics, 677–678:280–311. **https://doi.org/10.1016/j.tecto.2016.03.020**

Duggen, S., Hoernle, K., van den Bogaard, P., Rüpke, L., and Phipps Morgan, J., 2003. Deep roots of the Messinian salinity crisis. Nature, 422(6932):602–606. **https://doi.org/10.1038/nature01553**

Elsworth, G., Galbraith, E., Halverson, G., and Yang, S., 2017. Enhanced weathering and CO_2 drawdown caused by latest Eocene strengthening of the Atlantic meridional overturning circulation. Nature Geoscience, 10(3):213–216. **https://doi.org/10.1038/ngeo2888**

Ercilla, G., Juan, C., Hernández-Molina, F.J., Bruno, M., Estrada, F., Alonso, B., Casas, D., Farran, M.l., Llave, E., García, M., Vázquez, J.T., D'Acremont, E., Gorini, C., Palomino, D., Valencia, J., El Moumni, B., and Ammar, A., 2016. Significance of bottom currents in deep-sea morphodynamics: an example from the Alboran Sea. Marine Geology, 378:157–170. **https://doi.org/10.1016/j.margeo.2015.09.007**

Estrada, F., Ercilla, G., Gorini, C., Alonso, B., Vázquez, J.T., García-Castellanos, D., Juan, C., Maldonado, A., Ammar, A., and Elabbassi, M., 2011. Impact of pulsed Atlantic water inflow into the Alboran Basin at the time of the Zanclean flooding. Geo-Marine Letters, 31(5):361–376. **https://doi.org/10.1007/s00367-011-0249-8**

Expedition 339 Scientists, 2013. Expedition 339 summary. In Stow, D.A.V., Hernández-Molina, F.J., Alvarez Zarikian, C.A., and the Expedition 339 Scientists, Proceedings of the Integrated Ocean Drilling Program. 339: Tokyo (Integrated Ocean Drilling Program Management International, Inc.). **https://doi.org/10.2204/iodp.proc.339.101.2013**

Faccenna, C., Piromallo, C., Crespo-Blanc, A., Jolivet, L., and Rossetti, F., 2004. Lateral slab deformation and the origin of the western Mediterranean arcs. Tectonics, 23(1):TC1012. **https://doi.org/10.1029/2002TC001488**

Flecker, R., Ducassou, E., and Williams, T., 2023. Expedition 401 Scientific Prospectus: Mediterranean Atlantic Gateway Exchange. International Ocean Discovery Program. **https://doi.org/10.14379/iodp.sp.401.2023**

Flecker, R., Krijgsman, W., Capella, W., de Castro Martíns, C., Dmitrieva, E., Mayser, J.P., Marzocchi, A., Modestou, S., Ochoa, D., Simon, D., Tulbure, M., van den Berg, B., van der Schee, M., de Lange, G., Ellam, R., Govers, R., Gutjahr, M., Hilgen, F., Kouwenhoven, T., Lofi, J., Meijer, P., Sierro, F.J., Bachiri, N., Barhoun, N., Alami, A.C., Chacon, B., Flores, J.A., Gregory, J., Howard, J., Lunt, D., Ochoa, M., Pancost, R., Vincent, S., and Yousfi, M.Z., 2015. Evolution of the Late Miocene Mediterranean–Atlantic gateways and their impact on regional and global environmental change. Earth-Science Reviews, 150:365–392. **https://doi.org/10.1016/j.earscirev.2015.08.007**

Garcia-Castellanos, D., Micallef, A., Estrada, F., Camerlenghi, A., Ercilla, G., Periáñez, R., and Abril, J.M., 2020. The Zanclean megaflood of the Mediterranean – searching for independent evidence. Earth-Science Reviews, 201:103061. **https://doi.org/10.1016/j.earscirev.2019.103061**

García-Gallardo, Á., Grunert, P., Van der Schee, M., Sierro, F.J., Jiménez-Espejo, F.J., Alvarez Zarikian, C.A., and Piller, W.E., 2017a. Benthic foraminifera-based reconstruction of the first Mediterranean-Atlantic exchange in the early Pliocene Gulf of Cadiz. Palaeogeography, Palaeoclimatology, Palaeoecology, 472:93–107. **https://doi.org/10.1016/j.palaeo.2017.02.009**

García-Gallardo, Á., Grunert, P., Voelker, A.H.L., Mendes, I., and Piller, W.E., 2017b. Re-evaluation of the "elevated epifauna" as indicator of Mediterranean outflow water in the Gulf of Cadiz using stable isotopes ($\delta^{13}C$, $\delta^{18}O$). Global and Planetary Change, 155:78–97. **https://doi.org/10.1016/j.gloplacha.2017.06.005**

Glazkova, T., Hernández-Molina, F.J., Dorokhova, E., Mena, A., Roque, C., Rodríguez-Tovar, F.J., Krechik, V., Kuleshova, L., and Llave, E., 2022. Sedimentary processes in the Discovery Gap (Central–NE Atlantic): An example of a deep marine gateway. Deep Sea Research Part I: Oceanographic Research Papers, 180:103681. **https://doi.org/10.1016/j.dsr.2021.103681**

Grant, K.M., Rohling, E.J., Westerhold, T., Zabel, M., Heslop, D., Konijnendijk, T., and Lourens, L., 2017. A 3 million year index for North African humidity/aridity and the implication of potential pan-African Humid periods. Quaternary Science Reviews, 171:100–118. **https://doi.org/10.1016/j.quascirev.2017.07.005**

Guerra-Merchán, A., Serrano, F., Garcés, M., Gofas, S., Esu, D., Gliozzi, E., and Grossi, F., 2010. Messinian Lago-Mare deposits near the Strait of Gibraltar (Malaga Basin, S Spain). Palaeogeography, Palaeoclimatology, Palaeoecology, 285(3):264–276. **https://doi.org/10.1016/j.marpetgeo.2014.01.018**

Hernández-Molina, F.J., Larter, R.D., and Maldonado, A., 2017. Neogene to Quaternary stratigraphic evolution of the Antarctic Peninsula, Pacific Margin offshore of Adelaide Island: Transitions from a non-glacial, through glacially-influenced to a fully glacial state. Global and Planetary Change, 156:80–111. **https://doi.org/10.1016/j.gloplacha.2017.07.002**

Hernández-Molina, F.J., Llave, E., Preu, B., Ercilla, G., Fontan, A., Bruno, M., Serra, N., Gomiz, J.J., Brackenridge, R.E., Sierro, F.J., Stow, D.A.V., García, M., Juan, C., Sandoval, N., and Arnaiz, A., 2014a. Contourite processes associated with the Mediterranean Outflow Water after its exit from the Strait of Gibraltar: global and conceptual implications. Geology, 42(3):227–230. **https://doi.org/10.1130/G35083.1**

Hernández-Molina, F.J., Serra, N., Stow, D.A.V., Llave, E., Ercilla, G., and Van Rooij, D., 2011. Along-slope oceanographic processes and sedimentary products around the Iberian margin. Geo-Marine Letters, 31(5):315–341. **https://doi.org/10.1007/s00367-011-0242-2**

Hernández-Molina, F.J., Sierro, F.J., Llave, E., Roque, C., Stow, D.A.V., Williams, T., Lofi, J., Van der Schee, M., Arnáiz, A., Ledesma, S., Rosales, C., Rodríguez-Tovar, F.J., Pardo-Igúzquiza, E., and Brackenridge, R.E., 2016. Evolution of the Gulf of Cadiz margin and southwest Portugal contourite depositional system: tectonic, sedimentary and paleoceanographic implications from IODP Expedition 339. Marine Geology, 377:7–39. **https://doi.org/10.1016/j.margeo.2015.09.013**

Hernández-Molina, F.J., Stow, D.A.V., Alvarez-Zarikian, C.A., Acton, G., Bahr, A., Balestra, B., Ducassou, E., Flood, R., Flores, J.-A., Furota, S., Grunert, P., Hodell, D., Jimenez-Espejo, F., Kim, J.K., Krissek, L., Kuroda, J., Li, B., Llave, E., Lofi, J., Lourens, L., Miller, M., Nanayama, F., Nishida, N., Richter, C., Roque, C., Pereira, H., Sanchez Goñi, M.F., Sierro, F.J., Singh, A.D., Sloss, C., Takashimizu, Y., Tzanova, A., Voelker, A., Williams, T., and Xuan, C., 2014b. Onset of Mediterranean outflow into the North Atlantic. Science, 344(6189):1244–1250. **https://doi.org/10.1126/science.1251306**

Hernández-Molina, J., Llave, E., Somoza, L., Fernández-Puga, M.C., Maestro, A., León, R., Medialdea, T., Barnolas, A., García, M., Díaz del Río, V., Fernández-Salas, L.M., Vázquez, J.T., Lobo, F., Alveirinho Dias, J.M., Rodero, J., and Gardner, J., 2003. Looking for clues to paleoceanographic imprints: a diagnosis of the Gulf of Cadiz contourite depositional systems. Geology, 31(1):19–22. **https://doi.org/10.1130/0091-7613(2003)031%3C0019:LFCTPI%3E2.0.CO;2**

Hilgen, F., Aziz, H.A., Bice, D., Iaccarino, S., Krijgsman, W., Kuiper, K., Montanari, A., Raffi, I., Turco, E., and Zachariasse, W.-J., 2005. The global boundary stratotype section and point (GSSP) of the Tortonian Stage (Upper Miocene) at Monte Dei Corvi. International Union of Geological Sciences, 28(1):6–17. **https://doi.org/10.18814/epiiugs/2005/v28i1/001**

Hodell, D.A., Abrantes, F., Alvarez Zarikian, C.A., and the Expedition 397 Scientists, 2023. Expedition 397 Preliminary Report: Iberian Margin Paleoclimate. International Ocean Discovery Program. **https://doi.org/10.14379/iodp.pr.397.2023**

Hodell, D., Lourens, L., Crowhurst, S., Konijnendijk, T., Tjallingii, R., Jiménez-Espejo, F., Skinner, L., Tzedakis, P.C., and the Shackleton Site Project Members, 2015. A reference time scale for Site U1385 (Shackleton Site) on the SW Iberian Margin. Global and Planetary Change, 133:49–64. **https://doi.org/10.1016/j.gloplacha.2015.07.002**

Hsü, K.J., Ryan, W.B.F., and Cita, M.B., 1973. Late Miocene desiccation of the Mediterranean. Nature, 242(5395):240–244. **https://doi.org/10.1038/242240a0**

Iaccarino, S.M., and Bossio, A., 1999. Paleoenvironment of uppermost Messinian sequences in the western Mediterranean (Sites 974, 975, and 978). In Zahn, R., Comas, M.C., and Klaus, A. (Eds.), Proceedings of the Ocean Drilling Program, Scientific Results. 161: College Station, TX (Ocean Drilling Program). **https://doi.org/10.2973/odp.proc.sr.161.246.1999**

Intergovernmental Panel on Climate Change, 2014. Climate Change 2013 – The Physical Science Basis: Cambridge, UK (Cambridge University Press). **https://doi.org/10.1017/CBO9781107415324.013**

Iorga, M.C., and Lozier, M.S., 1999. Signatures of the Mediterranean outflow from a North Atlantic climatology: 1. Salinity and density fields. Journal of Geophysical Research: Oceans, 104(C11):25985–26009. **https://doi.org/10.1029/1999JC900115**

Ivanovic, R.F., Valdes, P.J., Flecker, R., Gregoire, L.J., and Gutjahr, M., 2013. The parameterisation of Mediterranean–Atlantic water exchange in the Hadley Centre model HadCM3, and its effect on modelled North Atlantic climate. Ocean Modelling, 62:11–16. **https://doi.org/10.1016/j.ocemod.2012.11.002**

Ivanovic, R.F., Valdes, P.J., Flecker, R., and Gutjahr, M., 2014a. Modelling global-scale climate impacts of the late Miocene Messinian salinity crisis. Climate of the Past, 10(2):607–622. **https://doi.org/10.5194/cp-10-607-2014**

Ivanovic, R.F., Valdes, P.J., Gregoire, L., Flecker, R., and Gutjahr, M., 2014b. Sensitivity of modern climate to the presence, strength and salinity of Mediterranean-Atlantic exchange in a global general circulation model. Climate Dynamics, 42(3):859–877. **https://doi.org/10.1007/s00382-013-1680-5**

Jolivet, L., and Faccenna, C., 2000. Mediterranean extension and the Africa-Eurasia collision. Tectonics, 19(6):1095–1106. **https://doi.org/10.1029/2000TC900018**

Juan, C., Ercilla, G., Estrada, F., Alonso, B., Casas, D., Vázquez, J.T., d'Acremont, E., Medialdea, T., Hernández-Molina, F.J., Gorini, C., El Moumni, B., and Valencia, J., 2020. Multiple factors controlling the deep marine sedimentation of the Alboran Sea (SW Mediterranean) after the Zanclean Atlantic mega-flood. Marine Geology, 423:106138. **https://doi.org/10.1016/j.margeo.2020.106138**

Juan, C., Ercilla, G., Hernández-Molina, F.J., Estrada, F., Alonso, B., Casas, D., García, M., Farran, M.l., Llave, E., Palomino, D., Vázquez, J.-T., Medialdea, T., Gorini, C., D'Acremont, E., El Moumni, B., and Ammar, A., 2016. Seismic evidence of current-controlled sedimentation in the Alboran Sea during the Pliocene and Quaternary: palaeoceanographic implications. Marine Geology, 378:292–311. **https://doi.org/10.1016/j.margeo.2016.01.006**

Kaboth-Bahr, S., Bahr, A., Zeeden, C., Toucanne, S., Eynaud, F., Jiménez-Espejo, F., Röhl, U., Friedrich, O., Pross, J., Löwemark, L., and Lourens, L.J., 2018. Monsoonal forcing of European ice-sheet dynamics during the late Quaternary. Geophysical Research Letters, 45(14):7066–7074. **https://doi.org/10.1029/2018GL078751**

Kaminski, M.A., Aksu, A., Box, M., Hiscott, R.N., Filipescu, S., and Al-Salameen, M., 2002. Late Glacial to Holocene benthic foraminifera in the Marmara Sea: implications for Black Sea–Mediterranean Sea connections following the last deglaciation. Marine Geology, 190(1):165–202. **https://doi.org/10.1016/S0025-3227(02)00347-X**

Karas, C., Nürnberg, D., Bahr, A., Groeneveld, J., Herrle, J.O., Tiedemann, R., and deMenocal, P.B., 2017. Pliocene oceanic seaways and global climate. Scientific Reports, 7(1):39842. **https://doi.org/10.1038/srep39842**

Kennett, J.P., 1982. Marine Geology: Englewood Cliffs, NJ (Prentice-Hall).

Khélifi, N., Sarnthein, M., Andersen, N., Blanz, T., Frank, M., Garbe-Schönberg, D., Haley, B.A., Stumpf, R., and Weinelt, M., 2009. A major and long-term Pliocene intensification of the Mediterranean outflow, 3.5–3.3 Ma ago. Geology, 37(9):811–814. **https://doi.org/10.1130/G30058A.1**

Knutz, P.C., 2008. Palaeoceanographic significance of contourite drifts. In Rebesco, M., and Camerlenghi, A. (Eds.), Contourites. Developments in Sedimentology, 60: (Elsevier), 511–535. **https://doi.org/10.1016/S0070-4571(08)10024-3**

Krijgsman, W., Capella, W., Simon, D., Hilgen, F.J., Kouwenhoven, T.J., Meijer, P.T., Sierro, F.J., Tulbure, M.A., van den Berg, B.C.J., van der Schee, M., and Flecker, R., 2018. The Gibraltar Corridor: Watergate of the Messinian Salinity Crisis. Marine Geology, 403:238–246. **https://doi.org/10.1016/j.margeo.2018.06.008**

LaRiviere, J.P., Ravelo, A.C., Crimmins, A., Dekens, P.S., Ford, H.L., Lyle, M., and Wara, M.W., 2012. Late Miocene decoupling of oceanic warmth and atmospheric carbon dioxide forcing. Nature, 486(7401):97–100. **https://doi.org/10.1038/nature11200**

Ledesma, S., 2000. Astrobiocronología y Estratigrafía de Alta Resolución del Neógeno de la Cuenca del Guadalquivir-Golfo de Cadiz [PhD dissertation]. University of Salamanca, Salamanca, Spain.

Legg, S., Briegleb, B., Chang, Y., Chassignet, E.P., Danabasoglu, G., Ezer, T., Gordon, A.L., Griffies, S., Hallberg, R., Jackson, L., Large, W., Özgökmen, T.M., Peters, H., Price, J., Riemenschneider, U., Wu, W., Xu, X., and Yang, J., 2009. Improving oceanic overflow representation in climate models: the gravity current entrainment climate process team. Bulletin of the American Meteorological Society, 90(5):657–670. **https://doi.org/10.1175/2008BAMS2667.1**

Llave, E., Hernández-Molina, F.J., García, M., Ercilla, G., Roque, C., Juan, C., Mena, A., Preu, B., Rooij, D.V., Rebesco, M., Brackenridge, R., Jané, G., Gómez-Ballesteros, M., and Stow, D., 2020. Contourites along the Iberian continental margins: conceptual and economic implications. Geological Society, London, Special Publications, 476(1):403–436. **https://doi.org/10.1144/SP476-2017-46**

Llave, E., Matias, H., Hernández-Molina, F.J., Ercilla, G., Stow, D.A.V., and Medialdea, T., 2011. Pliocene–Quaternary contourites along the northern Gulf of Cadiz margin: sedimentary stacking pattern and regional distribution. GeoMarine Letters, 31(5):377–390. **https://doi.org/10.1007/s00367-011-0241-3**

Lofi, J., 2018. Seismic Atlas of the Messinian Salinity Crisis Markers in the Mediterranean Sea, Volume 2: Paris (Société géologique de France).

Magill, C.R., Ausín, B., Wenk, P., McIntyre, C., Skinner, L., Martínez-García, A., Hodell, D.A., Haug, G.H., Kenney, W., and Eglinton, T.I., 2018. Transient hydrodynamic effects influence organic carbon signatures in marine sediments. Nature Communications, 9(1):4690. **https://doi.org/10.1038/s41467-018-06973-w**

Maldonado, A., Somoza, L.s., and Pallarés, L., 1999. The Betic orogen and the Iberian–African boundary in the Gulf of Cadiz: geological evolution (central North Atlantic). Marine Geology, 155(1):9–43. **https://doi.org/10.1016/S0025-3227(98)00139-X**

Martín, J.M., Braga, J.C., Aguirre, J., and Puga-Bernabéu, Á., 2009. History and evolution of the North-Betic Strait (Prebetic Zone, Betic Cordillera): a narrow, early Tortonian, tidal-dominated, Atlantic–Mediterranean marine passage. Sedimentary Geology, 216(3):80–90. **https://doi.org/10.1016/j.sedgeo.2009.01.005**

Martín, J.M., Puga-Bernabéu, Á., Aguirre, J., and Braga, J.C., 2014. Miocene Atlantic-Mediterranean seaways in the Betic Cordillera (southern Spain). Revista de la Sociedad Geológica de España, 27(1):175–186.

Martínez del Olmo, W., 2012. El Messiniense en el Golfo de Valencia y el Mar de Alborán: implicaciones paleogeográficas y paleoceanográficas. Revista de la Sociedad Geológica de España, 24(3-4):237–257.

Martínez del Olmo, W., and Martín, D., 2016. El Neógeno de la cuenca Guadalquivir-Cádiz (Sur de España). Revista de la Sociedad Geológica de España, 29(1):35–58.

Marzocchi, A., Lunt, D.J., Flecker, R., Bradshaw, C.D., Farnsworth, A., and Hilgen, F.J., 2015. Orbital control on Late Miocene climate and the North African monsoon: insight from an ensemble of sub-precessional simulations. Climate of the Past, 11(10):1271–1295. **https://doi.org/10.5194/cp-11-1271-2015**

Medaouri, M., Déverchère, J., Graindorge, D., Bracene, R., Badji, R., Ouabadi, A., Yelles-Chaouche, K., and Bendiab, F., 2014. The transition from Alboran to Algerian basins (Western Mediterranean Sea): chronostratigraphy, deep crustal structure and tectonic evolution at the rear of a narrow slab rollback system. Journal of Geodynamics, 77:186–205. **https://doi.org/10.1016/j.jog.2014.01.003**

Nelson, C.H., Baraza, J., Maldonado, A., Rodero, J., Escutia, C., and Barber Jr, J.H., 1999. Influence of the Atlantic inflow and Mediterranean outflow currents on late Quaternary sedimentary facies of the Gulf of Cadiz continental margin. Marine Geology, 155(1–2):99–129. **https://doi.org/10.1016/S0025-3227(98)00143-1**

Ng, Z.L., Hernández-Molina, F.J., Ledesma, S., Sierro, F.J., Duarte, D., Llave, E., Roque, C., and Arnáiz, Á., 2022. Late Miocene evolution of the eastern Deep Algarve basin: interaction of bottom currents and gravitational processes in a foredeep setting. Marine and Petroleum Geology, 141:105695. **https://doi.org/10.1016/j.marpetgeo.2022.105695**

Nisancioglu, K.H., Raymo, M.E., and Stone, P.H., 2003. Reorganization of Miocene deep water circulation in response to the shoaling of the Central American Seaway. Paleoceanography, 18(1):1006–1018. **https://doi.org/10.1029/2002PA000767**

Orszag-Sperber, F., 2006. Changing perspectives in the concept of "Lago-Mare" in Mediterranean Late Miocene evolution. Sedimentary Geology, 188–189:259–277. **https://doi.org/10.1016/j.sedgeo.2006.03.008**

Peixoto, J.P., and Kettani, M.A., 1973. The control of the water cycle. Scientific American, 228(4):46–63. **http://www.jstor.org/stable/24923025**

Penaud, A., Eynaud, F., Sánchez-Goñi, M., Malaizé, B., Turon, J.L., and Rossignol, L., 2011. Contrasting sea-surface responses between the western Mediterranean Sea and eastern subtropical latitudes of the North Atlantic during abrupt climatic events of MIS 3. Marine Micropaleontology, 80(1):1–17. **https://doi.org/10.1016/j.marmicro.2011.03.002**

Price, J.F., Baringer, M.O.N., Lueck, R.G., Johnson, G.C., Ambar, I., Parrilla, G., Cantos, A., Kennelly, M.A., and Sanford, T.B., 1993. Mediterranean Outflow mixing and dynamics. Science, 259(5099):1277–1282. **https://doi.org/10.1126/science.259.5099.1277**

Price, J.F., and O'Neil Baringer, M., 1994. Outflows and deep water production by marginal seas. Progress in Oceanography, 33(3):161–200. **https://doi.org/10.1016/0079-6611(94)90027-2**

Rahmstorf, S., 2006. Thermohaline ocean circulation. In Elias, S.A., Encyclopedia of Quaternary Sciences. Amsterdam (Elsevier), 739–750.

Riaza, C., and Martínez Del Olmo, W., 1996. Depositional model of the Guadalquivir – Gulf of Cadiz Tertiary basin. In Friend, P.F. and Dabrio, C.J., Tertiary Basins of Spain: The Stratigraphic Record of Crustal Kinematics. Cambridge (Cambridge University Press), 330–338. **https://doi.org/10.1017/CBO9780511524851.047**

Rodrigues, S., Roque, C., Hernández-Molina, F.J., Llave, E., and Terrinha, P., 2020. The sines contourite depositional system along the SW Portuguese margin: Onset, evolution and conceptual implications. Marine Geology, 430:106357. **https://doi.org/10.1016/j.margeo.2020.106357**

Rogerson, M., Bigg, G.R., Rohling, E.J., and Ramirez, J., 2012a. Vertical density gradient in the eastern North Atlantic during the last 30,000 years. Climate Dynamics, 39(3):589–598. **https://doi.org/10.1007/s00382-011-1148-4**

Rogerson, M., Colmenero-Hidalgo, E., Levine, R.C., Rohling, E.J., Voelker, A.H.L., Bigg, G.R., Schönfeld, J., Cacho, I., Sierro, F.J., Löwemark, L., Reguera, M.I., de Abreu, L., and Garrick, K., 2010. Enhanced Mediterranean-Atlantic exchange during Atlantic freshening phases. Geochemistry, Geophysics, Geosystems, 11(8):Q08013. **https://doi.org/10.1029/2009GC002931**

Rogerson, M., Rohling, E.J., Bigg, G.R., and Ramirez, J., 2012b. Paleoceanography of the Atlantic-Mediterranean exchange: overview and first quantitative assessment of climatic forcing. Reviews of Geophysics, 50(2):RG2003. **https://doi.org/10.1029/2011RG000376**

Rogerson, M., Rohling, E.J., and Weaver, P.P.E., 2006. Promotion of meridional overturning by Mediterranean-derived salt during the last deglaciation. Paleoceanography, 21(4):PA4101. **https://doi.org/10.1029/2006PA001306**

Rohling, E.J., 2007. Progress in paleosalinity: overview and presentation of a new approach. Paleoceanography, 22(3):PA3215. **https://doi.org/10.1029/2007PA001437**

Rouchy, J.M., Caruso, A., Pierre, C., Blanc-Valleron, M.-M., and Bassetti, M.A., 2007. The end of the Messinian salinity crisis: evidences from the Chelif Basin (Algeria). Palaeogeography, Palaeoclimatology, Palaeoecology, 254(3):386–417. **https://doi.org/10.1016/j.palaeo.2007.06.015**

Roveri, M., Flecker, R., Krijgsman, W., Lofi, J., Lugli, S., Manzi, V., Sierro, F.J., Bertini, A., Camerlenghi, A., De Lange, G., Govers, R., Hilgen, F.J., Hübscher, C., Meijer, P.T., and Stoica, M., 2014. The Messinian salinity crisis: past and future of a great challenge for marine sciences. Marine Geology, 352:25–58. **https://doi.org/10.1016/j.margeo.2014.02.002**

Ryan, W.B.F., Hsü, K.J., et al., 1973. Initial Reports of the Deep Sea Drilling Project, 13: Washington, DC (US Government Printing Office). **https://doi.org/10.2973/dsdp.proc.13.1973**

Schimmelmann, A., Lange, C.B., Schieber, J., Francus, P., Ojala, A.E.K., and Zolitschka, B., 2016. Varves in marine sediments: A review. Earth-Science Reviews, 159:215–246. **https://doi.org/10.1016/j.earscirev.2016.04.009**

Siegenthaler, U., and Sarmiento, J.L., 1993. Atmospheric carbon dioxide and the ocean. Nature, 365(6442):119–125. **https://doi.org/10.1038/365119a0**

Sierro, F.J., Delgado, J.A.G., Dabrio, C.J., Flores, J.A., and Civis, J., 1996. Late Neogene depositional sequences in the foreland basin of Guadalquivir (SW Spain). In Friend, P.F. and Dabrio, C.J., Tertiary Basins of Spain: The Stratigraphic Record of Crustal Kinematics. Cambridge (Cambridge University Press), 339–345. **https://doi.org/10.1017/CBO9780511524851.048**

Smethie, W.M., Jr., Fine, R.A., Putzka, A., and Jones, E.P., 2000. Tracing the flow of North Atlantic Deep Water using chlorofluorocarbons. Journal of Geophysical Research: Oceans, 105(C6):14297–14323. **https://doi.org/10.1029/1999JC900274**

Smith, A.G., and Pickering, K.T., 2003. Oceanic gateways as a critical factor to initiate icehouse Earth. Journal of the Geological Society, 160(3):337–340. **https://doi.org/10.1144/0016-764902-115**

Stow, D.A.V., and Faugères, J.C., 2008. Contourite facies and the facies model. In Rebesco, M., and Camerlenghi, A. (Eds.), Contourites. Developments in Sedimentology, 60: (Elsevier), 223–256. **https://doi.org/10.1016/S0070-4571(08)10013-9**

Suárez Alba, J., Martínez del Olmo, W., Serrano Oñate, A., and Leret Verdú, G., 1989. Estructura del sistema turbidítico de la Formación Arenas del Guadalquivir. In Libro homenaje a Rafael Soler y José. Madrid (Asociación de Geólogos y Geofísicos Españoles del Petróleo), 123–136.

Sykes, T.J.S., Ramsay, A.T.S., and Kidd, R.B., 1998. Southern hemisphere Miocene bottom-water circulation: a palaeobathymetric analysis. Geological Society, London, Special Publications, 131(1):43–54. **https://doi.org/10.1144/GSL.SP.1998.131.01.03**

Tans, P.P., Berry, J.A., and Keeling, R.F., 1993. Oceanic $^{13}C/^{12}C$ observations: a new window on ocean CO_2 uptake. Global Biogeochemical Cycles, 7(2):353–368. **https://doi.org/10.1029/93GB00053**

Taylforth, J.E., McCay, G.A., Ellam, R., Raffi, I., Kroon, D., and Robertson, A.H.F., 2014. Middle Miocene (Langhian) sapropel formation in the easternmost Mediterranean deep-water basin: evidence from northern Cyprus. Marine and Petroleum Geology, 57:521–536. **https://doi.org/10.1016/j.marpetgeo.2014.04.015**

Thomas, H., Bozec, Y., Elkalay, K., and de Baar, H.J.W., 2004. Enhanced open ocean storage of CO_2 from shelf sea pumping. Science, 304(5673):1005–1008. **https://doi.org/10.1126/science.1095491**

Uenzelmann-Neben, G., Weber, T., Grützner, J., and Thomas, M., 2017. Transition from the Cretaceous ocean to Cenozoic circulation in the western South Atlantic — a twofold reconstruction. Tectonophysics, 716:225–240. **https://doi.org/10.1016/j.tecto.2016.05.036**

van Aken, H.M., 2000. The hydrography of the mid-latitude northeast Atlantic Ocean: I: The deep water masses. Deep Sea Research Part I: Oceanographic Research Papers, 47(5):757–788. **https://doi.org/10.1016/S0967-0637(99)00092-8**

van der Schee, M., Sierro, F.J., Jiménez-Espejo, F.J., Hernández-Molina, F.J., Flecker, R., Flores, J.A., Acton, G., Gutjahr, M., Grunert, P., Garcia-Gallardo, A., and Andersen, N., 2016. Evidence of early bottom water current flow after the Messinian Salinity Crisis in the Gulf of Cadiz. Marine Geology, 380:315–329. **https://doi.org/10.1016/j.margeo.2016.04.005**

van Hinsbergen, D.J.J., Vissers, R.L.M., and Spakman, W., 2014. Origin and consequences of western Mediterranean subduction, rollback, and slab segmentation. Tectonics, 33(4):393–419. **https://doi.org/10.1002/2013TC003349**

Voelker, A.H.L., Lebreiro, S.M., Schönfeld, J., Cacho, I., Erlenkeuser, H., and Abrantes, F., 2006. Mediterranean outflow strengthening during northern hemisphere coolings: a salt source for the glacial Atlantic? Earth and Planetary Science Letters, 245(1):39–55. **https://doi.org/10.1016/j.epsl.2006.03.014**